

**MOLECULAR DYNAMICS SIMULATION STUDY
OF RESONANCE ABSORPTION PHENOMENA IN
INTENSE LASER-DRIVEN ATOMIC
NANO-CLUSTERS**

By

SAGAR SEKHAR MAHALIK

PHYS06201304008

Institute for Plasma Research, Gandhinagar

*A thesis submitted to the
Board of Studies in Physical Sciences*

*In partial fulfillment of requirements
for the Degree of*

DOCTOR OF PHILOSOPHY

of

HOMI BHABHA NATIONAL INSTITUTE

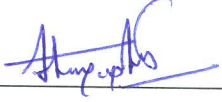
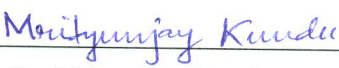
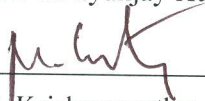

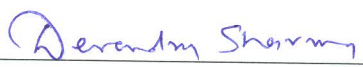


April, 2019

Homi Bhabha National Institute¹

Recommendations of the Viva Voce Committee

As members of the Viva Voce Committee, we certify that we have read the dissertation prepared by **Mr. Sagar Sekhar Mahalik** entitled “**Molecular dynamics simulation study of resonance absorption phenomena in intense laser-driven atomic nano-clusters**” and recommend that it may be accepted as fulfilling the thesis requirement for the award of Degree of Doctor of Philosophy.

	11/10/2019
Chairman- Prof. Sudip Sengupta	Date:
	11/10/2019
Guide/Convener- Dr. Mrityunjay Kundu	Date:
	11/10/19
Examiner- Prof. M. Krishnamurthy	Date:
	11/10/2019
Member 1- Prof. Subroto Mukherjee	Date:
	11/10/2019
Member 2- Dr. Devendra Sharma	Date:

Final approval and acceptance of this thesis is contingent upon the candidate's submission of the final copies of the thesis to HBNI.

I hereby certify that I have read this thesis prepared under my direction and recommend that it may be accepted as fulfilling the thesis requirement.

Date: 11/10/2019

Place: IPR, Gandhinagar



Dr. Mrityunjay Kundu

(Guide)

¹ This page is to be included only for final submission after successful completion of viva voce.

STATEMENT BY AUTHOR

This dissertation has been submitted in partial fulfilment of requirements for an advanced degree at Homi Bhabha National Institute (HBNI) and is deposited in the Library to be made available to borrowers under rules of the HBNI.

Brief quotations from this dissertation are allowable without special permission, provided that accurate acknowledgement of source is made. Requests for permission for extended quotation from or reproduction of this manuscript in whole or in part may be granted by the Competent Authority of HBNI when in his or her judgement the proposed use of the material is in the interests of scholarship. In all other instances, however, permission must be obtained from the author.

Sagar Sekhar Mahalik
Sagar Sekhar Mahalik

DECLARATION

I, hereby declare that the investigation presented in the thesis has been carried out by me. The work is original and the work has not been submitted earlier as a whole or in part for a degree/diploma at this or any other Institution or University.

Sagar Sekhar Mahalik
Sagar Sekhar Mahalik

List of Publications arising from the thesis

Journal:

1. **“Anharmonic resonance absorption of short laser pulses in clusters: A molecular dynamics simulation study”**, S. S. Mahalik and M. Kundu, [Physics of Plasmas](#) **23**, 123302 (2016).
2. **“Dynamical resonance shift and unification of resonances in short-pulse laser-cluster interaction”**, S. S. Mahalik and M. Kundu, [Physical Review A](#) **97**, 063406 (2018).
3. **“Collisionless absorption of short laser pulses in a deuterium cluster: dependence of redshift of resonance absorption peak on laser polarization, intensity and wavelength”**, S. S. Mahalik and M. Kundu, [\(Under review\)](#).

Conferences and Schools

International Participation:

1. **“Identification of nonlinear resonance absorption in a laser driven deuterium cluster using molecular dynamics simulation”**, Sagar Sekhar Mahalik and Mrityunjay Kundu, *10th Asia Plasma And Fusion Association (APFA), Institute for Plasma Research (IPR), Gandhinagar, Gujarat, India, December 14-18, 2015.*
2. **“Anharmonic Resonance Absorption Of Short Laser Pulses In Clusters : A Molecular Dynamics Simulation Study”**, Sagar Sekhar Mahalik and Mrityunjay Kundu, *International conference on Frontiers of Physics and Plasma Science (FPPS), Ujjain Engineering College, Ujjain, Madhya Pradesh, India, November 7-8, 2016.*
3. Laser Plasma Accelerator workshop, *International School for Theoretical Science (ICTS), Bangalore, India, March 6-17, 2017.*

4. **“Effect of laser wavelength on resonance absorption of ultrashort laser pulses in atomic clusters”**,

Sagar Sekhar Mahalik and Mrityunjay Kundu,

44th European Physical Society (EPS) Conference on Plasma Physics, Queen's university, Belfast, Northern Ireland, UK, June 26-30, 2017.

5. **“Dynamical resonance shift and unification of resonances in short-pulse laser cluster interaction”**,

Sagar Sekhar Mahalik and Mrityunjay Kundu,

60th Annual meeting of American Physical Society division of plasma physics (APS-DPP), Portland, Oregon, USA, November 5-9, 2018.

National Participation:

1. **“Plasma Oscillations By Molecular Dynamics Simulation”**,

Sagar Sekhar Mahalik and Mrityunjay Kundu,

30th National Symposium on Plasma Science & Technology (PLASMA 2015), Saha Institute of Nuclear Physics, Kolkata, India, December 1-4, 2015.

2. **“Effect of laser wavelength on resonance absorption of ultrashort laser pulses in a deuterium cluster”**,

Sagar Sekhar Mahalik and Mrityunjay Kundu,

32nd National Symposium on Plasma Science and Technology, Gandhinagar, India, November 7-10, 2017.

Sagar Sekhar Mahalik
Sagar Sekhar Mahalik

Dedicated
to
My Family

ACKNOWLEDGEMENTS

My journey, both academic and personal, to this point would not have been possible without the guidance and support of many amazing people. I consider myself to be very fortunate to have met these people and I would like to convey my deep gratitude to them here.

First and foremost, I would like to convey my sincere gratitude to my thesis supervisor Dr. Mrityunjay Kundu for giving me the opportunity to pursue my research work under his supervision. His excellent guidance, friendly attitude, constant support, and encouragement have greatly helped me throughout my PhD tenure. His comprehensive knowledge of computational techniques has really helped me in developing a new Molecular Dynamics simulation code from scratch, which has been used to carry out my research. His valuable guidance has solved many programming issues during the development of the MD code. I am also grateful to him for his invaluable advice during the writing of the manuscripts and the thesis. Apart from these, his personal discipline, calmness, efficient time management, hard work, and positive attitude have always inspired me throughout these years. I feel very fortunate to work under his guidance.

I am also indebted to my doctoral committee members, Prof. Sudip Sengupta (Chairman), Prof. Subroto Mukherjee and Dr. Devendra Sharma for timely monitoring the progress of my research work. Their useful suggestions and impactful comments during the doctoral committee reviews have greatly helped me to improve my basic understanding of plasma physics.

I would like to express my appreciation and gratitude to all my teachers of the Institute for Plasma Research (IPR) namely, late Prof. P. K. Kaw, Prof. A. Sen, Prof. Y. C. Saxena, Prof. S. K. Mattoo, Prof. G. Sethia, Prof. Amita Das, Prof. Subroto Mukherjee, Prof. R. Ganesh, Prof. Prabal K. Chattopadhyay, Prof. S. Sengupta, Dr. Ramasubramanian, Dr. Joydeep Ghosh, Dr. Devendra Sharma, Dr. Mrityunjay Kundu, Dr. Mainak Bandyopadhyay, Dr. Daniel Raju, Dr. R. Srinivasan, Dr. V. P. Anitha, Dr. Asim K. Chattopadhyay, Dr. G. Ravi and others who taught me basic plasma physics, experimental plasma physics, computational techniques and other disciplines of physics during the pre-PhD course work. I especially thank Prof. Subroto Mukherjee (Dean, Academics, and Student Affairs and Chairman, Academic Committee) for his guidance in various matters related to HBNI.

I would also like to acknowledge HBNI and IPR, for awarding me the student travel grant to attend and present my research work in EPS-2017, held at Northern Ireland, UK and APS-2018, held at Portland, USA. I am also thankful to the computer center staff, library staff and administrative staff of IPR for always being supportive and helpful.

I would also like to thank my seniors Vikram Sagar, Kshitish, Deepak, Ujjwal, Gurudatt, Rameswar, Sushil, Sanat, Pravesh, Sayak, Manjit, Aditya, Soumen, Vikram, Veda Prakash, Sandeep Rimza, Dushyant, Rana, Bibhu, Vara, Neeraj, Vidhi, Akanksha, Deepa, Rupendra, Chandrasekhar, Mangilal, Meghraj, Harish, Samir, Bhumika, Narayan, Sonu, Modhu, Arghya, Amit, Surabhi, Ratan, Umesh and Debraj and juniors Shivam, Trithendu, Arun, Rupak, Avnish, Gaurav, Subroto, Niraj, Srimanta, Dipshika, Garima, Girija, Yogesh, Arnab, Mayank, Priti, Chinmoy, Soumen, Hariprasad, Sanjeev, Karim, Tanmay, Satadal, Pradeep, Nidhi, Swapnali, Ayushi, Devshree, Pawandeep, Piyush, Jagannath, Prince, Satya, Ram, Vivek, Lavanya, Kalyani, other scholars and TTPs for making my stay at the hostel joyful and eventful. It is my pleasure to thank my batchmates Prabhakar, Sandeep, Chetan, Jervis, Atul, Deepak, Alamgir, Meenakshi, Pallavi and Harshita, for the wonderful times that we have shared over the past few years.

Special thanks to Narayan, Bhumika and Prabhakar, who have always been there to support me whenever I needed it the most. They have always stood by me through good and the bad moments to motivate me. I am grateful to them for their numerous help during the tough periods of my life. I find myself lucky to have friends like them in my life.

I would like to acknowledge my family members, who mean everything to me. Their unconditional love and endless support have been a constant source of encouragement to me. I am forever indebted to my parents, Mr. Kasinath Mahalik and Mrs. Sanjukta Mahalik for believing in me and standing with me in all situations. I would also like to thank my younger brother Nirmal (Kutu) and my elder sister Nilendri for their love, support and care.

Finally, I thank the Almighty for giving me the strength and patience during all the challenging moments in completing this thesis.

Sagar Sekhar Mahalik

Contents

Synopsis	v
List of Figures	xv
List of Tables	xix
1 Introduction	1
1.1 Introduction and overview	2
1.2 Clusters in intense laser fields	4
1.2.1 Ionization of atoms/ions in a cluster by laser field	5
1.2.2 Ionization of cluster by space-charge field : Ionization ignition	10
1.2.3 Ionization of a cluster by electron-ion collision	10
1.2.4 Laser energy absorption mechanisms in a cluster	13
1.2.5 Cluster expansion processes	17
1.2.6 Hydrodynamic expansion	17
1.2.7 Coulomb expansion	19
1.3 Plan of the thesis	20
2 Molecular Dynamics Simulation	25
2.1 Introduction	26
2.2 Flowchart of MD simulation	28
2.3 Initialization	29
2.4 The laser pulse	31
2.5 Governing Equations	32
2.6 Choice of artificial parameter r_0	33
2.7 Integration of the equation of motion	34
2.8 Test of the MD code	37
2.8.1 Single particle dynamics	37
2.8.2 Multi-particle dynamics in a 2D slab geometry	39
2.8.3 Verification of Mie-plasma frequency in a deuterium cluster	44
2.9 Improvement of the MD simulation code	49
2.10 Summary	52
3 Identification of anharmonic resonance absorption	53
3.1 Introduction	54

3.2	Model for anharmonic resonance absorption	57
3.2.1	Effective frequency of the electron sphere	60
3.2.2	Dynamics of the electron sphere in the laser field	63
3.3	Anharmonic resonance absorption using molecular dynamics simulation	67
3.3.1	Required details of molecular dynamics simulation	68
3.3.2	Laser energy absorption and outer ionization	69
3.3.3	Analysis of electron trajectory and finding the AHR	70
3.3.4	AHR in the frequency vs energy plane	73
3.4	Summary	76
4	Dynamical resonance shift and unification of resonances	77
4.1	Introduction	78
4.2	Wavelength shift of resonance absorption using RSM	81
4.2.1	RSM results with intensity variation for different \bar{Z}	83
4.2.2	RSM results with intensity variation for fixed \bar{Z}	85
4.3	Unified resonance absorption by MD simulation	88
4.3.1	Details of MD simulation	89
4.3.2	Calculation of Mie-plasma frequency in MD simulation	90
4.3.3	Dynamical resonance shift and unification of resonances	95
4.3.4	Time domain analysis of the resonance shift	99
4.3.5	Resonance shift with continuous short laser pulses	103
4.3.6	Resonance shift with cluster size variation	105
4.3.7	Resonance shift with different CEPs	107
4.4	Summary	109
5	Dependence of red-shift of absorption peak on laser polarization, intensity, and wavelength for a deuterium cluster	111
5.1	Introduction	112
5.2	Resonance absorption by MD simulation	114
5.2.1	Absorption and outer ionization with LP laser	115
5.2.2	Absorption and outer ionization with CP vs LP light	122
5.3	RSM results : Absorption and outer ionization with CP vs LP laser . . .	128
5.4	Summary	131

6	Conclusions and future scope	133
6.1	Conclusions	134
6.2	Future scope	136
A	Appendix	137
A.1	Atomic units and SI units conversion	137
A.2	Comparison between different parameters for a deuterium cluster and an argon cluster	138
	Bibliography	139

SYNOPSIS

Clusters are finite aggregate of atoms or molecules bound together via Van der Waals forces. Under specific conditions of pressure and temperature, their size may vary from sub-nanometer to a few tens of nanometers. The average atomic density of a cluster is low, typically on the order of the gas density $\sim 10^{17} - 10^{19} \text{cm}^{-3}$, while its local atomic density is close to the solid density $\sim 10^{22} - 10^{23} \text{cm}^{-3}$. Therefore, a cluster may serve as an intermediate state between solid and gas. The localized solid-like atomic density of a cluster and its smaller size as compared to laser wavelengths λ (typically longer than 100 nm) allow full penetration of the laser field into the cluster nano-plasma (immediately formed after the ionization of atoms of the cluster by the laser field) without any attenuation although laser frequency ω is lower than the plasma frequency ω_p , in contrast to the case of laser interaction with a solid target of thickness on the order of microns (e.g., thin foils). Therefore, laser-driven clusters are shown to be very efficient absorber of laser light (almost 90% absorption has been reported in the experiment [1]) as compared to isolated atoms, gas phase atoms and traditional solid targets, when they are irradiated by the same laser pulse. In a simplified picture, the dynamics of the laser-cluster interaction may be summarized as: (i) the leading edge of the laser pulse ionizes the constituent atoms through optical field ionization (OFI) and creates free electrons within the cluster (called inner ionization), (ii) these inner ionized electrons within the cluster experience the combined electric fields of the driving laser and transient local electrostatic field (due to charge separation) and may escape the cluster boundary (called outer ionization) after absorbing energy from the remaining part of the laser, thus creating an overall positive space-charge in the cluster due to bare ions, and (iii) finally the positively charged cluster explodes due to inter-ionic Coulomb repulsion

(called Coulomb explosion). The efficient coupling of laser light leads to the production of energetic KeV electrons [2–4], MeV ions (useful for driving fusion reaction with deuterium cluster plasma) [1, 2, 5, 6], generation of X-rays [7], and MeV neutrals [8] in experiments.

The experimental observation of unexpectedly high ionic charge states for rare gas clusters, energetic ions and energetic electrons above the energy of a free electron (known as ponderomotive energy) in the same laser field indicates a high degree of non-linear response of electrons involved in the laser-cluster interaction process. Electrons being much lighter than ions, they respond to the laser field much quicker and in the first instance laser energy is deposited to electrons while slow ion dynamics (e.g., Coulomb explosion) results as a secondary process after the electrons are displaced. Therefore, to explain the above experimental findings and to investigate various laser-cluster interaction processes, it is *important* to understand different absorption mechanisms by electrons for the extraordinary laser absorption in clusters. In spite of the various long research activities in this field since the early nineties, the laser energy coupling with cluster electrons is still debated. Laser energy is coupled to the electrons by collisions among charge particles and resonances. However, the collisional process of absorption becomes inefficient for infrared lasers with intensities $I_0 > 10^{16} \text{ Wcm}^{-2}$ and can be neglected since it scales as $\sim I_0^{-3/2}$. On the other hand, resonance absorption mechanism, considered as a collisionless process, includes both linear resonance (LR) and anharmonic resonance (AHR). In this thesis, we focus to study above collisionless resonance absorption processes (LR and AHR) which are frequency dependent phenomena and depend on the system's eigenfrequency and the driver's (here laser) frequency. In the present study, cluster plasma (nano-plasma) is considered as spherical and the eigenfrequency of the collective oscillation of the electron cloud is known as the Mie-plasma

frequency $\omega_M = \omega_p / \sqrt{3} = \sqrt{4\pi\rho/3}$ (atomic units are used, where $m_e = -e = 1$) which is $1/\sqrt{3}$ times ω_p due to finite spherical shape and here ρ is the ionic charge density. The charge density for which $\omega_p > \omega$, plasma is called as over-dense; in the opposite case of $\omega_p < \omega$, plasma is called as under-dense; and for $\omega_p = \omega$, plasma is called as critically-dense where $\rho_c = \omega^2/4\pi$ is the critical density. For the spherical cluster, LR happens when $\omega_M = \omega$ condition is met. The initial charge density ρ in a cluster after the OFI remains much above the critical density (i.e., plasma remains over-dense with $\omega_M > \omega$), but as the ionic background expands in later time due to mutual Coulomb repulsion, the charge density decreases which results decrease in ω_M and at a certain time it matches ω . Therefore, LR ($\omega_M = \omega$) occurs after a longer time (typically > 50 fs) during the Coulomb expansion. In experiments, with longer laser pulses, the importance of LR has been demonstrated through pump-probe technique [9–11]. LR absorption is often considered as the primary mechanism behind efficient coupling of laser energy to cluster electrons. However, for short laser pulses, background ions remain relatively frozen (cluster does not expand sufficiently), ω_M remains much above ω and LR ($\omega_M = \omega$) is not met. For this over-dense regime, efficient laser absorption by electrons takes place through AHR in the self-generated an-harmonic potential where a laser-driven electron's effective oscillation frequency $\Omega[(r(t))]$ dynamically meets ω , i.e., $\Omega[(r(t))] = \omega$. The extremely complex electron dynamics of a laser irradiated cluster has also sensitive dependence on both the laser and cluster parameters. The work reported in this thesis presents laser energy absorption processes (LR and AHR) in the short pulse regime and their dependency on different laser and cluster parameters (i.e, peak intensity, wavelength, pulse duration, cluster size and type etc.).

In the first problem, we identify the anharmonic resonance (AHR) absorption by 3D-MD simulation and a non-linear oscillator model, called rigid sphere model (RSM).

AHR occurring in an anharmonic potential was studied before for a laser-driven atomic cluster using particle-in-cell (PIC) simulations and models [12–14]. However, it is not rigorously verified so far by other first principle methods “e.g., molecular dynamics (MD)” simulation, although there are plenty of MD simulations [15–20] exist in different domains of laser-driven clusters. There are various advantages of MD simulations over PIC simulations. The main advantage of MD over PIC is the absence of computational grid and interpolation. In electro-static PIC (ES-PIC) simulations the field is computed on a grid of cells by solving the Poisson’s equation and then the field is interpolated from the grid to the positions of particles. Whereas, the Poisson’s equation is not solved in electro-magnetic PIC (EM-PIC) codes. In MD simulation the force on each particle is calculated as the sum over all forces from the rest of the particles in the system and the trajectory of each particle in the system is determined by solving Newton’s equations of motion. This unique feature of MD simulation makes the calculation simple for laser-cluster interaction study. Therefore, to prove AHR for a laser-driven cluster, a 3D-MD code with soft-core Coulomb interaction among charged particles has been developed. Also, for the first time, our MD simulation code clearly identifies the AHR process as a dominant collisionless absorption mechanism in an over-dense deuterium cluster irradiated by an ultra-short laser pulse [21]. The details of AHR will be described in chapter 3. In the next problem, we report the effect of laser wavelength on the resonance absorption with short laser pulses. The particular focus is given to find out an optimal regime of wavelength for maximum laser energy absorption. It is very trivial from the famous nano-plasma model [9] that for a laser-heated cluster, maximum energy transfer from the driver to the oscillatory electrons happens exactly at the linear resonance (the nanoplasma resonance), i.e., $\omega_M = \omega$ in the absence of other dissipation channels. However, there are some MD simulations of laser-heated clusters [19, 22, 23],

which contradict this perception and the role of above LR was denied without satisfactory physical explanation. Their contradictory results of LR should be re-examined in order to have a clear understanding of this physical phenomena. However, we find that for a given laser intensity, maximum laser absorption does not occur at the linear resonance wavelength $\lambda_M = \lambda$ (or frequency $\omega_M = \omega$), instead it is red-shifted in the regime of $(1 - 1.5)\lambda_M$. In this shifted band of wavelength, both LR and AHR absorption are shown to be dynamically unified leading to maximum absorption for a laser-heated cluster. We term this regime of combined resonances as unified dynamical linear resonance (UDLR) which will be explained in chapter 4 in detail. Next, in chapter 5, we study the dependence of UDLR and the red-shift of absorption peak for a different cluster i.e., deuterium (other than argon) for its universal acceptance. We also explore the effect of laser polarization on this red-shift of absorption peak. The thesis contains six chapters. A more systematic chapter-wise summary of the works carried out in this thesis is provided below.

Chapter-1: Introduction

This chapter provides a general introduction about the interaction of strong ultra-short laser fields with atomic clusters, important physical processes related to the laser-cluster interaction and its various applications. This chapter also contains a comprehensive review of previous theoretical modelling, experimental and simulation studies on laser-cluster interaction, followed by the motivations behind the present studies. It also highlights the importance of present studies in the field of laser-plasma interaction as far as collisionless absorptions are concerned. Finally, a brief outline indicating the chapter-wise organization of the contents of the thesis is given.

Chapter-2: Molecular Dynamics Simulation

This thesis work begins with the development of a 3D classical MD code as the main working tool. In this chapter, we describe the methodology of this newly developed MD code in detail. Before studying the various physics phenomena of laser-irradiated clusters in the next chapters, systematic numerical and analytical studies for single-particle and multi-particle dynamics are performed. To validate the MD code, energy conservation has also been checked for both the systems. An important physical phenomenon is the Mie-plasma oscillation of electron cloud against the ion background under small perturbation in the absence of any dissipation. This oscillation frequency is known as Mie-plasma frequency ω_M . Since, the focus of this thesis is to study resonance absorption processes (LR and AHR), which are frequency dependent phenomena, verification of the correct ω_M is *crucial* before we go for further studies. We first verify this ω_M in a 2D as well as in a 3D system (i.e., pre-ionized deuterium cluster) with analytical results for more than 100 Mie-plasma periods along with the energy conservation under a small perturbation of the electron cloud. The full 3D-MD code with soft-core Coulomb interaction among charge particles (electron-ion, electron-electron, ion-ion) is then employed to study the dynamical behaviour of a deuterium and argon clusters irradiated by different peak intensities between $I_0 = 5 \times 10^{14} - 5 \times 10^{17} \text{ Wcm}^{-2}$ in chapters 3, 4 and 5. The dipole approximation for the laser vector potential $A(z, t) = A(t) \exp(-i2\pi z/\lambda) \approx A(t)$ is assumed (i.e., spatial variation of the laser field is neglected), since the cluster size $R_0 < 10 \text{ nm}$ is much smaller than the skin depth $\delta \sim c/\omega_p$ and $\lambda = 100 - 800 \text{ nm}$ as considered in this thesis. To study high Z clusters (e.g., argon), we have further improved the MD code to include self-consistent ionization of atoms/ions assuming “over the barrier ionization (OBI)” model.

Chapter-3: Identification of anharmonic resonance absorption

In this chapter, the anharmonic resonance (AHR) absorption mechanism in a laser-driven pre-ionized deuterium cluster has been discussed and shown by using MD simulation and RSM. A linearly polarized, short 5-fs (fwhm) laser pulse of peak intensity $I_0 = 5 \times 10^{15} \text{ Wcm}^{-2}$ is considered. The size of the cluster is $R_0 = 2.05 \text{ nm}$, with number of neutral atoms $N = 1791$. By analyzing trajectories of individual MD electrons in the temporal domain and in the frequency versus energy plane and extracting their time-dependent frequencies $\Omega[r(t)]$ in the self-generated time-varying nonlinear plasma potential, we find that electrons become free from the cluster potential when the AHR condition is met, i.e., when $\Omega[r(t)]$ of an electron matches with the driving ω , i.e., $\Omega[r(t)] = \omega$. A simple RSM is also introduced to understand various features of AHR and also to corroborate the MD results.

Thus, in this chapter, the results with the MD approach and RSM analysis further prove that AHR process is a dominant collisionless mechanism of laser absorption in the short pulse regime of laser-cluster interaction. Present studies confirm the acceptance of AHR irrespective of the method of simulation that includes (i) a simple RSM, (ii) PIC simulation, and (iii) MD simulation (in the current work) for the first time.

Chapter-4: Dynamical resonance shift and unification of resonances

In this chapter, interactions of linearly polarized, short 5-fs (fwhm) laser pulses of different peak intensities $\sim 10^{15} \text{ Wcm}^{-2} - 10^{17} \text{ Wcm}^{-2}$ and $\lambda = 100 - 800 \text{ nm}$ with an argon cluster of $R_0 = 2.91 \text{ nm}$ are studied by the improved MD simulation including self-consistent ionization. We show an optimal regime of λ for the range of intensities $\sim 10^{15} \text{ Wcm}^{-2} - 10^{17} \text{ Wcm}^{-2}$ to attain maximum absorption of laser energy at a

given intensity and pulse energy. At this optimal condition, different absorption processes (LR and AHR) are shown to dynamically work together within a single short 5-fs (fwhm) pulse to maximize absorption. Our results reveal that, for a given peak intensity and a plasma density ρ , the efficient coupling of laser energy to cluster electrons does not happen at the well-known wavelength of linear resonance $\lambda_M = \lambda$; instead it happens at a red-shifted wavelength in the marginally over-dense regime of wavelength $\Lambda_d \approx (1 - 1.5)\lambda_M$ depending upon the percentage of the outer ionization that in turn depends on the field strength of the laser [24]. At this shifted band of Λ_d (typically lies in the ultra-violet regime), evolution of the cluster happens through very efficient unification of possible resonances in various stages, including (i) the LR in the initial time of plasma creation, (ii) the LR in the Coulomb expanding phase in the later time and (iii) anharmonic resonance (AHR) in the marginally over-dense regime for a relatively longer pulse duration below 5-fs (fwhm), leading to maximum laser absorption accompanied by maximum removal of electrons from cluster and also maximum allowed average charge states \bar{Z} of argon ions in the cluster. We termed this combined resonances as the unified dynamical linear resonance (UDLR) where ω_M is time-dependent. Increasing the laser intensity, the absorption maxima are found to shift further to a higher wavelength in the band of $\Lambda_d = (1 - 1.5)\lambda_M$ than staying permanently at the expected λ_M as in the nano-plasma model. In this marginally over-dense band of Λ_d , the unification of both AHR and dynamical LR is found to be more efficient than a longer $\lambda > 400$ nm due to significant time taken by the system near the LR during the rise of ω_M , where the system constantly experiences the near-LR enhanced effective field $E_{eff} \approx E_0/(\omega_M^2 - \omega^2)$ for a longer time. MD results are also justified by the simple RSM, where non-interacting electrons in a predefined potential of the ion sphere are driven by identical laser fields as in MD. The dependence of red-shift of the absorption

peak with different cluster size, different pulse type and also with carrier-envelope phase (CEP) of the laser pulse within the short 5 fs (fwhm) laser pulse has been reported by MD simulation. We conclude that there is always a redshift of the absorption peak with respect to λ_M in the marginally over-dense band of $\Lambda_d = (1 - 1.5)\lambda_M$ irrespective of laser intensity, cluster size, and pulse type. Also, it is confirmed by the MD simulation that the redshift is hardly affected by different CEPs for this short duration of the laser pulse.

Our results agree with the general observation from the nano-plasma model [9] that absorption peaks exist, but it is red-shifted in the band of $\Lambda_d \approx (1 - 1.5)\lambda_M$. It is perhaps misleading to look for the absorption maxima *exactly* at the λ_M in presence of non-zero outer ionization at higher intensities since linear Mie-resonance theory is invalid here. This new finding in laser atomic cluster study may be useful to guide an optimum control experiment in the short-pulse regime where maximum energy is required to transfer from laser-fields to charge particles and/or radiations.

Chapter-5: Dependence of red-shift of absorption peak on laser polarization, intensity, and wavelength for a deuterium cluster

In the previous chapter, we have restricted the study of UDLR for one type of atom (e.g., argon) and also for one degree of polarization, e.g., linear polarization. To justify and validate the above mentioned UDLR in the wavelength band of $\Lambda_d = (1 - 1.5)\lambda_M$, in this chapter, we have further extended our study for a different cluster type, i.e., deuterium (other than argon) for its universal acceptance and also explore the effect of laser polarization on the UDLR and the red-shift of the resonance absorption peak. For both linear polarization (LP) and circular polarization (CP) cases, we show that for a given intensity $< 10^{17} \text{ Wcm}^{-2}$ the optimized wavelength for maximum laser absorption in deuterium

cluster lies in the band of wavelengths $\lambda \approx 330 \pm 67$ nm instead of the commonly expected LR wavelength of $\lambda_M = 263$ nm. MD simulation and the RSM show gradual red-shift of the absorption maxima towards higher wavelengths in the marginally over-dense band of $\Lambda_d \approx (1 - 1.5)\lambda_M$ from λ_M of LR with increasing laser intensity; and for higher intensities $> 10^{17} \text{ Wcm}^{-2}$ absorption peak disappears as outer ionization saturates at 100% for both LP and CP. This disappearance of the resonance absorption peak should not be misinterpreted as the negligible (or no) role of Mie-resonance. In fact, in this marginally over-dense band of $\Lambda_d \approx (1 - 1.5)\lambda_M$, both AHR and dynamical LR with near-LR enhanced effective field $E_{eff} = E_0/(\omega_M^2 - \omega^2)$ contribute in unison very efficiently - UDLR happens - to maximize absorption and outer ionization for both LP and CP. It is also found that before the absorption peak, laser absorption due to LP and CP laser pulses are almost equally efficient (CP case being inappreciably higher than LP) for all intensities and λ . However, after the absorption peak, at lower intensities, absorption due to LP inappreciably dominates absorption due to CP with increasing λ which gradually reverses at higher intensities. Neglecting marginal differences for LP and CP cases, which may not be differentiated in real experiments, we conclude that laser absorption and outer ionization are almost same irrespective of the states of laser polarization for intensities $< 10^{17} \text{ Wcm}^{-2}$. Coulomb explosion of deuterium cluster is also found to be almost independent of the laser polarization. MD results are also supported by the RSM analysis as done in chap.4.

Chapter-6: Conclusions and future scope

This chapter presents a summary of the main results presented in this thesis and also explores several possible future directions.

List of Figures

1.1	Schematic of different ionization processes of an atom with ionization potential I_p	7
1.2	Schematic of a driven electron (filled red circle) inside the anharmonic potential (green curve)	16
2.1	Flowchart diagram of the MD scheme.	28
2.2	Initial Gaussian velocity distribution of neutral atoms	30
2.3	Illustration of the velocity Verlet integration scheme.	35
2.4	Results for single particle motion in a 2D harmonic potential	38
2.5	Results for non-interacting particles in a two dimensional harmonic potential $\frac{1}{2}\omega_p^2(x^2 + y^2)$	40
2.6	Results for multi-particle system interacting via Coulomb potential	42
2.7	FFT of the center of mass (CM) position co-ordinate of electrons of 2D slab geometry	44
2.8	Results for the deuterium cluster	47
2.9	FFT of the center of mass (CM) position co-ordinate of electrons for a deuterium cluster	48
3.1	Schematic of the rigid sphere model (RSM)	58
3.2	Normalized effective frequency Ω/ω of the electron sphere versus its excursion amplitude r_m for a deuterium cluster	62
3.3	RSM results of AHR for a deuterium cluster in the temporal domain	64
3.4	RSM results of AHR for a deuterium cluster in the frequency vs. energy plane	65

3.5	Total absorbed energy and fractional outer ionization versus the laser intensity for a deuterium cluster	69
3.6	Normalized self-generated space-charge field ($E^{sc}(t)/E_0$) and normalized total field ($E_t(t)/E_0$) versus normalized excursion $x(t)/R$	71
3.7	MD results of AHR for a deuterium cluster in temporal domain	72
3.8	MD results of AHR for a deuterium cluster in frequency vs. energy plane	74
4.1	RSM results of resonance shift with intensity variation for different \bar{Z} .	84
4.2	RSM results of resonance shift with intensity variation for fixed \bar{Z} . . .	86
4.3	Temporal variation of normalized Mie-frequency $\omega_M(t)/\omega$, for the argon cluster	91
4.4	Typical Coulomb explosion scenario for the Argon cluster corresponding to MD results	94
4.5	MD results for dynamical resonance shift for an argon cluster	96
4.6	Temporal analysis of dynamical resonance shift	99
4.7	MD results of resonance shift with continuous short laser pulses	104
4.8	MD results of resonance shift with cluster size variation	106
4.9	MD results of resonance shift with different CEPs	108
5.1	MD results for dynamical resonance shift for a deuterium cluster with LP laser	116
5.2	MD results showing average kinetic energy $\overline{\mathcal{E}}_k$ per electron versus λ at $I_0 = 5 \times 10^{17} \text{Wcm}^{-2}$	118
5.3	MD results of resonance shift with cluster radius variation for a fixed charge density of deuterium cluster	121
5.4	Comparative MD results for a deuterium cluster with LP vs. CP laser . .	123

5.5	Comparison of temporal variation normalized Mie-frequency $\omega_M(t)/\omega$, (b) total absorbed energy $\overline{\mathcal{E}}_t$ per atom, and (c) fractional outer ionization of electrons \overline{N} for LP and CP lasers	127
5.6	RSM results for absorption and outer ionization with CP vs LP laser . .	129

List of Tables

2.1	Parameters for verification of plasma frequency in a 2D slab geometry. .	41
2.2	Parameters used to study Mie-plasma oscillation for deuterium cluster. .	46
2.3	Ionization potential and corresponding threshold intensity of the deuterium atoms/ions.	51
2.4	Ionization potentials and corresponding threshold intensities of the argon atoms/ions.	51
A.1	SI units of various physical quantities, which is related to 1 atomic unit of the corresponding quantity.	138
A.2	Comparison between different parameters for a deuterium cluster and an argon cluster containing the same number of atom $N = 1791$. For laser pulse of wavelength $\lambda = 800$ nm, the critical density is defined as $\rho_c = 1.75 \times 10^{27} m^{-3}$	138

1

Introduction

In this chapter, we give an overview of the interaction of strong ultra-short laser fields with atomic clusters, important physical processes related to the laser-cluster interaction and its various applications. This chapter also contains a comprehensive review of previous theoretical modelling, experimental and simulation studies on laser-cluster interaction relevant to this thesis, followed by the motivations behind the present studies. It also highlights the importance of present studies in the field of laser-plasma interaction as far as collisionless absorption processes are concerned. Finally, a brief outline of the remaining chapters of the thesis is given.

1.1 Introduction and overview

In the past few decades, there has been a rapid progress in ultra-high intensity short-pulse laser technology. At present, laser intensity higher than 10^{21} Wcm^{-2} and with durations on the femtosecond and even attoseconds time scale are available in the laboratories [25–27]. This technological development of high power laser has facilitated the understanding of the behaviour of matter under the influence of intense short laser pulses. Extensive studies on laser-matter interactions have been performed on the atomic targets in low density ($< 10^{19} \text{ atoms/cm}^3$) gas phase [27, 28] and in high density ($\sim 10^{23} \text{ atoms/cm}^3$) solid phase [29–31]. The gas phase atoms under intense laser pulse produce electrons and ions with low energies, therefore are considered as poor absorbers of laser light. On the other hand, the interaction of high power lasers with solid targets creates a high density plasma and a significant fraction of the laser energy can be deposited into the solid density plasma due to subsequent interactions with the laser pulse which successfully produce energetic charge particles in the MeV energy range [32]. However, since only a portion of solid target is irradiated by the laser, heat is conducted to the cold bulk. Therefore, the absorbed laser energy can not be fully utilized for accelerating charge particles in laser-solid interactions.

In the intermediate regime between solid and gas phases, an atomic cluster combining the advantage of both solid and gaseous properties [33] has been shown to act as a unique target for high energy particle generation. Therefore, the interaction of laser with atomic cluster has been the topic of considerable interest since early nineties [34–37]. These clusters are actually finite aggregate of atoms or molecules bound together via Van der Waals forces. Experimentally clusters can be formed by an adiabatic expansion of a certain gas into the vacuum chamber through a supersonic nozzle. Adiabatic

expansion of the gas leads to sudden cooling and then results in condensation into clusters. The size distribution and number density of clusters is experimentally determined by controlling the backing pressure, temperature, nozzle geometry, and other experimental factors [38]. Under specific conditions of pressure and temperature, cluster size may vary from sub-nanometer to a few tens of nanometers. In an experimental system, the average atomic density of a cluster is low, typically on the order of the gas density $\sim 10^{17} - 10^{19} \text{ cm}^{-3}$, while its local atomic density is close to the solid density $\sim 10^{22} - 10^{23} \text{ cm}^{-3}$. The localized solid-like atomic density of a cluster and its smaller size as compared to laser wavelengths λ (typically longer than 100 nm) allow full penetration of the laser field into the cluster nano-plasma (immediately formed after the ionization of atoms of the cluster by the laser field) without any attenuation, in contrast to the case of laser interaction with a solid target of thickness on the order of microns (e.g., thin foils). Therefore, laser-driven clusters are shown to be very efficient absorbers of laser light (almost 90% absorption has been reported in the experiment [1]) as compared to isolated atoms, gas phase atoms and traditional solid targets, when they are irradiated by the same laser pulse. The efficient coupling of laser light leads to the production of energetic KeV electrons [2–4], MeV ions (useful for driving fusion reaction with deuterium cluster plasma) [1, 2, 5, 6], generation of x-rays [7], high order harmonics [39–41], and MeV neutrals [8] in experiments. High neutron yield also have been found from fusion reaction in deuterium clusters [42–44]. Therefore, clusters irradiated with strong laser pulses can serve as efficient table-top radiation sources of x-rays, energetic KeV electrons, MeV ions, and MeV neutrals. The energetic electrons and ions from laser irradiated clusters can be used in biological imaging as well as medical therapies. One important example would be proton beam radiation therapy for cancer treatment.

The experimental observation of unexpectedly high ionic charge states for rare gas clusters, energetic ions and energetic electrons above the energy of a free electron (known as ponderomotive energy) in the same laser field indicates a high degree of non-linear response of electrons involved in the laser-cluster interaction process. Therefore, to explain the above experimental findings and to investigate various laser-cluster interaction processes, it is *important* to understand different absorption mechanisms by electrons for the extraordinary laser absorption in clusters.

The goal of the research presented in the present thesis is to study the laser energy absorption to the cluster electrons using molecular dynamics (MD) simulations. In particular, our focus is to study the collision-less resonance absorption processes which includes both linear resonance (LR) and anharmonic resonance (AHR) which are frequency dependent phenomena and depend on the system's eigenfrequency and the driver's (here laser) frequency. Further we study dependency of resonance absorption on different laser and cluster parameters (i.e., peak intensity, wavelength, laser polarization, cluster size and type etc.). In Sec. 1.2, we introduce different atomic processes, preliminary theoretical concepts useful for laser-cluster interaction. Sec. 1.3 summarizes the plan of the thesis.

1.2 Clusters in intense laser fields

The interaction of strong laser fields with atomic nano-clusters comprises a wide range of physical phenomena, e.g., inner ionization, energy absorption, outer ionization, and cluster expansion. In a simplified picture, the dynamics of the laser-cluster interaction may be summarized as follows. The leading edge of the laser pulse ionizes the constituent atoms and creates free electrons within the cluster (called *inner ionization*). Subsequent interactions lead to absorption of laser energy by electrons and removal of

those energetic electrons from the time-dependent cluster potential (called *outer ionization*). As an electron crosses the cluster boundary or leaves the cluster completely, a local electrostatic (ES) field due to charge non-neutrality is developed. This ES field together with the laser field may lead to further inner ionization (called *ionization ignition* [15]) and creation of higher charge states which are forbidden by the laser field alone. Subsequent outer ionization of electrons leaves the cluster with a net positive charge which explodes due to inter-ionic Coulomb repulsion (*cluster expansion*).

We first discuss various inner ionization mechanisms of a cluster, exposed to intense laser fields in Sec. 1.2.1. We discuss ionization ignition and collisions between electron and ion (inverse bremsstrahlung) in Sec. 1.2.2 and Sec. 1.2.3 respectively. Then we discuss the mechanism of energy absorption in Sec. 1.2.4, followed by a complete discussion of different cluster expansion models in Sec. 1.2.5.

1.2.1 Ionization of atoms/ions in a cluster by laser field

In order to understand inner ionization of atoms/ions in a cluster, one should first consider ionization of single atom under an intense laser pulse. The same concept of ionization mechanism can then be applied to a cluster which consists of N number of atoms. The ionization of an atom by the laser field (also called as optical field ionization (OFI)) can take two different routes depending on the laser intensity and frequency: (i) multi-photon ionization (MPI) and (ii) tunnel ionization (TI) which are distinguished by the Keldysh parameter γ [45] defined as,

$$\gamma = \sqrt{\frac{I_p}{2U_p}}, \quad (1.1)$$

Chapter 1. Introduction

where I_p is the ionization potential of an atom and U_p is the pondermotive energy of an electron which is the cycle average of the electron's kinetic energy in a linearly polarized oscillating laser field given by,

$$U_p(\text{eV}) = \frac{1}{2}m_e\langle v_e^2 \rangle = \frac{e^2 E_0^2}{4m_e \omega^2} = 9.33 \times 10^{-14} I_0 (\text{Wcm}^{-2}) \lambda^2 (\mu\text{m}^2). \quad (1.2)$$

Here e , m_e , and v_e are electron charge, mass, and velocity respectively. E_0 is the electric field amplitude of the laser of intensity I_0 , wavelength λ and frequency ω . The MPI regime [46–53] is defined for $\gamma > 1$ and the TI regime [45, 52–55] is defined for $\gamma < 1$. Figures 1.1(a)-(d) present the schematic of different ionization processes for an atom by the laser field, which are briefly discussed below.

1.2.1.1 Multiphoton ionization (MPI)

Multiphoton ionization (MPI) process is a dominant ionization process for lower laser intensities $< 10^{13} \text{Wcm}^{-2}$, where ponderomotive potential (U_p) is much smaller than the photon energy ($\hbar\omega$) and the ionization potential. In MPI, a bound electron of an atom absorbs more than one photon from the incident laser field and acquires enough energy higher than the ionization potential of the atom to escape into the continuum (Fig. 1.1(a)). MPI can be modelled by lowest order perturbation theory [46, 49, 50, 52, 53, 56], and in this case the ionization rate is defined as,

$$W_n = \sigma_n I^n, \quad (1.3)$$

where n is the number of photons required for ionization, σ_n is the generalized multiphoton ionization cross section, and I is the incident laser intensity.

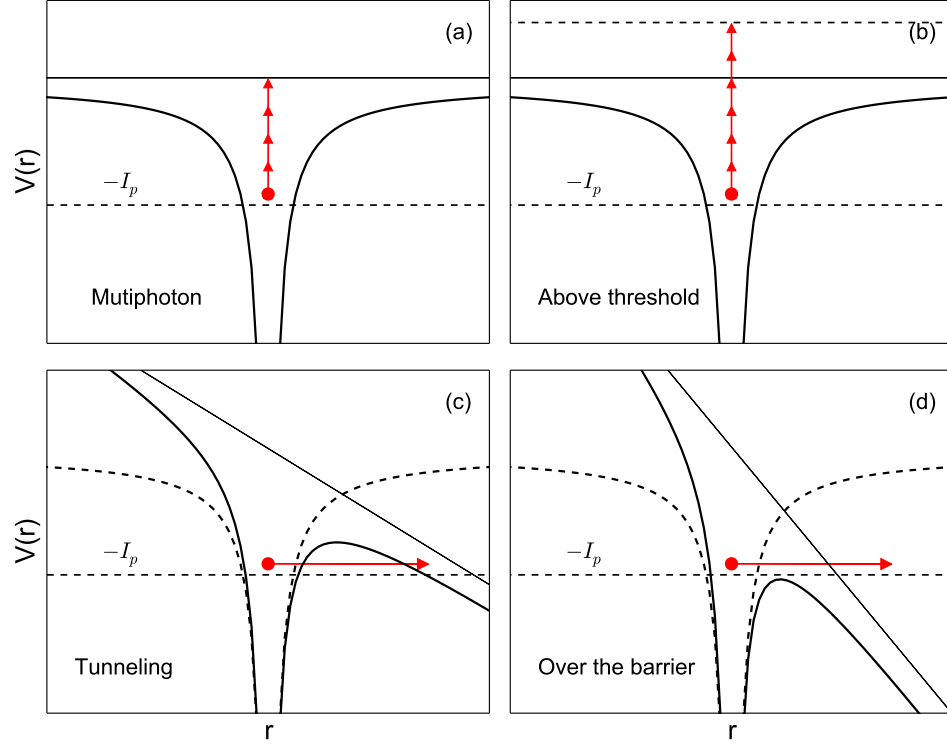


Figure 1.1: Schematic of different ionization processes of an atom with ionization potential I_p . (a) Multiphoton ionization (MPI): A bound electron overcome the potential barrier by absorbing required number of photons to overcome the potential barrier and escapes to the continuum with lower kinetic energy. (b) Above threshold ionization (ATI): A bound electron overcome the potential barrier by absorbing more photons than required to overcome the potential barrier and escapes to the continuum with higher kinetic energy. (c) Tunnelling ionization (TI): In the intermediate laser intensities the electric field bend the potential barrier but still the barrier remains above the ionization level and in that case the bound electron can tunnel through the resulting barrier into the continuum. (d) Over-the-barrier ionization (OBI): In the very strong laser field, the electric field bend the barrier below the ionization level and electron can directly escape to the continuum.

1.2.1.2 Above threshold ionization (ATI)

Experimentally it has been observed that, an electron can sometimes absorbs more photons from the incident laser field than the required minimum to overcome the binding potential and it can be released with a higher kinetic energy (Fig. 1.1(b)). This excess-

Chapter 1. Introduction

photon ionization is known as “above threshold ionization” (ATI) [52, 57–63]. The ATI ionization rate follows similar form as Eq. (1.3),

$$W_{n+s} = \sigma_{n+s} I^{n+s}, \quad (1.4)$$

where s is the excess number of photons absorbed by the electron above the threshold of n photons (the required minimum). The excess kinetic energy carried by the electron after ATI can be written from the modified Einstein’s photoelectric effect equation as,

$$K.E. = (n + s)\hbar\omega - I_p. \quad (1.5)$$

1.2.1.3 Tunnel ionization (TI)

In the intermediate laser intensities $10^{14} \text{ Wcm}^{-2} \leq I \leq 10^{15} \text{ Wcm}^{-2}$, the laser electric field is strong enough to distort the atomic potential and the bound electron can tunnel through the resulting barrier into the continuum (see Fig. 1.1(c)). This mechanism is called as tunnel ionization (TI), which is a semi-classical process and the interaction is non-perturbative. The transition from multiphoton to tunnelling ionization takes place when $\gamma \approx 1$. The ionization rate of TI can be described by semi-classical approach through Ammosov-Delone-Krainov (ADK) formula [55],

$$W_t = \omega_a \frac{(2l+1)(l+|m|)!}{2^{|m|}|m|!(l+|m|)!} \left(\frac{2e}{n^*}\right)^{n^*} \frac{I_p}{2\pi n^*} \times \left(\frac{2E}{\pi(2I_p)^{3/2}}\right)^{1/2} \left(\frac{2(2I_p)^{3/2}}{E}\right)^{2n^*-|m|-1} \\ \times \exp\left[-\frac{2(2I_p)^{3/2}}{3E}\right]. \quad (1.6)$$

Here, ω_a is the atomic unit of frequency ($\omega_a = 4.13 \times 10^{16} \text{ s}^{-1}$), l and m are the orbital and magnetic quantum number of the tunnelling electron, n^* is the effective principal

quantum number ($n^* = Z[2I_p(eV)]^{-1/2}$), E and I_p are the laser field and the ionization potential for a given charge state Z respectively in atomic units.

1.2.1.4 Over the barrier ionization (OBI)

In the TI regime, the barrier is not sufficiently lowered, i.e, the initial electron energy level is still below the barrier. If the laser intensity is increased further ($I \geq 10^{15} \text{ Wcm}^{-2}$) and exceeds a certain critical value, the laser field can lower the atomic potential even further so that the barrier is fully suppressed below the energy level of the electron, and the electron can escape to the continuum directly without tunnelling, which is schematically shown in Fig. 1.1(d). This ionization mechanism which occurs above the barrier is called as over-the-barrier (OBI) ionization [52, 63–65]. The critical field strength and the corresponding intensity above which OBI occurs can be calculated from the net effective atomic potential [64] (in a.u.),

$$V(r) = -\frac{Z}{r} - Er. \quad (1.7)$$

The effective force $\sim \partial V / \partial r$ vanishes at the turning point $r = r_{\max} = \sqrt{Z/E}$, where effective potential is $V_{\max} = V(r_{\max}) = -2r_{\max}E = -2\sqrt{ZE}$. Equating V_{\max} with $I_p(Z)$, we obtain the critical laser field for OBI (in a.u.) as,

$$E_c = I_p^2(Z)/4Z. \quad (1.8)$$

The corresponding critical laser intensity $I_c = \frac{1}{2}\epsilon_0 c E_c^2$ reads (in a.u.),

$$I_c = \left(\frac{c}{8\pi}\right) \frac{I_p^4}{16Z^2}. \quad (1.9)$$

1.2.2 Ionization of cluster by space-charge field : Ionization ignition

Ionization ignition model was first proposed by Rose-Petruck et al. [15] to explain the unexpectedly higher charge states of ions inside a laser-driven cluster as compared to the situation where the same laser is focused into a single atom. Initially free electrons are created inside the cluster by any of the ionization mechanisms described above depending upon the laser intensity and also the photon energy. These inner ionized electrons are then governed by the oscillating laser field and some of them are outer ionized, which results an additional electric field within the cluster due to the charge imbalance. The combined effective field of the laser and the space charge field may further increase inner ionization rate inside the cluster, thus the name “ionization ignition”. Various studies [17, 66, 66–71] in laser-cluster interaction clearly mention the importance of this mechanism. However, this ionization ignition rate can be hampered in presence of excessive trapped electrons inside the cluster, because they shield the laser field and reduce the inner ionization rate [9, 37, 39, 70–73]. Therefore, the relative importance of ionization ignition and shielding depends on the percentage of inner ionization and outer ionization. The shielding of laser field is maximum at the center of the cluster as compared to the surface, which results higher charge states of ions at the cluster boundary than the ions at the cluster center [70, 71].

1.2.3 Ionization of a cluster by electron-ion collision

All the ionization mechanisms described above are important in the early stage of the laser pulse interacting with a cluster which form a nano-plasma having density nearly equal to the solid density $\sim 10^{23} \text{ cm}^{-3}$. This high electron density (n_e) inside the cluster allows further increase of the level of ionization through inelastic collisions between

electrons and ions. The collisional ionization rate average over all collisions, can be calculated from the empirical formula, given by Lotz [74, 75],

$$W_{ci} = n_e \overline{v_e \sigma_i}, \quad (1.10)$$

where v_e is electron velocity and σ_i is the collisional ionization cross-section defined as,

$$\sigma_i = a_i q_i \frac{\ln(K_e/I_p)}{K_e I_p}. \quad (1.11)$$

Equation (1.11) is valid for large kinetic energy (K_e) of the projectile electron compared to the ionization potential of the target ion, $K_e > I_p$. Here a_i is an empirical constant $4.5 \times 10^{-14} \text{ eV}^2 \text{ cm}^2$, q_i is the number of electrons in the outer shell of the ion. Separating the contribution due to the thermal motion of the projectile electron and its laser driven motion we can write Eq. (1.10) as,

$$W_{ci} = W_{ci}^{KT} + W_{ci}^{las}, \quad (1.12)$$

where W_{ci}^{KT} and W_{ci}^{las} individually satisfy Eq. (1.10). To calculate the ionization rate W_{ci}^{KT} by thermal electrons in the cluster, a Maxwellian electron distribution is assumed which obeys [76],

$$\frac{dn_e}{n_e} = \frac{2}{kT_e} \left(\frac{K_e}{\pi kT_e} \right)^{1/2} \exp(-K_e/kT_e) dK_e \quad (1.13)$$

where k is Boltzmann constant, and T_e is electron temperature. Using Eq. (1.11) and Eq. (1.13) we obtain,

$$\begin{aligned}
 W_{ci}^{KT} &= 2n_e a_i q_i \int_{I_p}^{\infty} \sqrt{\frac{2}{\pi(kT_e)^3}} \frac{\ln(K_e/I_p)}{I_p} \exp(-K_e/kT_e) dK_e \\
 &= n_e \frac{a_i q_i}{I_p (kT_e)^{1/2}} \int_{I_p/kT_e}^{\infty} \frac{e^x}{x} dx.
 \end{aligned} \tag{1.14}$$

The ionization rate W_{ci}^{las} due to electrons driven by the laser field is calculated again from the Lotz formula (Eq. (1.11)) as [9],

$$W_{ci}^{las} = n_e \overline{v_e} \sigma_i = n_e \sigma_i \frac{E_0}{\omega} |\sin(\omega t)|, \tag{1.15}$$

where $v_e = \frac{E_0}{\omega} \sin(\omega t)$ is the velocity of the electron in a linearly polarized laser field $E = E_0 \cos \omega t$. The cycle average rate of the ionization over one laser period T is,

$$W_{ci}^{las} = \frac{2n_e}{\pi} \int_{\tau_i}^{\pi/2} \sigma_i \frac{E_0}{\omega} \sin(\tau) d\tau, \tag{1.16}$$

where $\tau = \omega t$ and $\tau_i = \omega t_i$ is the time at which energy of the projectile electron becomes I_p . Noting that $K_e = 2U_p \sin^2 \tau$, one obtain W_{ci}^{las} as,

$$W_{ci}^{las} = n_e \frac{a_i q_i}{\pi I_p} \frac{1}{\sqrt{U_p}} \int_{I_p}^{2U_p} \frac{\ln(K_e/I_p)}{K_e I_p} \frac{dK_e}{\sqrt{1 - K_e/2U_p}}. \tag{1.17}$$

Collisional ionization is relatively unimportant in the ionization of small clusters [17, 70, 73]. However, the contribution of collisional ionization increases with increase in cluster size and pulse width, but decreases with increase in laser intensity. In this thesis we neglect collisional ionization and only consider the ionization due to the laser field and the effect of neighbouring ions (ionization ignition). Since the intensity regime considered in this thesis is above 10^{15} Wcm^{-2} , OBI mechanism is chosen in the molecular dynamics simulations described in Chapter 2 (see Sec. 2.9).

1.2.4 Laser energy absorption mechanisms in a cluster

It is known that coupling of laser energy to cluster electrons is very efficient which is one of the prominent features of laser-cluster interaction. Therefore, investigation of underlying physical processes is very much important. Various mechanisms and models have been proposed earlier to understand the laser absorption processes in plasmas including inverse bremsstrahlung heating (collisional heating), vacuum heating, $\vec{J} \times \vec{B}$ heating and resonance absorption which are briefly described below, since some of the processes are also relevant to laser-cluster interactions.

1.2.4.1 Inverse bremsstrahlung

A free electron oscillating in the laser field does not gain energy directly from the field. But, in a plasma due to the presence of ions, electron's motion is perturbed by the collision with the ions and thereby transfers laser energy into thermal energy of the electron during its scattering in the Coulomb field of the ions. This absorption mechanism is called as inverse bremsstrahlung (or collisional heating) [77–79], which is considered in various works [9, 35, 72, 80–83] in the context of laser-cluster interaction.

The electron-ion Coulomb collision frequency ν_{ei} [35, 84] is determined by the Rutherford formula integrated over the scattering angle, which reads (in atomic units)

$$\nu_{ei} = \frac{4\sqrt{2}\pi Z n_e}{3T_e^{3/2}} \ln \Lambda. \quad (1.18)$$

Here, $\ln \Lambda$ is the standard Coulomb logarithm, which has values in the range of 10 – 20 [85]. Equation (1.18) is valid in the low frequency regime ($\nu_{ei} \ll \omega$), i.e., when thermal electron energy (T_e) is greater than the pondermotive energy U_p of the electron oscillating in the laser field of strength E_0 . In the high frequency regime ($\nu_{ei} \gg \omega$), the

electron oscillation velocity under the action of the laser field is appreciably larger than its thermal velocity (i.e., $T_e < U_p$) and v_{ei} given by [86],

$$v_{ei} = \frac{16ZN_e\omega^3}{E_0^3} \ln\Lambda. \quad (1.19)$$

We can see that v_{ei} depends on n_e , T_e , E_0 , ω . In the interaction of super-intense laser pulses with atomic cluster, inverse bremsstrahlung is important for high n_e and low T_e . However, due to $v_{ei} \sim E_0^{-3}$, at high laser intensities, collisional absorption process is ineffective and can be neglected [13, 87, 88].

1.2.4.2 Vacuum heating

“Vacuum heating” is a collisionless laser energy absorption mechanism initially proposed by Brunel for the case of laser-solid interaction, also called as Brunel heating [89–92]. According to Brunel’s original proposition [89], when an intense laser field obliquely incident on a sharply bounded overdense plasma; electrons are dragged in to the vacuum and then due to the laser field reversal, in the next half-cycle of the pulse, electrons are pushed back inside the target with a velocity on the order of the ponderomotive velocity $v_0 = E_0/\omega$. When transition time of emerging electrons across the target matches the laser period, a substantial fraction energy from the laser field is absorbed. In laser-irradiated clusters “vacuum heating” mechanism is used in many works [12, 93–96] to describe the laser energy absorption, which is not well justified and remains to be a debate for a few nanometer size clusters. We shall discuss more on this in chapter 3.

1.2.4.3 $\vec{J} \times \vec{B}$ heating

When the laser intensity becomes very high $> 10^{18} \text{ Wcm}^{-2}$, the ponderomotive velocity $v_o = E_0/\omega$ of an electron becomes comparable to speed of light c and the electron mo-

tion becomes relativistic. In this relativistic regime of intensity, the magnetic field of the laser \vec{B} significantly influences the electron's trajectory by the Lorentz force component $\vec{v}_e \times \vec{B}$ and the electron is accelerated by gaining large amount of energy from the laser. This mechanism is known as $\vec{J} \times \vec{B}$ heating mechanism [97]. This mechanism is discriminated in this thesis by restricting the laser intensity below 10^{18} Wcm^{-2} , where laser magnetic field is $|B(t)| \approx |E(t)|/c \ll 1$ and can be neglected.

1.2.4.4 Resonance absorption

Among the various collisionless absorption mechanisms (e.g., vacuum heating, $\vec{J} \times \vec{B}$ heating described before), resonance absorption is a very well known process in case of laser-plasma interaction [31]. A bulk plasma of charge density $\rho = Zn_i$ has a natural frequency of oscillation which is called as plasma frequency $\omega_p = \sqrt{4\pi\rho}$ [85]. If we excite the plasma with an external laser field of frequency ω , then resonance occurs when $\omega_p = \omega$ called as linear resonance (LR). This effect can greatly enhance the laser energy coupling to the plasma electrons. In the case of a finite size spherical cluster, the natural frequency of the collective oscillation of the electrons cloud is known as the Mie-plasma frequency $\omega_M = \omega_p/\sqrt{3}$ (with corresponding Mie-plasma wavelength λ_M) and in this case LR occurs when $\omega_M = \omega$ (or $\lambda_M = \lambda$). The initial charge density of the cluster after the optical field ionization (OFI) remains much above the critical charge density $\rho_c = \omega^2/4\pi$ (i.e., plasma remains over-dense with $\omega_M > \omega$ for $\lambda = 800 \text{ nm}$). When the cluster expands in the later time, the ionic charge density of the cluster drops and at a certain time it will pass through the LR condition $\omega_M = \omega$, which occurs after a long time (typically $> 50 \text{ fs}$) during the Coulomb expansion phase for 800 nm laser. This LR mechanism was first proposed for large clusters by Ditmire et al [9] through a hydrodynamic model of the laser-cluster interaction, called as “nanoplasma model”.

For this resonance absorption, electric field is resonantly enhanced inside the cluster and the electrons gain enormous energy from this strong electric field. Thus, LR during the cluster expansion is often considered as the primary mechanism behind efficient coupling of laser energy to cluster electrons. The importance of this LR mechanism in the Coulomb expanding phase of the cluster has also been experimentally demonstrated in pump-probe technique [9–11, 98].

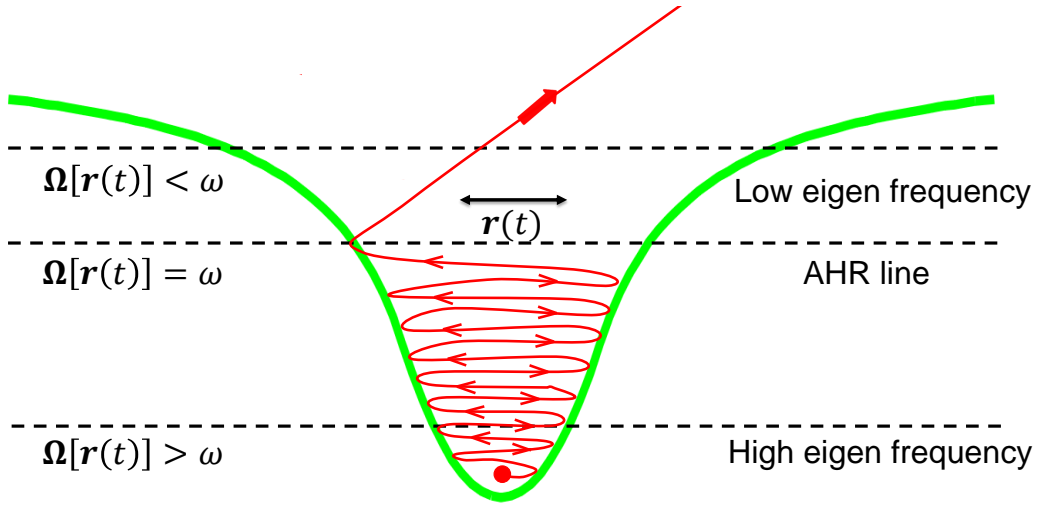


Figure 1.2: Schematic of a driven electron (filled red circle) inside the anharmonic potential (green curve). In the bottom potential, the oscillation frequency $\Omega[r(t)]$ of the electron is very high as compared to the laser frequency ω (i.e., $\Omega[r(t)] > \omega$). As the electron is driven up in the potential, its excursion amplitude increases and $\Omega[r(t)]$ gradually decreases. If $\Omega[r(t)]$ matches with ω (shown by AHR line), then AHR occurs and electron leaves the cluster by absorbing energy from the laser.

However, for a short laser pulse duration < 15 fs or early time of a long laser pulse, background ions remain relatively frozen and ω_M remains much above the laser frequency ω for $\lambda > 400$ nm. In this regime, an electron may pass through anharmonic resonance (AHR) when its dynamical frequency $\Omega[r(t)]$ in the anharmonic potential

gradually decreases and finally meets the driving ω [14, 99]. Schematically it is shown in Fig. 1.2 and explained in its caption. The role of AHR as a dominant collisionless process in the case of laser-cluster interaction is also established by theory [13, 87, 100] and particle-in-cell (PIC) simulations [12, 14, 93, 99]. AHR also finds its place for laser absorption in over-dense structured targets [101, 102]. One of the goals of this thesis is to re-examine AHR through molecular dynamics (MD) simulation, which is described in chapter 3 and also in Ref. [21].

1.2.5 Cluster expansion processes

Expansion of a cluster, happening during or after the laser pulse, mainly categorized as hydrodynamic expansion and Coulomb expansion [35]. Hydrodynamic expansion occurs due to the force associated with the hot electrons present in the cluster. These hot electrons expand and drag the cold and heavy ions outward with them [9, 103]. However, Coulomb expansion is driven by repulsive Coulomb forces between ions as soon as some of the electrons are outer ionized leaving behind some bare ions [43, 104–106]. Therefore, one can say the relative importance of these two different expansion mechanisms depend on the number of inner electrons and outer electrons during the interaction, which in turn depend upon the laser intensity and cluster size. Now, we will separately discuss both these cluster expansion mechanisms in brief.

1.2.6 Hydrodynamic expansion

For large and high Z clusters, if the impinging laser pulse is not strong enough to remove the electrons out of cluster, then the interior of the cluster can essentially be treated as a quasi-neutral nano-plasma. The temperature T_e of these trapped electrons significantly increases due to collisional heating. The electrons inside the nano-plasma expand which

Chapter 1. Introduction

simultaneously drag the cold ions outward with them, thus the cluster expands hydrodynamically. The hydrodynamic pressure P_e of hot electrons of temperature T_e and number density n_e inside the cluster may be determined by the ideal gas law (in a.u.),

$$P_e = n_e T_e, \quad (1.20)$$

and the rate of hydrodynamic expansion of the cluster is given by [35],

$$\left(\frac{dR}{dt}\right)^2 = \frac{3T_{e0}(Z - Q/N)}{M_i} \left[1 - \left(\frac{R_0}{R}\right)^2\right]. \quad (1.21)$$

Here M_i is the mass of an ion, R_0 and T_{e0} are the initial cluster radius and the initial electron temperature respectively. It can be shown that $T_e = T_{e0}(R_0/R)^2$ [35]. The above rate equation (1.21) assumes saturation of inner and outer ionization, Z is the average ion charge of $N = n_i V$ ions, with n_i as the ion number density inside volume V . If Q number of electrons are outer ionized, then the net electron density becomes $n_e = n_i(Z - Q/n_i V) = n_i(Z - Q/N)$. In the limit when $R \rightarrow \infty$, the cluster expands with a constant speed which is equal to the ion plasma sound speed $C_s = \sqrt{3T_{e0}(Z - Q/N)/M_i}$ [35]. By solving Eq. (1.21) we may find the characteristic time t_e for a cluster to double its initial radius R_0 as (in a.u.):

$$t_e = R_0 \sqrt{\frac{M_i}{Z T_e}}. \quad (1.22)$$

The typical time scale for hydrodynamic expansion lies in picoseconds. For example, assuming a deuterium cluster of $Z = 1$, $M_i = 2 \times 1836m_e$, $T_e = 100$ eV and $R_0 = 10$ nm, the time required to double its radius is found to be $t_e = 0.15$ picoseconds.

1.2.7 Coulomb expansion

Coulomb explosion occurs for both large and small clusters. If the intensity of the impinging laser pulse is strong enough, then the laser quickly remove all or few of the electrons out of the cluster much faster than the ions are able to move. Ideally, if all the electrons are outer ionized, then the cluster explodes due to repulsive Coulomb forces between the ions. The rate of Coulomb expansion of the ion sphere with total charge $Q_p = NZ$ and total mass $M_p = NM_i$ is given by [35] (in a.u.),

$$\frac{M_p}{2} \left(\frac{dR}{dt} \right)^2 = Q_p^2 \left(\frac{1}{R_0} - \frac{1}{R} \right) \quad (1.23)$$

Assuming the initial conditions $R(t_0) = R_0$, $\dot{R}(t_0) = 0$, solution for Eq (1.23) is given by,

$$t = t_0 + \sqrt{\frac{M_p R_0^3}{2Q_p^2}} \left(\sqrt{p^2 - p} + \ln(\sqrt{p} + \sqrt{p-1}) \right), \quad (1.24)$$

where, $p = R(t)/R_0$ is the expansion ratio of the cluster and t is the time needed to increase the radius of the cluster from R_0 to R . The time required for the cluster to expand to twice (i.e., $p = R(t)/R_0 = 2$) is found to be [35],

$$t = 1.6 \sqrt{\frac{M_i R_0^3}{NZ^2}}. \quad (1.25)$$

Assuming $R_0 = r_\omega N^{1/3}$ (r_ω is the Wigner-Seitz radius of the cluster) [35], we can write Eq. (1.25) as, $t = 1.6 \sqrt{M_i r_\omega^3 / Z^2}$. Therefore, Coulomb explosion time for a cluster depends on the ion mass and the ion charge, However, it does not depend on the initial cluster radius (R_0). For example, assuming a deuterium cluster with $Z = 1$, $M_i = 2 \times 1836m_e$ and $r_\omega = 0.17$ nm, one can obtain the time required for the deuterium cluster to

double the radius $t = 13.6$ femtoseconds. The electrostatic energy $\mathcal{E}_c = Q_p^2/2R$ stored in the cluster [9] can be used to obtain the Coulomb pressure $P_c = (\mathcal{E}_c/R)/4\pi R^2$, i.e., the force per unit area as:

$$P_c = \frac{Q_p^2}{8\pi R^4}. \quad (1.26)$$

One can see from Eq. (1.26) that the Coulomb pressure scales with the cluster radius as $\sim 1/R^4$, while hydrodynamic pressure scales as $\sim 1/R^3$ (through N_e , see Eq. (1.20)). Therefore, P_c decreases more rapidly during the cluster expansion than P_e . Coulomb pressure is thus more important for smaller clusters.

1.3 Plan of the thesis

The aim of the thesis is to study collisionless laser energy absorption processes (LR and AHR) in the short-pulse regime and their dependency on different laser and cluster parameters, i.e., peak intensity, wavelength, pulse duration, laser polarization, cluster size and cluster type etc. To this end, we have developed a three dimensional MD simulation code with soft-core Coulomb interaction among charged particles which we describe in detail in chapter 2.

In the first problem, we identify the anharmonic resonance (AHR) absorption by 3D-MD simulation and a non-linear oscillator model, called rigid sphere model (RSM). AHR occurring in an anharmonic potential was studied before for a laser-driven atomic clusters using particle-in-cell (PIC) simulations and models [12–14]. However, it is not rigorously verified so far by other first principle methods e.g., molecular dynamics (MD) simulation, although there are plenty of MD simulations [15–20] exist in different domains of laser-driven clusters. In this thesis, we clearly identify the AHR process as a dominant collisionless absorption mechanism in an over-dense deuterium cluster

irradiated by an ultra-short laser pulse through our MD simulation code for the first time. We show that electrons become free from the cluster potential when the AHR condition is met, i.e., when $\Omega[r(t)]$ of an electron matches with the driving ω , i.e., $\Omega[r(t)] = \omega$, explained in chapter 3 in detail.

In the next problem, we report the effect of laser wavelength on the resonance absorption with short laser pulses. The particular focus is given to find out an optimal regime of laser wavelength for maximum laser energy absorption. It is very trivial from the famous nano-plasma model [9] that for a laser-heated cluster, maximum energy transfer from the driver to the oscillatory electrons happens exactly at the linear resonance condition (the nanoplasma resonance) $\omega_M = \omega$ in the absence of other dissipation channels. However, there are some MD simulations of laser-heated clusters [19, 22, 23], which contradict this perception and the role of above LR was denied without satisfactory physical explanation. Their contradictory results of LR should be re-examined in order to have a clear understanding of this physical phenomena. However, we find that for a given laser intensity, maximum laser absorption does not occur at the linear resonance wavelength $\lambda_M = \lambda$ (or frequency $\omega_M = \omega$), instead it is red-shifted in the regime of $(1 - 1.5)\lambda_M$. In this shifted band of wavelength, both LR and AHR absorption are shown to be dynamically unified leading to maximum absorption for a laser-heated cluster. We term this regime of combined resonances as unified dynamical linear resonance (UDLR) which is explained in chapter 4 in detail.

In chapter 5, we have further extended our study for a different cluster type, i.e., deuterium (other than argon) for its universal acceptance and also explore the effect of laser polarization on the UDLR and the red-shift of the resonance absorption peak. It is found that there is always a redshift of the absorption peak with respect to λ_M in the marginally over-dense band of $\Lambda_d \approx (1 - 1.5)\lambda_M$ irrespective of cluster atom type,

and laser polarization. We also find that the absorption peak gradually disappears for both LP and CP cases at higher intensities $> 10^{17} \text{ Wcm}^{-2}$ due to quick saturation of outer ionization at 100%. On the other hand, for lower intensities, laser absorption due to different polarization of the laser pulse (both LP and CP) are almost equally efficient. However, after absorption peak, at lower laser intensities, absorption due to LP inappreciably dominates absorption due to CP with increasing λ which gradually reverses its character at higher intensities.

Thesis organization

A brief outline of the remaining chapters of the thesis is provided below.

- **Chapter 2** describes the development of a three-dimensional MD simulation code, which is the main working tool to obtain the results presented in this thesis. Detail numerical techniques with various benchmarking results are also presented.
- **Chapter 3** presents the identification of anharmonic resonance (AHR) absorption mechanism in an over-dense pre-ionized deuterium nano-cluster irradiated by an ultra-short laser pulse.
- **Chapter 4** reports the unified dynamical linear resonance (UDLR) and the shifting of the resonance absorption peak from the expected LR for a short-pulse laser interacting with an argon cluster.
- **Chapter 5** illustrates the collisionless absorption of short laser pulses in a deuterium cluster and also explores the effect of laser polarization on the dynamical shift of the resonance absorption.
- Finally, in **chapter 6**, we present the conclusions of the work reported in the thesis with some scope for future works.

Note that atomic units are used throughout the thesis, unless stated otherwise. In atomic units $m_e = -e = 4\pi\epsilon_0 = \hbar = 1$, $c = 137$. Here ϵ_0 is the permittivity of vacuum, $-e$ and m_e are the charge and the mass of the electron, \hbar is the Planck constant, and c is speed of light. The conversion between atomic units and SI units is summarised in appendix A (see A.1). We consider two different clusters e.g., deuterium and argon throughout the thesis. Different parameters for both the clusters are given in table A.2.

2

Molecular Dynamics Simulation

In this chapter, we present the methodology of the newly developed three dimensional (3D) classical molecular dynamics (MD) simulation code. We present numerical and analytical studies for single-particle dynamics and multi-particle dynamics in detail for the validation of the MD code. Most importantly, Mie-plasma frequency is verified for a pre-ionized deuterium cluster nano-plasma, which is extremely important to study the resonance phenomena (the main goal of this thesis work) and energy conservation is also shown. We further discuss the improved MD code that includes self-consistent ionization of atoms/ions assuming “over the barrier ionization (OBI)” model.

2.1 Introduction

Over the past years, numerical simulation has become an extremely powerful tool to understand and interpret the experimental results even at the microscopic level. Numerical simulation facilitates to study the essence of various physical phenomena in an extensive parameter range where experimental and analytical studies have their limitations. Numerical simulations are also used to validate the correctness of theoretical models. So, it serves as a link between a theoretical model and an experiment. Mainly there are two different approaches to study laser-cluster interaction, namely, fluid model and particle model. The fluid model [9, 103, 107] is a macroscopic description, it only describes the average picture of laser-cluster interaction where the individual particle behaviour is not included. Also, fluid model fails to explain various features of laser-cluster interactions due to the small finite size of the cluster and the relatively small number of particles. So, fluid model is not appropriate when the information at the individual particle level is desired. On the other hand the particle simulation model [14–17, 20, 108, 109] can provide a detailed quantitative description of laser-cluster interaction dynamics at the microscopic level. Therefore, the particle simulation model is more suitable for laser-cluster interaction study to predict ionization, charge states, and energy absorption. The particle simulation method is categorized in two types: (i) particle-particle (e.g., MD), and (ii) particle-mesh (e.g., particle-in-cell). Both these models take into account the classical equation of motion to get the temporal evolution of the particles. In MD simulation the force on each particle is calculated as the sum over all forces from the rest of the particles in the system and the trajectory of each particle in the system is determined by solving Newton's equation of motion [110–112]. The force due to the external laser field is also added to this force. Since it takes into account the interactions between all

particles present in the system, the computational time scales as $N(N-1) \sim N^2$. Therefore, MD simulation requires large computational power and can be prohibited for a bigger cluster. It is important to understand that PIC is a method to solve the Vlasov equation by means of particle sampling. In PIC simulation [113, 114] the field is computed on a grid of cells and then the field is interpolated from the grid to the particle's positions. Therefore, the computational cost in PIC simulation scales as $\sim N \log(N)$. The main advantage of MD over PIC is the absence of computational grid and interpolation, which also facilitates its extension to 3D geometry more easily as compared to PIC simulation. The lesser number of particles in a medium sized cluster (as considered in this work) makes the MD simulation suitable to study various physical phenomena of laser-cluster interaction.

In this thesis, we use MD simulation method to study resonance absorption phenomena (both LR and AHR) in a laser-driven cluster. Before studying the various physics phenomena of laser-irradiated clusters in the next chapters 3, 4, 5, systematic numerical and analytical studies for single-particle dynamics and multi-particle dynamics are performed. To validate the MD code, energy conservation has also been rigorously checked for both the cases. Since, the focus of this thesis is to study resonance absorption processes (LR and AHR), which are frequency dependent phenomena, verification of the correct plasma frequency (ω_p) of the electron cloud oscillating against the ionic background under a small perturbation of the electron cloud is *crucial* before we go for further studies. We first verify this plasma frequency ω_p in a 2D slab geometry and then extend our study to verify the exact Mie-plasma frequency $\omega_M = \omega_p/\sqrt{3}$ in a pre-ionized spherical deuterium cluster and compare the results with the desired analytical solutions. Energy conservation is also taken care for all the cases, including the plasma oscillation at ω_p for 2D slab plasma and the Mie-plasma oscillation at ω_M for the spher-

ical plasma case. Further, to study high Z clusters (e.g., argon), we have improved the MD code to include self-consistent ionization of atoms/ions assuming “over the barrier ionization (OBI)” model 1.2.1.4. In the subsequent sections of this chapter, we discuss the basic principle of MD simulation, initial configuration, the laser pulse profile used in the simulation, governing equation of motion (EOM), the time integration scheme and the numerical benchmarked results.

2.2 Flowchart of MD simulation

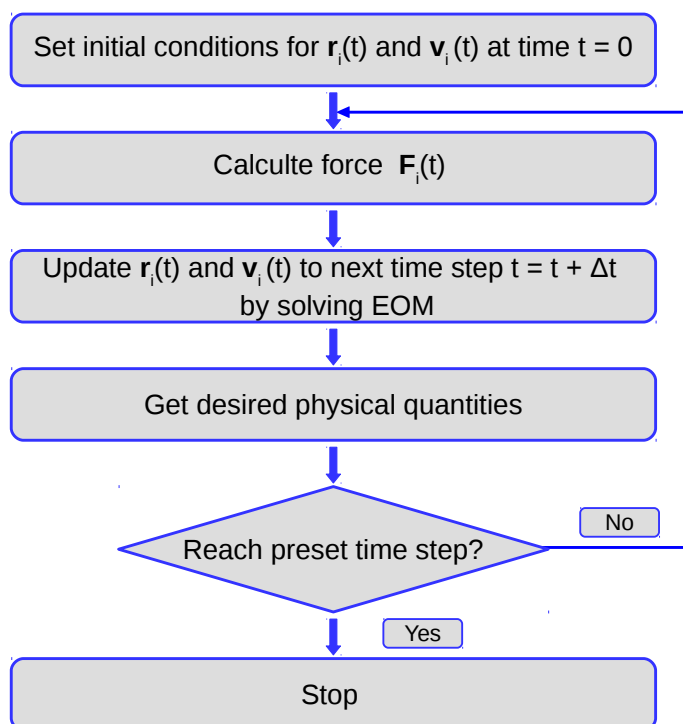


Figure 2.1: Flowchart diagram of the MD scheme.

Molecular dynamics simulation is a computational method for studying the dynamical behaviour of N -particle system by solving equation of motion of each particle experiencing inter-particle force and external force (e.g., laser). The complete flowchart for

the MD algorithm is given in Fig. 2.1 which is self-explanatory.

2.3 Initialization

To start a simulation we need to define the initial positions $\mathbf{r}_i(t_0)$ and velocities $\mathbf{v}_i(t_0)$ of the particles at time t_0 , so that we can predict the trajectories of the particles in a later time by solving the corresponding EOM. Usually, these initial positions and velocities of N particles are chosen in such a way that the system is in equilibrium. We perform simulations with various initial configurations of the charge-neutral cluster, but results of average absorbed energy, outer ionization, and cluster charging are found to be less sensitive to initial configurations for the chosen cluster and laser parameters in this work.

The initial benchmarking results in chapter 2 and the results presented in chapter 3 are obtained by taking a uniform spatial distribution of the particles inside the simulation volume. Each particle is assigned with zero initial velocity. The system is charge neutral and there is no net force on the system at time $t = t_0$.

In the next part, for results presented in chapters 4 and 5, we use a different set of initial configuration, where spatial distribution is taken as random inside the simulation volume and the velocity assignment to the particles is done by Gaussian random distribution. The generation of Gaussian random number is done by the Box-Muller algorithm [115] generated by Box-Muller transformation. The Box-Muller method uses random numbers from [0,1] drawn from the standard normal distribution and the detailed method can be found in Ref. [115]. We need to set the center of mass (CM) velocity as zero to prevent the system from drifting in space and it is done by summing up all the velocities, then divide by the number of atoms (i.e., the average velocity) and subtract this average velocity from each velocity vector. After setting CM velocity to zero, all the velocities are rescaled by a constant factor T_{sf} in order to adjust with

the desired temperature T . The scaling factor T_{sf} is chosen such that the instantaneous temperature is same as the desire temperature and it can be defined as,

$$T_{sf} = \sqrt{\frac{3NK_B T}{\sum_{i=1}^N m_i \mathbf{v}_i^2}} \quad (2.1)$$

where, $\mathbf{v}_i^2 = \mathbf{v}_{i,x}^2 + \mathbf{v}_{i,y}^2 + \mathbf{v}_{i,z}^2$. Each component of the velocity is then scaled by T_{sf} . The initial velocity distribution of the particles using Box-Muller tranformation is reproduced and shown in Fig. 2.2. The full width at half maximum (fwhm) of the velocity distribution refers to the initial temperature of the system.

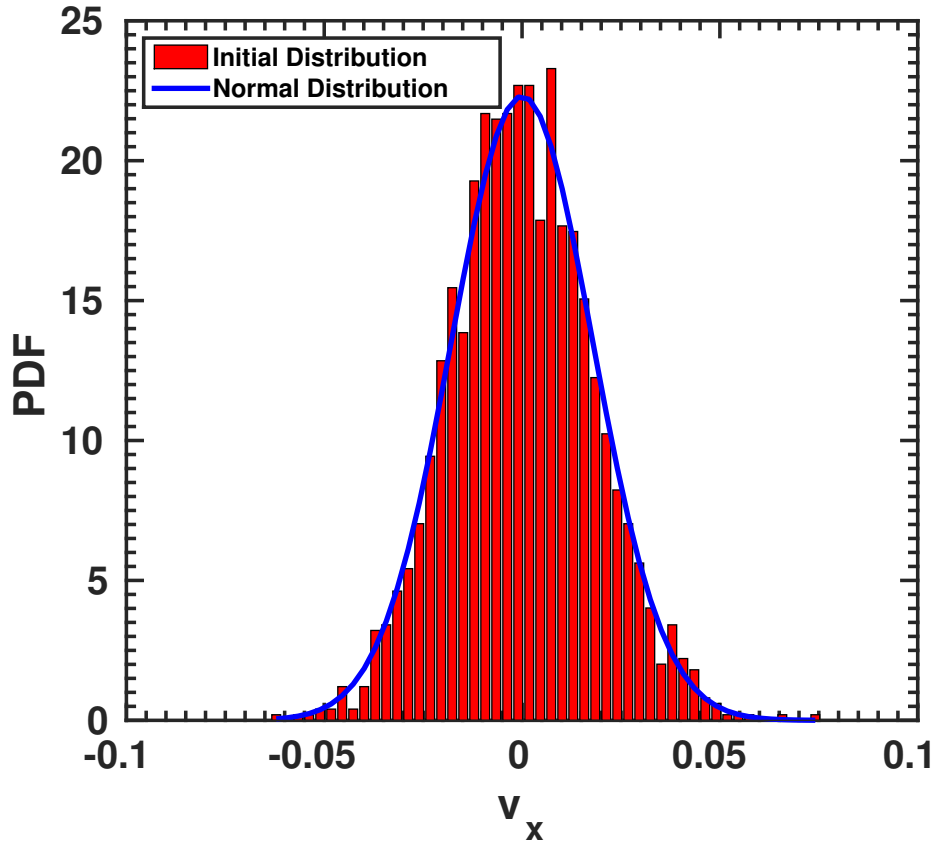


Figure 2.2: Initial Gaussian velocity distribution of neutral atoms along x-direction, generated by Box-Muller transformation. Solid blue curve is the fitted normal distribution.

2.4 The laser pulse

The dipole approximation for the laser vector potential $\vec{A}(z, t) = \vec{A}(t) \exp(-i2\pi z/\lambda) \approx \vec{A}(t)$ is assumed (i.e., spatial variation of the laser field is neglected), since the cluster size R_0 (< 10 nm) is much smaller than the skin depth $\lambda_s \sim c/\omega_p$ of laser for the laser wavelength $\lambda = 100 - 800$ nm as considered in this thesis. In general, we write

$$\vec{A}(t) = \frac{E_0}{\omega} \sin^2(\omega t/2n) \left[\delta \cos(\omega t) \hat{x} + \sqrt{1-\delta^2} \sin(\omega t) \hat{y} \right], \quad (2.2)$$

for $0 \leq t \leq nT$. Here δ is the degree of ellipticity ($0 \leq \delta \leq 1$); $\delta = 1, 1/\sqrt{2}$ for LP and CP respectively; n is the number of laser period T ; $\tau = nT$ is the total pulse duration and $E_0 = \sqrt{8\pi I_0/c}$ is the field strength for the peak intensity I_0 . The components of driving laser electric field $\vec{E}_l(t) = -d\vec{A}/dt$ along x, y and z directions are,

$$\vec{E}_l^x(t) = \delta \frac{E_0}{\omega} \begin{cases} \sum_{i=1}^3 c_i \omega_i \sin(\omega_i t) & \text{if } 0 \leq t \leq nT \\ 0 & \text{otherwise;} \end{cases} \quad (2.3)$$

$$\vec{E}_l^y(t) = \sqrt{1-\delta^2} \frac{E_0}{\omega} \begin{cases} \sum_{i=1}^3 c_i \omega_i \cos(\omega_i t) & \text{if } 0 \leq t \leq nT \\ 0 & \text{otherwise;} \end{cases} \quad (2.4)$$

$$\vec{E}_l^z(t) = 0. \quad (2.5)$$

Where $c_1 = 1/2, c_2 = c_3 = -1/4, \omega_1 = \omega, \omega_2 = (1 + 1/n)\omega$, and $\omega_3 = (1 - 1/n)\omega$. Note that the ponderomotive energy $U_p = E_0^2/4\omega^2$ is the same for both LP and CP. For LP, only the x-component of laser electric field $\vec{E}_l^x(t)$ survives which may vanish at the completion of each laser cycle. Whereas, for CP, electric field components $\vec{E}_l^x(t), \vec{E}_l^y(t)$ in x, y do not vanish simultaneously. Note that, the results presented in chapter 3 and

chapter 4 we consider the LP laser for the study of various resonance absorption phenomena. To study the dependency of laser polarization on resonance absorption we take both LP and CP lasers in chapter 5.

2.5 Governing Equations

The motion of a charge particle in the combined field of laser and space-charge is discussed now. The EOM of i -th particle in a laser field polarized in x and propagating in z (in the dipole approximation) reads

$$m_i \frac{d\vec{v}_i}{dt} = \vec{F}_i(r_i, v_i, t) + \hat{x}q_i E_l(t) + q_i \vec{v}_i \times \hat{y}B_l(t), \quad (2.6)$$

where $\vec{F}_i = \sum_{j=1, i \neq j}^{N_p} q_i q_j \vec{r}_{ij} / r_{ij}^3$ is the Coulomb force on i -th particle of charge q_i due to all j -th particles each of charge q_j . The space-charge field is calculated from the negative gradient of the interacting Coulomb potential $\phi_i = \sum_{j=1, i \neq j}^{N_p} q_j / r_{ij}$. $E_l(t)$ and $B_l(t)$ are the electric and magnetic part of the laser field. Usually, $B_l(t) \approx E_l(t)/c \ll 1$ for intensities $< 10^{18} \text{ Wcm}^{-2}$. The Coulomb potential has a singularity at a zero inter-particle separation $r_{ij} \rightarrow 0$, which leads to an unphysical increase in \vec{F}_i . To avoid such steep increase in the Coulomb force \vec{F}_i , a smoothing parameter r_0 is added with r_{ij} . The modified Coulomb force on i -th particle and the corresponding potential at its location are,

$$\vec{F}_i = \sum_{j=1, i \neq j}^{N_p} \frac{q_i q_j \vec{r}_{ij}}{(r_{ij}^2 + r_0^2)^{3/2}}, \quad \phi_i = \sum_{j=1, i \neq j}^{N_p} \frac{q_j}{(r_{ij}^2 + r_0^2)^{1/2}}. \quad (2.7)$$

This modification of the force allows a charge particle to pass through another charge particle in the same way as in the PIC simulation. Thus it helps to study collisionless energy absorption processes in plasmas, e.g., resonances.

2.6 Choice of artificial parameter r_0

In MD calculation, the choice of the artificial parameter r_0 is very much crucial for smoothing the interaction potential and the force to mitigate the Coulomb singularity for the closest approach of two charge particles, otherwise, Eq. (2.6) gives an unphysical solution. We note that the artificial free parameter r_0 in most of the earlier works has been chosen by considering *only* the energy conservation point of view in the simulation. In Refs.[16, 70, 105], $r_0 = 0.02$ nm for electron-electron interaction and $r_0 = 0.1$ nm for electron-ion interaction have been taken which do not violate the energy conservation in the case of xenon cluster. In Ref. [116], $r_0 = 0.15$ nm for argon and $r_0 = 0.12$ nm for xenon cluster were chosen such that the minimum of the electron-ion interaction potential agrees with the ionization potential of the neutral atom. MD codes in Refs. [19, 22, 23, 117–120] have reported similar kind of r_0 values as in Refs. [16, 70, 105]. Some of the authors have also chosen large r_0 on the order of cluster radius [15, 121] and energy conservation is still obeyed. However, neither of the earlier works reported what happens to the plasma oscillation frequency of electrons in the absence of a laser pulse.

In our simulation, the frequency of oscillation (ω_M) of electrons is found to be sensitive on the value of the r_0 while conservation of energy is obeyed even for larger values of the r_0 . But energy conservation *alone* can not grant correctness of particle dynamics in simulations. To get correct oscillation frequency (ω_M) one can not choose r_0 arbitrarily and a law has to be enforced. For a very small separation $r_{ij} \ll r_0$, the space-charge field on the i -th particle $\vec{E}_i^{sc} = \vec{F}_i/q_i$ has to be linear in r_{ij} and its slope has to be ω_M^2 , i.e., $\vec{E}_i^{sc} = \vec{F}_i/q_i = \omega_M^2 \vec{r}_{ij}$ in order to get correct plasma oscillations at ω_M . From Eq. (2.7), we find that $\vec{E}_i^{sc} = \vec{F}_i/q_i \approx \sum_j (q_j/r_0^3) \vec{r}_{ij} \approx (Q_0/r_0^3) \vec{r}_{ij}$ for $r_{ij} \ll r_0$; assuming Q_0 is the total uniformly distributed charge of type j inside the sphere of radius r_0 where all r_{ij}

are nearly same for collective plasma oscillations. From the above two expressions of space-charge field $\vec{E}_i^{sc} = \omega_M^2 \vec{r}_{ij}$ and $\vec{E}_i^{sc} \approx (Q_0/r_0^3) \vec{r}_{ij}$ we get $\omega_M^2 = Q_0/r_0^3$. For uniform ionic charge density ρ we write $\rho = Q/(4\pi/3)R^3 = Q_0/(4\pi/3)r_0^3$ which gives $Q/R^3 = Q_0/r_0^3 = 4\pi\rho/3 = \omega_M^2$. Thus we get $Q_0/r_0^3 = N_0Z/r_0^3 = Q/R^3 = NZ/R^3$ and $r_0 = R(N_0/N)^{1/3}$; where Z is the uniform charge state of ions in the cluster, N_0, N are the number of ions inside the sphere of radius r_0 and R , $Q_0 = N_0Z$, $Q = NZ$ are the total ionic charge in the sphere of radius r_0 and in the cluster respectively. At this point N_0 remains arbitrary. We note that r_0 should be as small as possible, but non-zero. For a non-zero ionic charge density there should be at least one ion (to provide the restoring force to an electron) in the sphere of radius r_0 . Therefore, setting $N_0 = 1$, we find that $r_0 = R/N^{1/3}$ is the most legitimate choice [122] which is equal to the well known Wigner-Seitz radius $r_\omega = R/N^{1/3}$ for a given cluster that leads to correct Mie-plasma oscillation at ω_M if the law of force is of Coulombic in nature. Therefore, in our MD simulations, we use $r_0 = r_\omega$ that produces correct plasma oscillation frequency as well as energy conservation.

2.7 Integration of the equation of motion

After specifying the initial positions and velocities of the particles in the system, the force on each particle is calculated from Eq. (2.7). Knowing the force on each particle, the next step is to integrate the EOM (2.6) which needs an integration algorithm. Various integration algorithms are used in MD simulation to integrate the EOM. We use velocity Verlet algorithm [110, 123] where we consider the Taylor expansion of the position coordinate $\mathbf{r}(t)$ and velocity $\mathbf{v}(t)$ of a particle at time t . It is a modification of the Verlet algorithm [124]. The standard implementation scheme of this algorithm is shown in Fig. 2.3. The equations for $\mathbf{r}(t)$ and $\mathbf{v}(t)$ at time $t = t + \Delta t$ are respectively,

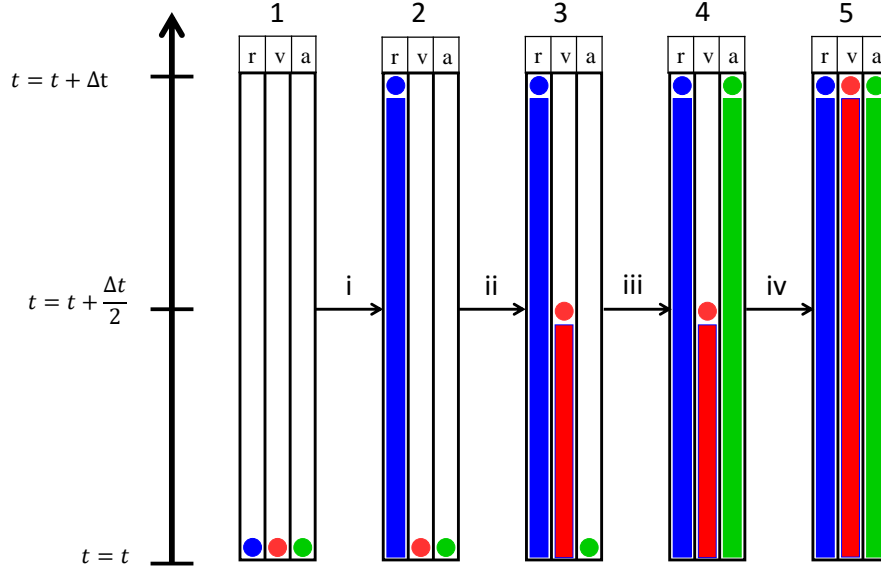


Figure 2.3: Illustration of the velocity Verlet integration scheme.

$$\mathbf{r}(t + \Delta t) = \mathbf{r}(t) + \mathbf{v}(t)\Delta t + \frac{1}{2}\mathbf{a}(t)\Delta t^2, \quad (2.8)$$

$$\mathbf{v}(t + \Delta t) = \mathbf{v}(t) + \frac{\mathbf{a}(t) + \mathbf{a}(t + \Delta t)}{2}\Delta t. \quad (2.9)$$

The instantaneous acceleration at each time step is given by $\mathbf{a}(t) = \mathbf{F}(t)/m_i$, and the force $\mathbf{F}(t)$ is calculated from the interaction potential using Eq. (2.7). The intermediate steps followed in velocity Verlet integration algorithm are as follows: (i) Starting from initial position $\mathbf{r}(t)$, velocity $\mathbf{v}(t)$, and acceleration $\mathbf{a}(t)$ at time t , we calculate new position $\mathbf{r}(t + \Delta t)$ in step $1 \rightarrow 2$

$$\mathbf{r}(t + \Delta t) = \mathbf{r}(t) + \mathbf{v}(t)\Delta t + \frac{1}{2}\mathbf{a}(t)\Delta t^2.$$

Chapter 2. Molecular Dynamics Simulation

(ii) Calculate the intermediate velocity (half velocity) in step $2 \rightarrow 3$

$$\mathbf{v}(t + \Delta t/2) = \mathbf{v}(t) + (1/2)\mathbf{a}(t)\Delta t.$$

(iii) Compute new acceleration $\mathbf{a}(t + \Delta t)$ using new position $\mathbf{r}(t + \Delta t)$ in step $3 \rightarrow 4$

$$\mathbf{a}(t + \Delta t) = \frac{\mathbf{F}(\mathbf{r}(t + \Delta t))}{m}.$$

(iv) Compute the new velocity from the new acceleration and half velocity in step $4 \rightarrow 5$,

$$\mathbf{v}(t + \Delta t) = \mathbf{v}(t + \Delta t/2) + (1/2)\mathbf{a}(t + \Delta t)\Delta t = \mathbf{v}(t) + \frac{1}{2}[\mathbf{a}(t) + \mathbf{a}(t + \Delta t)]\Delta t.$$

The advantage of the velocity Verlet scheme is that it preserves time reversal symmetry and phase space volume [111]. In this scheme both the positions and velocities of particles are defined at the same instant of time contrary to Leapfrog integration scheme. As a consequence, it gives better energy conservation, because the kinetic and potential energy depends on the velocities and the positions at the same time. Velocity Verlet integration scheme also conserves total energy even when relatively large time steps are used [110] and the accuracy reaches up to $O(\Delta t)^4$. It also consumes less computational power as compared to RK4 integration algorithm [125]. Due to all these advantages, we use the velocity Verlet integration algorithm in our MD simulation. Since time integration algorithm is based on the finite difference method, the choice of a time step Δt is important in MD simulation. The EOM (2.6) can be integrated by choosing a small Δt . The most important criterion for choosing a Δt is that the integration algorithm conserves the total energy of the system for a longer period of time and also represents accurate frequency of the system. In our MD simulation we use $\Delta t = 0.01$ a.u. ≈ 0.24 as, to resolve the highest ω_M corresponding to highest Z of the plasma.

2.8 Test of the MD code

In this section, we report the validation of the MD code with simple examples and the results obtained from the simulations are compared with respective analytical solutions.

2.8.1 Single particle dynamics

We start by verifying numerical solution of the classical motion of a single particle of $m = 1$, $q = -1$ in a continuous laser field with the analytical result. We take the potential as harmonic potential $\frac{1}{2}\omega_p^2(x^2 + y^2)$. The EOM of the particle with a continuous laser field $E_0 \cos(\omega t)$, polarized along x-direction reads,

$$\frac{d^2x(t)}{dt^2} = -\omega_p^2 x(t) - E_0 \cos(\omega t), \quad (2.10)$$

$$\frac{d^2y(t)}{dt^2} = -\omega_p^2 y(t). \quad (2.11)$$

The solution to equations (2.10) and (2.11) with initial condition $x(0) = 0, v_x(0) = 1$ and $y(0) = 0, v_y(0) = 1$ are respectively,

$$x(t) = \frac{E_0}{(\omega_p^2 - \omega^2)} \cos(\omega_p t) + \frac{\sin(\omega_p t)}{\omega_p} - \frac{E_0}{(\omega_p^2 - \omega^2)} \cos(\omega t), \quad (2.12)$$

$$v_x(t) = -\frac{E_0 \omega_p}{(\omega_p^2 - \omega^2)} \sin(\omega_p t) + \cos(\omega_p t) + \frac{E_0 \omega}{(\omega_p^2 - \omega^2)} \sin(\omega t), \quad (2.13)$$

$$y(t) = \frac{\sin(\omega_p t)}{\omega_p}, \quad (2.14)$$

$$v_y(t) = \cos(\omega_p t). \quad (2.15)$$

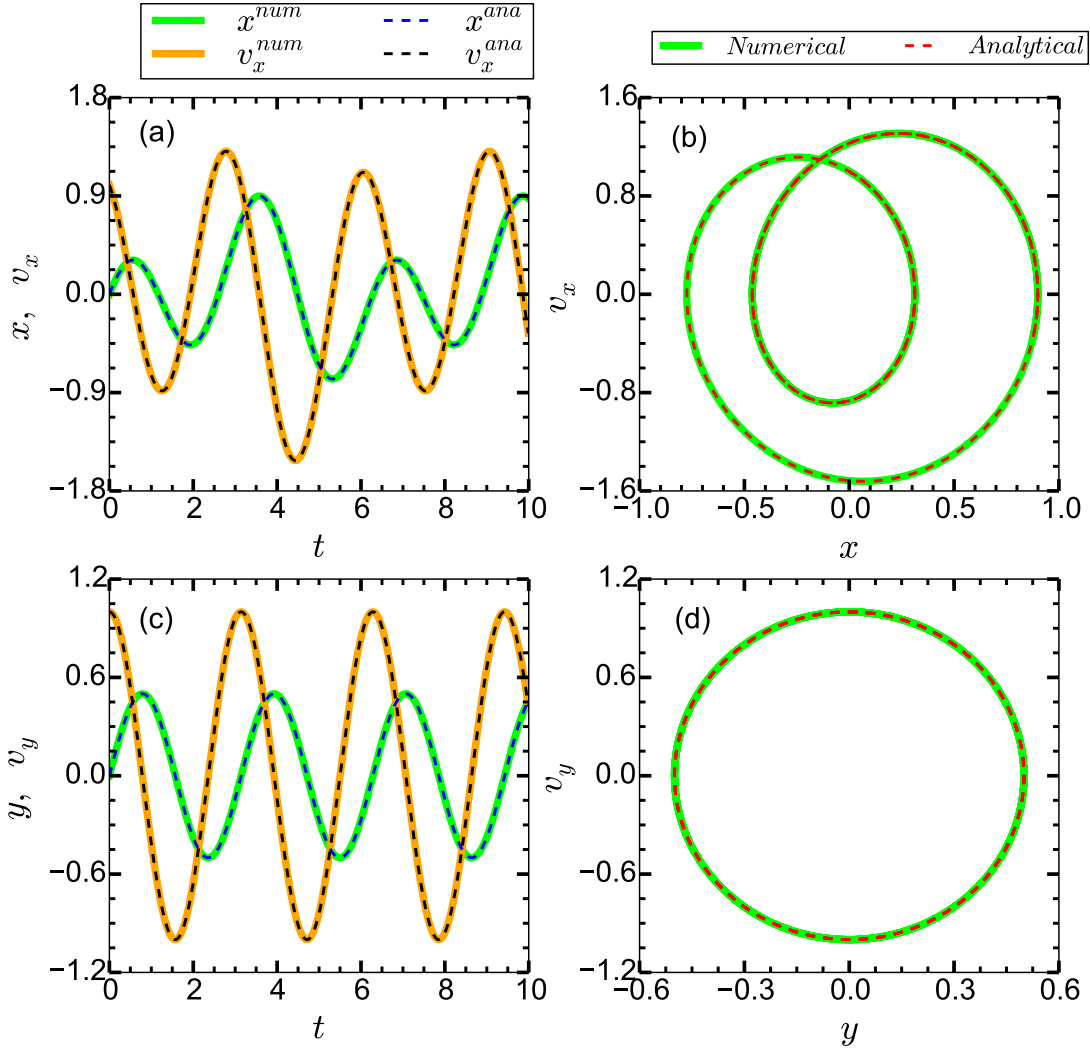


Figure 2.4: Results for single particle motion in a 2D harmonic potential $\omega_p^2(x^2 + y^2)/2$ with continuous laser field $E_0 \cos(\omega t)$ long x-direction. Evolution of position and velocity along both the x and y directions are shown in subplots (a) and (b) respectively and corresponding phase space plots are shown in subplots (c) and (d). Numerical results are compared with the analytical results which show a good matching.

Figure 2.4 shows the dynamics of the single particle along x, y directions. Here, we have taken $q/m = -1$, $E_0 = 1$ a.u., $\omega_p = 2$ a.u., and $\omega = 1$ a.u. The simulation results (solid line) for temporal evolution of position and velocity are also plotted with the analytical results (dashed line), which show a very good agreement.

2.8.2 Multi-particle dynamics in a 2D slab geometry

In this section, we describe the multi-particle dynamics in a 2D slab geometry. We simulate the dynamics of $N = 100$ number of non-interacting particles ($q = -1$ and $m = 1$), which are moving in a two dimensional harmonic potential $\omega_p^2(x^2 + y^2)/2$. All the particles are symmetrically and uniformly distributed in a 2D square box of dimension $l_x = l_y = 100$ a.u. as shown in Fig. 2.5(a). The initial velocities are assumed zero for all particles. The governing EOMs along x, y directions are,

$$\frac{d^2x_i(t)}{dt^2} = -\omega_p^2x_i(t), \quad \frac{d^2y_i(t)}{dt^2} = -\omega_p^2y_i(t). \quad (2.16)$$

The solutions to Eq. (2.16) with initial conditions $x_i(0) = x_{0i}$, $y_i(0) = y_{0i}$ and $v_{x_i}(0) = v_{y_i}(0) = 0$ are,

$$x_i(t) = x_{0i} \cos(\omega_p t), \quad y_i(t) = y_{0i} \cos(\omega_p t), \quad (2.17)$$

$$v_{x_i}(t) = -x_{0i} \omega_p \sin(\omega_p t), \quad v_{y_i}(t) = -y_{0i} \omega_p \sin(\omega_p t). \quad (2.18)$$

The kinetic energy, potential energy, and total energy of the system are obtained as,

$$E_k = \frac{1}{2} \sum_{i=1}^N m_i (v_{x_i}^2 + v_{y_i}^2), \quad (2.19)$$

$$E_p = \frac{1}{2} \sum_{i=1}^N m_i \omega_p^2 (x_i^2 + y_i^2), \quad (2.20)$$

$$E_t = E_k + E_p. \quad (2.21)$$

Figure 2.5 shows the dynamics of the all particles in time. Initial distributions are shown in Fig. 2.5(a), the inter-particle distance is $\delta a = 10$ a.u., excursion of all the electrons and phase space of the system are plotted together with numerical results in subplots

2.5(b) and 2.5(d) respectively. All particles repeatedly come back to their respective initial position at equal interval of time which shows the periodic nature. The sum total of kinetic energy and potential energy remains constant with time, showing the conservation of energy of the system of particles in Fig. 2.5(c). Here also numerical results reasonably match with the analytical results.

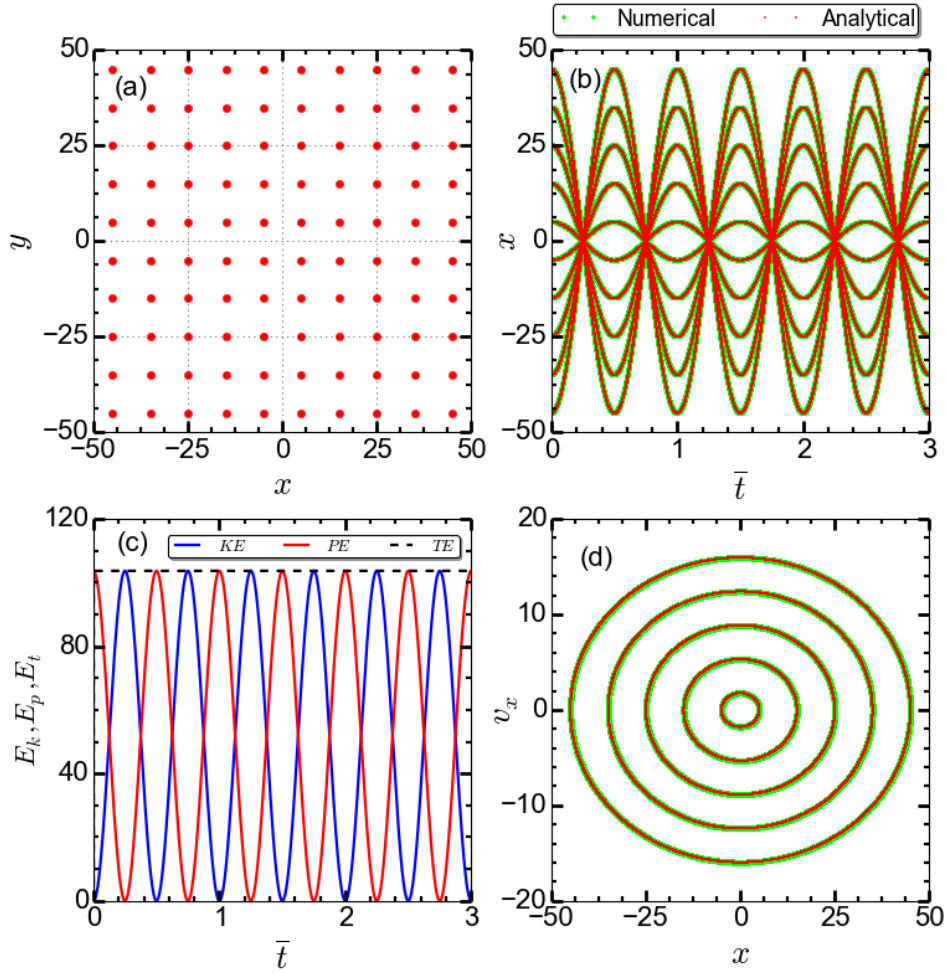


Figure 2.5: Results for non-interacting particles in a two dimensional harmonic potential $\frac{1}{2}\omega_p^2(x^2 + y^2)$. (a) uniform distribution of 100 particles having $q/m = 1$ in a 2D grid of size $L_x = L_y = 100$ a.u., (b) evolution of all particles with time in x-direction. Both numerical (dotted green line) and analytical (dotted red line) results are plotted simultaneously showing good matching, (c) variation of KE, PE and TE with time, which shows conservation of energy and (d) phase space plot for the system.

2.8.2.1 Reproducing the plasma frequency in a 2D slab geometry

In an extension to our study in Sec. 2.8.2, now we consider both the charge species (i.e., electron and ion) and also the interaction between all particles. We take the interaction potential as Coulomb potential (2.7). We validate the MD code by verifying the electron plasma oscillation frequency and energy conservation. Plasma frequency is described by the collective motion of the electrons which oscillate with a constant frequency ω_p in the static ion background potential when a very small perturbation is given to the electron system [85]. The parameters taken in the simulation are listed in the Table 2.1.

Quantity	Symbol	value
Number of ions	N_i	100
Number of electrons	N_e	100
Ion density	ρ_i	0.01 a.u.
Box dimension	$L_x = L_y$	100 a.u.
Smoothing parameter	r_0	2.0 a.u.
Distance between individual particles	δa	10 a.u.
Charge of ion	q_i	1.0 au.
Charge of electron	q_e	-1.0 au.
Mass of ion	m_i	1836.0 a.u.
Mass of electron	m_e	1.0 a.u.
The value of plasma frequency	ω_p	0.3545 a.u.
Displacement	δx	0.2 a.u.

Table 2.1: Parameters for verification of plasma frequency in a 2D slab geometry.

We assume 100 immobile ions and 100 electrons which are distributed symmetrically in 2D space as shown in Fig. 2.6(a). The electron-ion system is macroscopically charge neutral. Now we give a small perturbation of $\delta x = 0.2$ a.u. to the electrons w.r.t. ion background along +x direction at time $t = 0$ (see Fig. 2.6(b)). The restoring force pro-

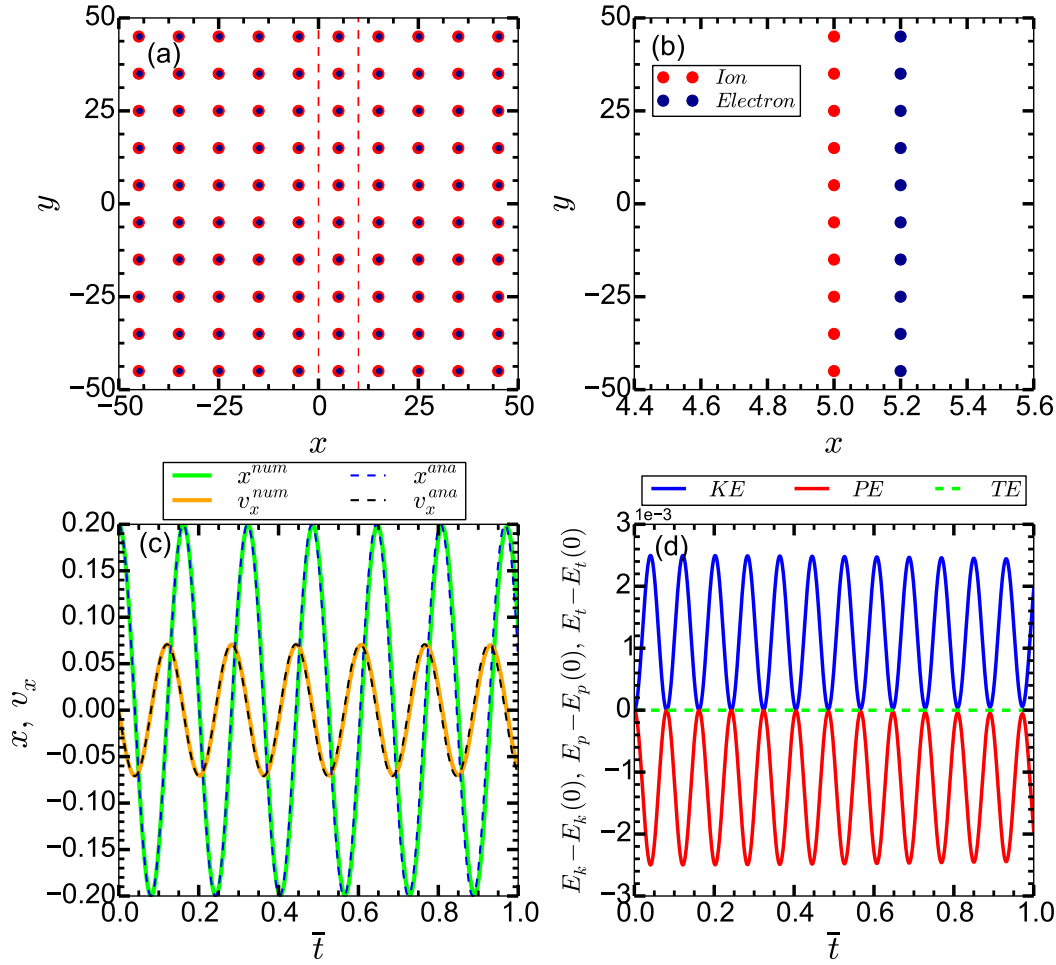


Figure 2.6: Results for multi-particle system interacting via Coulomb potential. (a) initial distribution of electron and ion system, each electron is displaced by $\delta x = 0.2$ a.u. along the +x-direction at time $t = 0$ from their parent ion, (b) zoomed part of one layer of ion and electron system has been shown for better clarity, (c) oscillation of center of mass of the electron cloud plotted with analytical result, and (d) evolution of kinetic energy (KE), potential energy (PE), and total energy (TE) showing conservation of energy. Initial PE and TE of the system are subtracted from their corresponding PE and TE of the system.

duced due to the local charge imbalance will pull the electrons back to their original position and that will lead to oscillations of the electrons against the background ions with the plasma frequency ω_p determined by the density ρ_i of the ionic background as

$\omega_p = \sqrt{4\pi\rho_i}$. Each electron should satisfy $\delta\ddot{x} + \omega_p^2\delta x = 0$. However, for collective oscillation we take oscillation of center of mass of the electrons and write EOM of the center of mass of the electrons as,

$$\ddot{x}_{CM} + \omega_p^2 x_{CM} = 0. \quad (2.22)$$

The analytical solution of Eq. (2.22) with initial conditions $x_{CM}(0) = a_0$, $\dot{x}_{CM}(0) = 0$ gives, $x_{CM}(t) = x_{0CM} \cos(\omega_p t)$ and $v_x(t) = -x_{0CM} \sin(\omega_p t)$. The CM oscillation of the electrons is given by $x_{CM}(t) = \sum_1^{N_e} m_e x_i(t) / N_e$ which matches with the analytical results very well in Fig. 2.6(c). One of the important tests to verify that MD simulation is working correctly or not is to test the conservation of energy of the system. The TE of the system is given by $E_t = E_k + E_p$ where,

$$E_k = \frac{1}{2} \sum_{i=1}^N m_i \mathbf{v}_i^2, \quad E_p = \sum_{j=1, i \neq j}^N q_i \phi_i. \quad (2.23)$$

Figure 2.6(d) shows the variation of KE (solid blue line), PE (solid red line), and TE (dashed black line) with time. The initial potential energy and total energy are subtracted from their corresponding values. The results show the conservation of energy as the total energy (dashed black line) is constant over time. Figure 2.7 shows the Fourier transform (FT) of center of mass oscillation of electrons which gives the collective oscillation frequency, i.e., plasma frequency ω_p . Numerical result (dashed-circle) from MD simulation plotted with the analytical FFT of the excursion of CM (solid line) $x_{CM}(t) = x_{0CM} \cos(\omega_p t)$ showing excellent matching that confirms the collective oscillation of the electrons at the plasma frequency ω_p . Thus, energy conservation and fairly accurate plasma frequency are represented by our MD simulations.

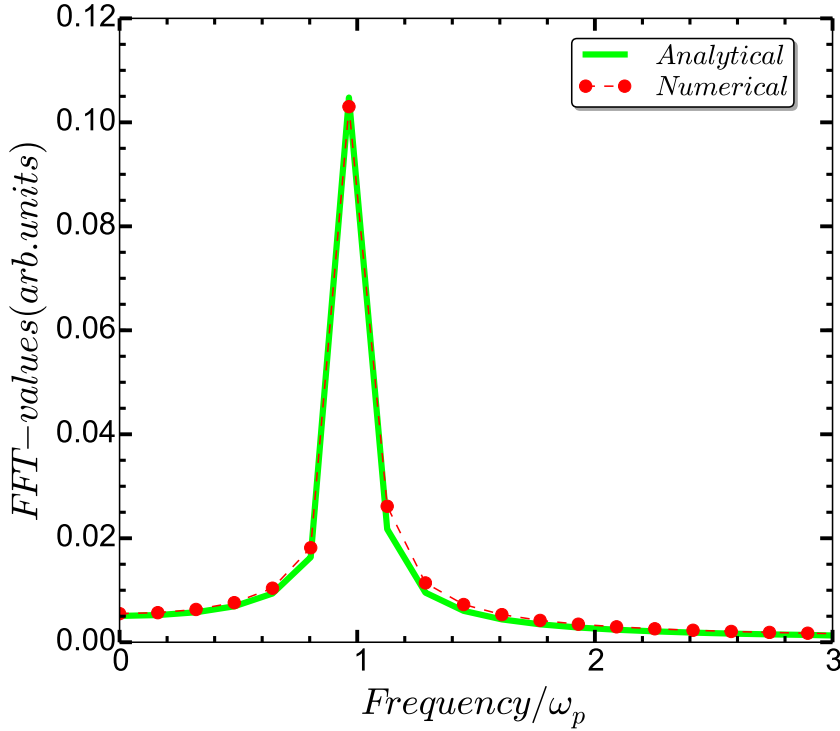


Figure 2.7: FFT of the center of mass (CM) position co-ordinate of electrons. Frequency is normalized by ω_p . MD simulation result (numerical, dashed-circle) matches with the analytical result (solid line).

2.8.3 Verification of Mie-plasma frequency in a deuterium cluster

In this section we show the validation of our MD code by identifying the desired Mie-plasma frequency $\omega_M = \omega_p / \sqrt{3}$ for the spherical deuterium cluster plasma under small perturbation and also by verifying conservation of total energy of the system. Although there are plenty of MD simulations for clusters [15–20, 22, 23, 70, 105, 116–122, 126, 127], verification of this natural oscillation through MD simulation is rarely reported which is extremely important, particularly to study frequency dependent phenomena, e.g., anharmonic and harmonic resonance absorption in laser driven plasmas. Otherwise, resonance physics may be missing in simulations and subsequent MD results could be

misleading. In fact, MD codes in Refs.[19, 22, 23, 117] could not find the signature of resonances in laser cluster interaction and the reason was unknown; while experiments [9, 11, 128, 129], theory and PIC simulation [12–14, 87, 93, 99, 100] studies clearly indicated its importance.

To prove that our MD code is capable of producing oscillation of electrons at the Mie-plasma frequency ω_M in the absence of a laser field, the deuterium cluster of radius $R = 2.05$ nm, and number of atoms $N = 1791$ is considered. To make homogeneously charged positive background in which electrons will oscillate, all N_i ions ($N_i = N = 1791$) are uniformly distributed initially. It gives ionic charge density $\rho_i = 0.007$ a.u. and $\omega_M = \sqrt{4\pi\rho_i/3} = 0.1735$ a.u.. A fewer number of N_e electrons (forming a homogeneous sphere of radius $R/2$) is uniformly and symmetrically distributed about the center of the spherical ion background and the whole system is at rest. This may represent a situation when most of the electrons are removed from the cluster by a laser field, and the remaining cold electrons occupying the central region collectively oscillate with the frequency ω_M . Electrons are now uniformly shifted (small perturbation) from the ionic background along x . The space-charge field due to the local charge imbalance acts like a restoring field. Whether these electrons will oscillate at ω_M is determined by the homogeneity of the charge density ρ_i and the linearity of the restoring field decided by the amount of perturbation. These are ensured by making the ion background homogeneous and keeping perturbation small so that electrons do not cross the cluster boundary. Under this condition one may write EOM of the center of mass of the electron cloud as $\ddot{x} = -\omega_M^2 x$, giving $x = x_0 \cos(\omega_M t)$ with initial conditions $x(0) = x_0$, $\dot{x}(0) = 0$; and verify the MD simulation results as in the Sec. 2.8.2.1. The values of all the parameters taken in the simulation are listed in Table 2.2.

Quantity	Symbol	value
Number of ions	N_i	1791
Number of electrons	N_e	1791
Ion density	ρ_i	0.007 a.u.
Cluster radius	R	38.88 a.u. (≈ 2.05 nm)
Wigner-Seitz radius of cluster	r_w	3.22 a.u. (≈ 0.17 nm)
Distance between individual particles	δa	5.184 a.u.
Charge of ion	q_i	1.0 au.
Charge of electron	q_e	-1.0 au.
Mass of ion	m_i	1836.0 a.u.
Mass of electron	m_e	1.0 a.u.
The value of Mie-plasma frequency	ω_M	0.1735 a.u.
Ratio of ω_M and ω	ω_M/ω_p	3.05 (at $\lambda = 800$ nm)
Displacement	δx	6 a.u.

Table 2.2: Parameters used to study Mie-plasma oscillation for deuterium cluster.

Figure 2.8(a) shows the initial distribution of electrons and ions. The CM excursion of MD electrons is given by $x_{CM}(t) = \sum_1^{N_e} m_e x_i(t)/N_e$ and CM velocity $V_{CM}(t) = \sum_1^{N_e} m_e v_i(t)/N_e$ which match corresponding analytical results as shown in Fig. 2.8(b). Figure 2.8(c) shows the variation of KE (solid blue line), PE (solid red line), and TE (dashed green line) with time. The initial potential energy and initial total energy are subtracted from their corresponding values. The results shows the conservation of energy. Phase space variables (x, v_x) are plotted in Fig. 2.8(d).

It can be inferred from Figs. 2.8 (b, d) that the electron cloud oscillates with a constant frequency ω_M . The Fourier transform (FT) of the center of mass position $x_{CM}(t) = \sum_1^{N_e} m_e x_i(t)/N_e$ of MD electrons also give the collective oscillation frequency of the electron cloud which is plotted with the FT of the analytical solution of $x = x_0 \cos(\omega_M t)$

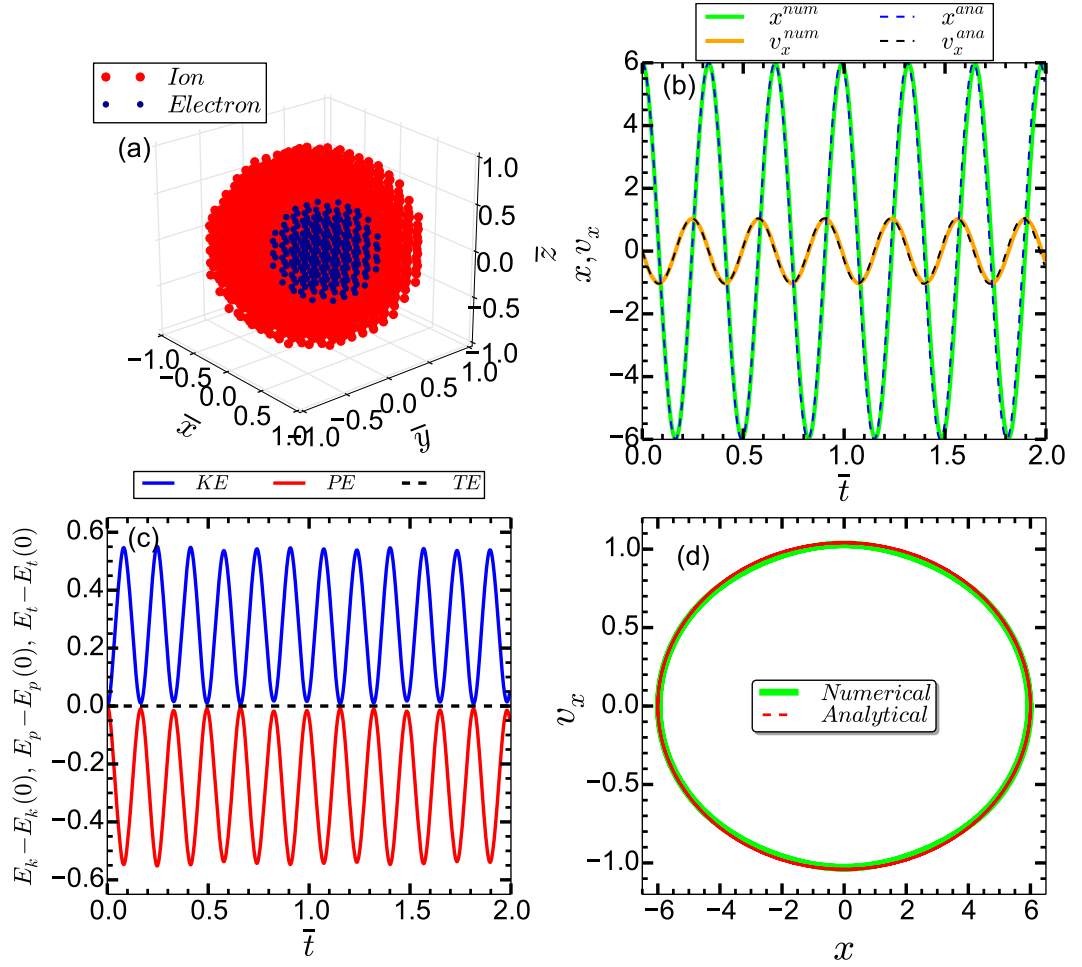


Figure 2.8: (a) Initial distribution of ions (red dots) and electrons (blue dots) at time $t = 0$. There are 1791 number of ions and with cluster radius $R = 2.05$ nm. $N_e = 251$ electrons are forming a homogeneous sphere of radius $R/2$. All the electrons are uniformly shifted from the ionic background along $+x$ direction, (b) The center of mass oscillation of electrons cloud with respect to ion cloud. The excursion $x(t)$ (solid green line) and velocity $v_x(t)$ (solid orange line) calculated from the MD code matches very well with the analytical result $x(t) = x_0 \cos(\omega_M t)$ (dashed blue line) and $v_x(t) = -x_0 \sin(\omega_M t)$ (dashed black line), (c) variation of KE, PE, and TE with time showing conservation of energy as TE (dashed black line) remains constant with time, (d) numerical results for phase space plot for CM oscillation of the electron cloud (solid green line) plotted with the analytical result (red dashed line).

in Fig. 2.9 after the normalization by ω_M similar to the case of Fig. 2.7. An excellent match between the numerical MD (dashed-circle) result and analytical (solid line) re-

sult confirms the collective oscillation of electrons at the Mie-plasma frequency ω_M . Extensive simulations have been performed for other values of smoothing parameters $r_0 = 0.5r_\omega, 2r_\omega, 3r_\omega, 4r_\omega$ to check the effect of r_0 on the plasma oscillation dynamics. As time progresses, we find 5-20% reduction in the amplitude of plasma oscillation with 5 – 10% elongation in the plasma period compared to the case of $r_0 = r_\omega$ and the desired analytical solution. Therefore, in all MD simulations in this thesis we keep $r_0 = r_\omega$ (it may vary depending upon cluster type) which leads to both energy conservation and reproducing accurate natural oscillation frequency of the system. Our MD simulation is thus capable of representing ω_p or ω_M depending upon the shape of the finite size of plasma.

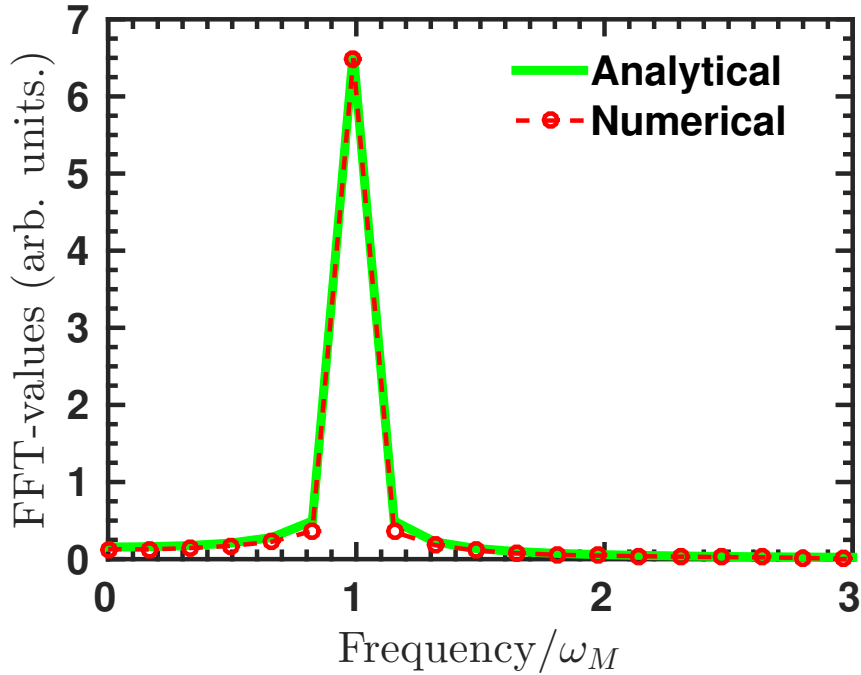


Figure 2.9: FFT of the center of mass (CM) position co-ordinate of electrons for a deuterium cluster of radius $R = 2.05$ nm, and number of atoms $N = 1791$. Frequency is normalized by ω_M . MD simulation result (numerical, dashed-circle) matches with the analytical result (solid line) for the entire range of frequency.

2.9 Improvement of the MD simulation code

In this section, we describe the additional improvement to our MD code (mainly inclusion of ionization) which is used to simulate various results in chapter 4 and 5.

Initialization

The clusters are assumed to be initially neutral and atoms are distributed randomly inside the initial cluster radius R_0 . The thermal velocity assignment of neutral atoms in the cluster is done by Gaussian random distribution generated by the Box-Muller transformation as described in Sec. 2.3. The velocity distribution relates to the initial temperature of the neutral cluster which is taken as one-fifth of the room temperature ≈ 0.025 eV for simplicity. Once thermal velocity is assigned, then we post process the data to correlate with the position of the atoms in the cluster in such a way that the surface atoms in the cluster have larger thermal velocities as compared to the core atoms.

Inclusion of ionization

For laser intensities above 10^{15} Wcm $^{-2}$ (considered in this thesis), the electric field of the laser is strong enough to bend down the Coulomb potential and the bound electron is escaped from the potential. This mechanism is called “over the barrier ionization” (OBI) mechanism [52, 63, 64], already described in chapter 1 (see Sec. 1.2.1.4). The laser intensity is appropriately chosen such that it ionizes all neutral atoms initially at the same time $t = t_i$ and produces first ionization state $Z = 1$. The value of t_i depends upon laser intensity and wavelength. At a fixed intensity, values of t_i may have minor differences depending upon the phase of the pulses of different wavelengths near t_i . The

Chapter 2. Molecular Dynamics Simulation

critical laser field $E_c = |\vec{E}_l(t_i)|$ for this OFI can be rewritten from Eq. 1.8,

$$E_c = I_p^2(Z)/4Z, \quad (2.24)$$

where $I_p(Z)$ is the ionization potential corresponding to Z . The values of I_p for the only charge state of deuterium cluster ions and for different Z of argon cluster ions (as considered in this thesis) are listed in Table 2.3 and 2.4 respectively with their corresponding critical laser intensity to get that value of Z . After the initial ionization by OFI, the nano-plasma is formed with equal number of electrons and ions $N_e = N_i$. As time advances, the laser field $\vec{E}_l(t > t_i)$ may displace few electrons along the laser polarization and space charge field $|\vec{E}_{sc}(\vec{r}_i, t)|$ is created at each ion position \vec{r}_i due to the breaking of charge neutrality (may be at a microscopic level) which may exceed $|\vec{E}_l(t)|$. $\vec{E}_{sc}(\vec{r}_i, t)$ at the ion position \vec{r}_i is contributed by all electrons and all other ions at $\vec{r} \neq \vec{r}_i$. Thus, the effect of plasma environment is taken into account for the ionization of ions. The total instantaneous field $\vec{E}(\vec{r}_i, t) = \vec{E}_l(t) + \vec{E}_{sc}(\vec{r}_i, t)$, including the plasma field, may create even higher $Z > 1$ of ions (ionization ignition, see Sec. 1.2.2) by satisfying the condition

$$|\vec{E}(\vec{r}_i, t)| \geq I_p^2(Z+1)/4(Z+1), \quad (2.25)$$

and the number of electrons increase dynamically. The position and velocity of a newly born electron are assumed to be the same as the parent ion conserving the momentum and energy. For simplicity, we use standard $I_p(Z)$ of argon atom/ions as in Refs.[15, 17, 19, 22, 71, 117, 130], whereas due to the additive effect of the plasma field $\vec{E}_{sc}(\vec{r}_i, t)$ higher charge states Z are created (in this work) for cluster atoms/ions than predicted by OFI (2.24) for isolated argon atoms/ions, if only laser field is considered. By sophisticated MD simulations, it has been shown that electronic levels of atoms in

a cluster may differ from those of a single atom [20, 131]. The electronic energies in cluster-ions are also lowered by electronic screening and by the presence of other plasma ions. We have not yet considered these corrections in $I_p(Z)$, which will be included in future work.

Deuterium ion	Z	I_p (eV)	I_0 (Wcm⁻²)
D_2^{+1}	1	13.6	1.0×10^{15}

Table 2.3: Ionization potential and corresponding threshold intensity of the deuterium atoms/ions.

Argon ions	Z	I_p (eV)	I_0 (Wcm⁻²)
Ar^{+1}	1	15.76	1.35×10^{15}
Ar^{+2}	2	27.63	3.18×10^{15}
Ar^{+3}	3	40.74	6.68×10^{15}
Ar^{+4}	4	59.81	1.74×10^{16}
Ar^{+5}	5	75.02	2.76×10^{16}
Ar^{+6}	6	91.01	4.16×10^{16}
Ar^{+7}	7	124.32	1.06×10^{17}
Ar^{+8}	8	143.46	1.44×10^{17}
Ar^{+9}	9	422.45	8.58×10^{18}
Ar^{+10}	10	478.69	1.14×10^{19}

Table 2.4: Ionization potentials and corresponding threshold intensities of the argon atoms/ions.

2.10 Summary

In this chapter, we have presented the detail technique of the newly developed 3D-MD code. Initial studies for single particle dynamics and multi particle dynamics have been performed. Energy conservation has also been verified for both the systems. The plasma frequency in a 2D slab geometry has been verified with analytical result. The full 3D-MD code has been employed to verify the Mie-plasma frequency in a pre-ionized deuterium cluster. Next, we have improved the MD code to include self-consistent ionization by “OBI” model to study high Z clusters (e.g., argon) in chapters [4](#) and [5](#).

3

Identification of anharmonic resonance absorption

*The objective of this chapter * is to identify anharmonic resonance (AHR) absorption mechanism in an over-dense pre-ionized deuterium nano-cluster irradiated by an ultra-short laser pulse using the newly developed 3D-MD simulation code (discussed in chapter 2). AHR was shown before by a model and particle-in-simulations (PIC) [14]. However, AHR remains to be a debate and still obscure in multi-particle plasma simulations. Present study confirms the universal acceptance of AHR as a collisionless mechanism of absorption in the short pulse regime in clusters irrespective of the method of simulation. A simple anharmonic oscillator model called rigid sphere mode (RSM) has also been introduced to understand various features of AHR and also to corroborate the MD results.*

* **S. S. Mahalik** and M. Kundu, “Anharmonic resonance absorption of short laser pulses in clusters: A molecular dynamics simulation study”, [Physics of Plasmas](#) (23), 123302 (2016)

3.1 Introduction

Laser-driven atomic clusters absorb large fraction of laser energy compared to traditional solid and gas targets. Solid like overdense plasma density of a cluster and its smaller size (of a few nanometer) than the wavelength of 800 nm laser pulse (typically used in experiments) allow full penetration of laser field without its attenuation, contrary to micron-sized solids, leading to nearly 90% laser absorption in clusters [1]. MeV ions [1, 2, 5, 6, 108, 132–136], KeV electrons [2–4, 136–139], x-rays [7, 140–142] and MeV neutrals [8] in experiments are the consequence of efficient coupling of laser energy with cluster. Clearly, without the efficient electron acceleration, the subsequent ion acceleration, x-ray generation and neutral atom acceleration can not happen. Therefore, investigation of underlying physical process of coupling of laser energy with electrons is very important. For infrared lasers (800 nm wavelength or above) with intensities $I_0 > 10^{16} \text{ Wcm}^{-2}$, collisional process of absorption through electron-ion collision can be neglected since it scales as $\sim I_0^{-3/2}$. However, collisionless process of absorption continues irrespective of the laser intensity and the wavelength as long as the plasma is overdense.

Among the various collisionless processes, linear resonance (LR) occurs when Mie-plasma frequency $\omega_M(t)$ of the Coulomb expanding cluster meets the laser frequency ω . In experiments, it is achieved by a pump-probe technique [10, 36, 37] where a pump pulse first ionizes the cluster, $\omega_M(t)$ rises above ω , subsequent outer ionization of electrons leads to cluster expansion causing decrease of $\omega_M(t)$ towards ω , and after a suitable delay (typically > 100 fs) a probe pulse hits the expanding cluster to meet the LR condition $\omega_M(t) \approx \omega$ [9]. However, to make this LR to happen at a later time, we need to remove as many electrons by a laser from the cluster potential in an early time.

Otherwise Coulomb expansion is not possible. Therefore, one must know how those electrons absorb energy in an early time of a long pulse laser. For a short pulse, ionic background can not expand sufficiently, $\omega_M(t)$ does not fall upto ω to meet LR; *but* energy absorption by electrons still persists. Therefore, we concentrate on the mechanism of energy absorption in the short pulse regime which is also applicable for the early duration of a longer pulse much before the LR can happen.

The role of $\vec{v} \times \vec{B}$ heating [97] as a collisionless mechanism is discriminated here by restricting the laser intensity below 10^{17} Wcm^{-2} where B field of the laser is negligible. One may surmise the “Brunel effect” or the “vacuum heating” as a probable collisionless process in the early time of interaction when plasma boundary is sharp [89]. Firstly, the “vacuum” as mentioned by Brunel may not be a real vacuum. Electrostatic field exists in the target vicinity (as we shall show here) that plays a crucial role for an electron’s dynamics before it is liberated from the target or directed into the target. It can not gain a net energy, unless there is any nonlinear interaction through the nonlinear space-charge field within the target and/or in the target vicinity. Therefore, “vacuum heating” is improper. The *crucial* assumption in this model is that electrons experience *no net* field while they return to the target. As a consequence Brunel’s electron flow becomes laminar, meaning that their trajectories do not cross each other within a laser period irrespective of the laser intensity. We point out that, since different electrons originate from different parts of the target they experience different electrostatic fields and originate with different initial phases. When driven by a laser, their trajectory crossing is unavoidable at a later time. Detail analysis showing deficiency in Brunel’s “vacuum heating” is given in Ref. [143]. Brunel electrons, upon returning to the target, experience a field free region due to complete cancellation of induced electrostatic field by the laser field. Thus, the velocities acquired during their traversal in the vacuum are fully re-

Chapter 3. Identification of anharmonic resonance absorption

tained, they do not have chance to give energy back (even partly) to the electromagnetic field. In the context of laser-cluster interaction, induced electrostatic fields can not be fully compensated by the laser field (induced field may exceed the laser field) and cluster interior is rarely field free (as shown in this work) during the laser interaction. Otherwise, ionization ignition [15] can not happen and higher charge states [17, 67, 69, 144] of ions can not be created. In this sense, Brunel effect is incomplete, warrant a re-look into the problem and search for an appropriate mechanism behind the laser absorption.

On the other hand, let us suppose that there is an anharmonic potential created at the target front (or in the target interior) due to the laser interaction. Such a potential is inevitably formed (for any finite size target) at the ion-vacuum boundary (where laser interacts first) due to $\sim 1/r$ fall of the potential which may be asymmetric. Anharmonicity in the potential also appears due to local charge non-uniformity (via ionization, concentrated electron cloud etc.) in a laser driven plasma. The frequency Ω of an electron in such a potential is dependent on its position r . When driven by a laser field, its r changes with time which makes $\Omega(r)$ time dependent, i.e., $\Omega[r(t)]$. An initially bound electron, starting from some location in the overdense plasma potential, while becoming free must experience the $\sim 1/r$ Coulomb tail of the potential and the corresponding $\Omega[r(t)]$ of the electron must meet ω while trying to come out of the potential. This dynamical resonance - the anharmonic resonance (AHR) - occurring in an anharmonic potential was studied before using a model and three dimensional PIC simulations of laser driven clusters [14]. However, collisionless processes and AHR phenomenon remain to be a debate [88, 143, 145]. In numerical simulations it is often obscured due to many body nature of interaction, since it needs clear examination of individual electron trajectory, identification of corresponding $\Omega[r(t)]$ and a dynamical mapping of $\Omega[r(t)]$ on to ω . To prove AHR for a laser driven cluster a three dimensional MD simulation code with soft-

core Coulomb interactions among charge particles has been developed. By following the trajectory of each MD electron and identifying its time-dependent frequency $\Omega[r(t)]$ in the self-generated anharmonic plasma potential it is found that electron leaves the potential and becomes free only when AHR condition $\Omega[r(t)] = \omega$ is met. Thus, for the first time, our MD simulation clearly identifies AHR process in the laser cluster interaction. We further introduce a non-linear oscillator model that brings out most of the features of MD electrons while passing the AHR. Thus, we bridge the gap between PIC simulations, analytical models and MD calculations.

We consider a single deuterium cluster of radius $R = 2.05$ nm, Wigner-seitz radius $r_w = R/N^{1/3} \approx 0.17$ nm and number of atoms $N = 1791$. It is irradiated by 800 nm wavelength laser pulses of various intensity giving density $\rho \approx 27.3\rho_c$ and $\omega_p^2/3\omega^2 = \omega_M^2/\omega^2 \approx 9.24$; where $\rho_c = \omega^2/4\pi$ is the critical density at 800 nm and ω_p is the plasma frequency. These parameters of the cluster are kept unchanged throughout this chapter.

The outline of the present chapter is as follows: Section 3.2 illustrates AHR by a simple model of a cluster while Sec.3.3 proves the hypothesis of AHR by detailed MD simulations. A summary of the present study is given in Sec.3.4.

3.2 Model for anharmonic resonance absorption

Before studying the laser-cluster interaction by MD simulations, we show here various features of AHR by a model of a cluster which will provide an easy interpretation of MD results in Sec.3.3. Although the rigid sphere model is a very simple approximation of clusters, it provides significant qualitative understanding of efficient energy absorption by clusters. The schematic of a simple RSM is shown in Fig. 3.1. In the model, cluster is assumed to be pre-ionized and consists of homogeneously charged spheres of massive ions and much lighter electrons of equal radii $R_i = R_e = R_0$. When their centers coincide

Chapter 3. Identification of anharmonic resonance absorption

plasma becomes charge neutral. The motion of ions can be neglected for short laser pulses < 50 fs and non-relativistic laser intensities $< 10^{18} \text{ Wcm}^{-2}$ as considered in this work. Thus ion sphere provides a sharp boundary with zero density gradient scale-length at the vacuum plasma boundary.

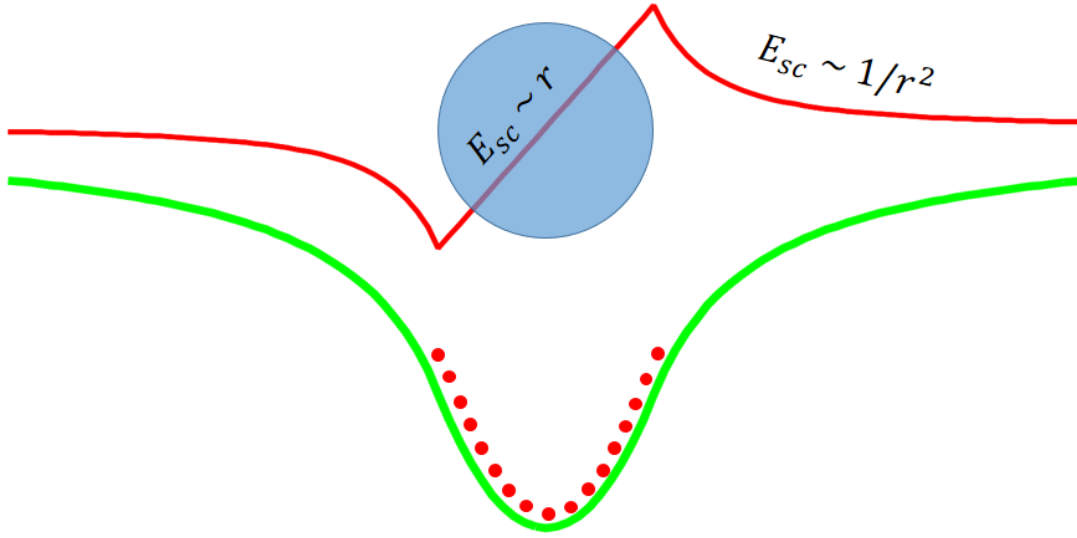


Figure 3.1: Schematic of the rigid sphere model. The positively charged ion sphere is at rest which provides the background potential 3.3 shown in solid green line in which non-interacting electron spheres (red dots) are uniformly placed. Corresponding electrostatic restoring field 3.2 is plotted with solid red line which shows field is harmonic inside the cluster and becomes anharmonic outside the cluster boundary.

The equation of motion (EOM) of the electron sphere in a linearly polarized laser field along x -direction reads

$$\frac{d^2 \vec{r}}{dt^2} + \frac{\vec{r}}{r} g(r) = \hat{x} (q_e/m_e) E_l(t)/R_0 \quad (3.1)$$

where $\vec{r} = \vec{x}/R_0$ and $r = |\vec{r}|$. The electrostatic restoring field

$$g(r) = \omega_M^2 \times \begin{cases} r & \text{if } 0 \leq r \leq 1 \\ 1/r^2 & \text{if } r \geq 1, \end{cases} \quad (3.2)$$

can be derived by Gauss's law. It shows that as long as the excursion r of the center of the electron sphere remains inside the ion sphere, it experience a harmonic oscillation with a constant eigen-frequency ω_M . Crossing the boundary of the ion sphere, it begins to experience the Coulomb force and its motion becomes anharmonic with gradual reduction in the eigen-frequency for increasing excursion from the center of the ion sphere. The nonlinear restoring field (3.2) is simpler than used earlier [99, 146]. Nevertheless, it exhibits all features AHR phenomena elegantly, e.g., prompt generation of electrons within a time much shorter than a laser period, crossing of electron trajectories and subsequent non-laminar electron flow [88]. It neglects the interaction of diffuse boundary of the electron sphere with the sharp boundary of the ion sphere, *but* allows us to calculate $\Omega[r]$ of the electron sphere analytically for an arbitrary excursion which is not possible with the $g(r)$ in Refs.[99, 146]. The electrostatic potential corresponding to Eq.(3.2) reads

$$\phi(r) = \omega_M^2 R_0^2 \times \begin{cases} 3/2 - r^2/2 & \text{if } 0 \leq r \leq 1 \\ 1/r & \text{if } r \geq 1. \end{cases} \quad (3.3)$$

The cluster size being much smaller than the laser wavelength $\lambda = 800$ nm as considered in this work, the dipole approximation for the laser vector potential $A(z, t) = A(t) \exp(-i2\pi z/\lambda) \approx A(t)$ is assumed. Thus, the effect of propagation of light (directed in z) is disregarded. The driving field of the laser can be derived from the re-

Chapter 3. Identification of anharmonic resonance absorption

lation $E_l(t) = -dA/dt$ which is already shown in chapter 2. Here we re-write the expression for the electric field component of the laser derived from the vector potential $A(t) = (E_0/\omega) \sin^2(\omega t/2n) \cos(\omega t)$ for $0 < t < nT$;

$$E_l(t) = (E_0/\omega) \begin{cases} \sum_{i=1}^3 c_i \omega_i \sin(\omega_i t) & \text{if } 0 < t < nT \\ 0 & \text{otherwise;} \end{cases} \quad (3.4)$$

where n is the number of laser period T , nT is the total pulse duration and E_0 is the field strength corresponding to an intensity $I_0 = E_0^2$. $c_1 = 1/2, c_2 = c_3 = -1/4, \omega_1 = \omega, \omega_2 = (1 + 1/n)\omega$, and $\omega_3 = (1 - 1/n)\omega$. Eq.(3.4) leads to the correct dynamics of a free electron [71] even for very short sub-cycle pulses in contrast to the often used \sin^2 -pulses [13, 18, 36, 87].

3.2.1 Effective frequency of the electron sphere

In the absence of a driver, the eigen-period T of oscillation of the electron sphere in the potential (3.3) can be calculated from

$$T = \frac{4R}{\sqrt{2}} \int_0^{r_m} \frac{dr}{\sqrt{\Phi(r_m) - \Phi(r)}}. \quad (3.5)$$

Here $\Phi(r_m) = q_e \phi(r_m)$ is the potential energy stored in the oscillator at an initial distance $r = r_m$ from where it is left freely in the potential at a time $t = 0$. For $0 \leq r_m \leq 1$, Eq. (3.5) yields a constant $T = 2\pi/\omega_M$ and the effective frequency of oscillation of the electronic sphere as

$$\Omega(r) = 2\pi/T = \omega_M. \quad (3.6)$$

When $r_m > 1$, we write $T = T_1 + T_2$ with $T_1/4$ as the time required for $r = 1$ to $r = 0$

and $T_2/4 = \frac{R}{\sqrt{2}} \int_{r_m}^1 \frac{dr}{\sqrt{\Phi(r_m) - \Phi(r)}}$ is the time required for $r = r_m$ to $r = 1$ which give

$$\begin{aligned} T_1 &= \frac{4}{\omega_M} \left[\sin^{-1} \left(\sqrt{r_m / (3r_m - 2)} \right) \right], \\ T_2 &= \frac{(2r_m)^{3/2}}{\omega_M} \left[\sin^{-1} \left(\sqrt{(r_m - 1)/r_m} \right) + \sqrt{(r_m - 1)/r_m^2} \right]. \end{aligned} \quad (3.7)$$

The expression for T_1 is obtained from the harmonic solution $r_{\text{in}} = \sqrt{R^2 + v_R^2 / \omega_M^2} \sin(\omega_M(t - T_2/4) + \arctan(\omega_M R / v_R))$ inside the cluster satisfied by the electron that enters the surface of the cluster with the velocity $v_R = -\omega_M R \sqrt{2(r_m - 1)/r_m}$ (obtained from the energy conservation) at $t = T_2/4$. If the electron starts at the surface of the cluster, i.e., at $r_m = 1$, we get $T_1 = 2\pi/\omega_M$, $T_2 = 0$ and recover Eq.(3.6) with $T = T_1$. The effective frequency $\Omega(r) = 2\pi/(T_1 + T_2)$ now depends on the excursion amplitude $r = r_m$, since the electron sphere interacts with the nonlinear part of the restoring field. In a laser field excursion changes with time. Thus $\Omega[r(t)]$ depends on t when $r(t) > 1$. In more realistic MD simulations of clusters, there is no pre-defined potential (as Eq.(3.3)) in which electrons oscillate. Therefore, finding $\Omega(r)$ analytically is not possible in MD. From Eq. (3.1) we formally write (in analogy with a harmonic oscillator) the square of $\Omega(r)$ as the ratio of restoring field to the excursion of the electron sphere [14]

$$\Omega^2[r(t)] = \frac{g[r(t)]}{r(t)} = \frac{\text{restoring field}}{\text{excursion}}. \quad (3.8)$$

Note that for a harmonic oscillator above relation yields the correct eigen frequency Ω_h with $g(r) = \Omega_h^2 r$.

Analytical result of the normalized effective frequency Ω/ω using (Eqns.(3.6)-(3.7)) as a function of excursion (r_m) of the electron sphere in the potential (3.3) is plotted

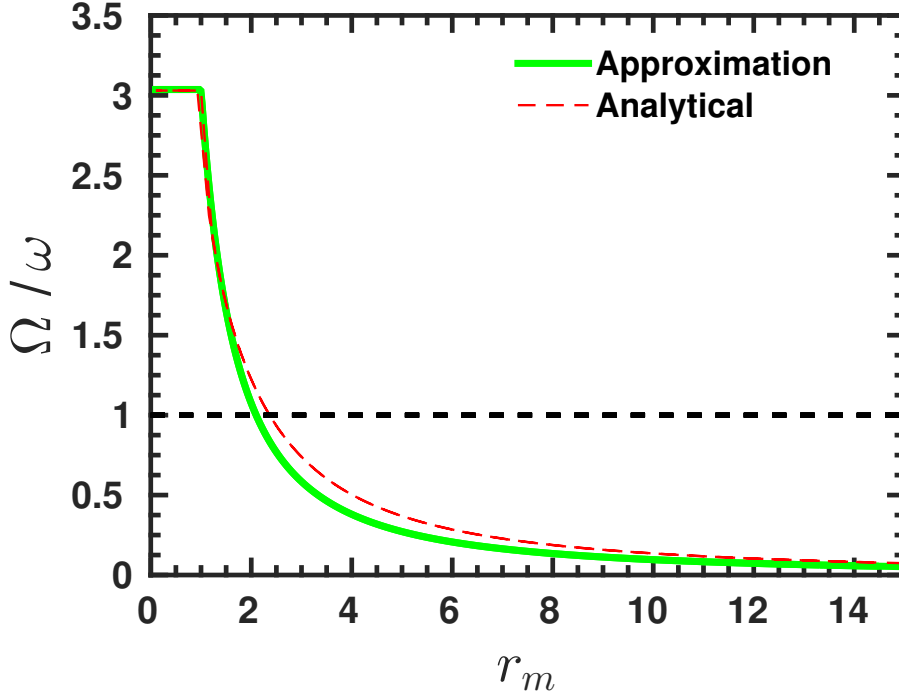


Figure 3.2: Normalized effective frequency Ω/ω of the electron sphere versus its excursion amplitude r_m for a deuterium cluster of radius $R = 2.05$ nm, Wigner-seitz radius $r_w \approx 0.17$ nm and number of atoms $N = 1791$, density $\rho \approx 27.3\rho_c$ and $\omega_M^2/\omega^2 \approx 9.24$; where $\rho_c = \omega^2/4\pi$ is the critical density at $\lambda = 800$ nm. Numerical approximation using Eq.(3.8) and the analytical result using Eqns.(3.6)-(3.7) are comparable. Vertical dashed lines indicate AHR is expected near $r_m \approx 2$ according to Eq.(3.8) and $r_m \approx 2.5$ according to Eq.(3.7).

in Fig. 3.2. Numerical solution of Eq. (3.1) (without the laser field) gives $r(t)$ and corresponding Ω/ω from Eq. (3.8). This numerical approximation is also plotted in Fig. 3.2 which matches reasonably well with the analytical Ω/ω . As the electron sphere moves away from harmonic region of the potential, Ω/ω starts decreasing. At a distance of $r_m \approx 2$, the AHR condition $\Omega/\omega \approx 1$ is satisfied. If the laser field is strong enough to bring the electron sphere at a value of $r(t) = r_m \approx 2$, the electron sphere may gain significant energy from the laser field via such AHR.

3.2.2 Dynamics of the electron sphere in the laser field

The dynamical behaviour of the electron sphere (for the above cluster) irradiated by a $n = 5$ -cycle pulse (3.4) of duration $nT = 13.5$ fs and peak intensity 5×10^{15} W/cm² is now studied. Figure 3.3(a-d) depicts the normalized value of the square of the frequency $\overline{\Omega}^2(r) = \Omega^2(r)/\omega^2$ using Eq.(3.8), excursion $\bar{x} = x/R$, total energy $\overline{\mathcal{E}}_t = \mathcal{E}_t/U_p$ and the laser field $\overline{E}_l = E_l/E_0$ versus the normalized time $\bar{t} = t/T$ for the electron sphere placed at four different initial locations $|\bar{x}| < 1$ in the potential. Initially, spheres are bound with different energies (near $\overline{\mathcal{E}}_t \approx -4$) where they experience a constant frequency $\Omega[r(0)] = \omega_M$. Up to $t/T \lesssim 2.0$, in Fig.3.3(a), the laser field strength is not sufficient to liberate the electron sphere from the potential. In the oscillating laser field, at times \bar{x} exceeds unity with a decrease in $\overline{\Omega}^2$ from $\omega_M^2/\omega^2 \approx 9.24$ and the corresponding increase in $\overline{\mathcal{E}}_t$. The decrease of $\overline{\Omega}^2[r(t)]$ being insufficient to meet the AHR condition $\overline{\Omega}^2[r(t)] \approx 1$ (dashed horizontal line), particle can not absorb sufficient energy to come out completely but pulled back towards the potential center (see the reversal of \bar{x} and $\overline{\Omega}^2$ near $t/T \approx 1.9$) by the restoring force due to the ion sphere. As it reverses its direction and emerges on the other side of the potential with $\bar{x} < 0$; the increasing laser field towards its peak value (i.e., $\overline{E}_l \sim 1$) after $t/T \approx 2.0$ helps $|\bar{x}|$ to exceed unity with a fast drop of $\overline{\Omega}^2$ for $t/T > 2.1$. Around $t/T \approx 2.2$ (indicated by vertical dashed line), $\overline{\Omega}^2$ meets the AHR condition with $|\bar{x}| \approx 2$. The fact that AHR truly occurs at an excursion $|\bar{x}| \approx 2$ is in agreement with Fig.3.2. It also justifies the robustness of the formal approximation (Eq.(3.8)) for retrieving the effective frequency from the numerical model. After the AHR (i.e., $t/T > 2.2$) particle becomes completely free with $\overline{\Omega}^2[r(t)] \approx 0$ and final energy $\overline{\mathcal{E}}_t \geq 0$.

Figures 3.3(c-d) show electron spheres undergoing AHR at $t/T = 2.7, 3.2, 3.7$ respectively. Since initial positions are different, they have different initial phases and

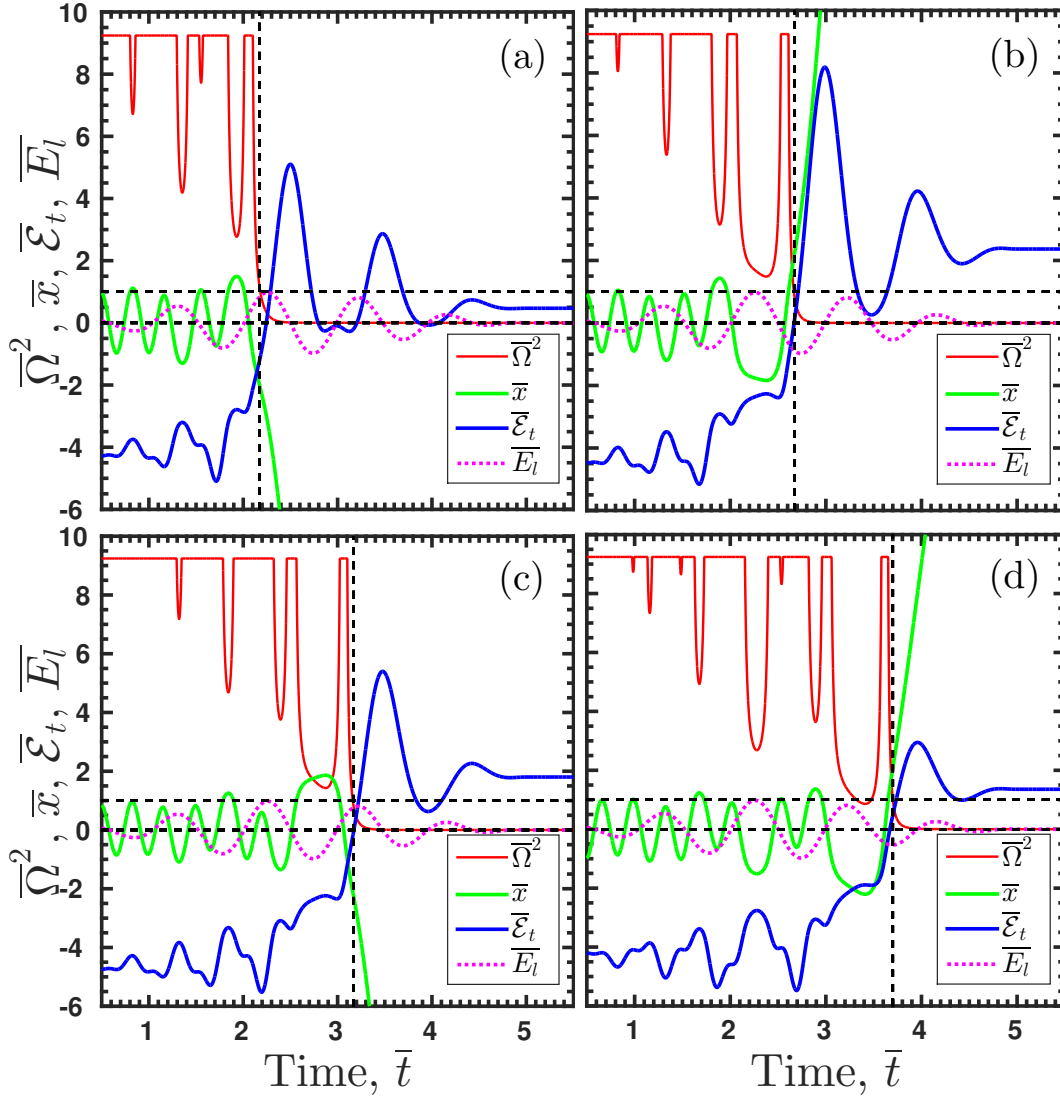


Figure 3.3: Normalized value of the square of the effective frequency $\bar{\Omega}^2(r)$, excursion \bar{x} , total energy $\bar{\mathcal{E}}_t$ and the laser field \bar{E}_l versus the normalized time $\bar{t} = t/T$ for four electron spheres undergoing AHR at successive times (a) $\bar{t} = 2.2$, (b) $\bar{t} = 2.7$, (c) $\bar{t} = 3.2$, (d) $\bar{t} = 3.7$. The deuterium cluster of Fig.3.2 is irradiated by a $n = 5$ -cycle pulse of peak intensity $5 \times 10^{15} \text{ W/cm}^2$.

experience different restoring fields and total fields even though same laser field acts on them. As a result they are emitted at different times from the potential experiencing the AHR with different laser field strengths. Electron spheres experiencing AHR at a higher driving field strength generally acquire higher energies after the pulse as in Figs.3.3(a-

c). Some electrons may also exhibit [as in Fig.3.3(d)] multiple AHR: they leave the cluster potential through AHR, return to the cluster interior by the laser field (or by the stronger restoring field than the laser field) and finally become free with a net positive energy via the AHR.

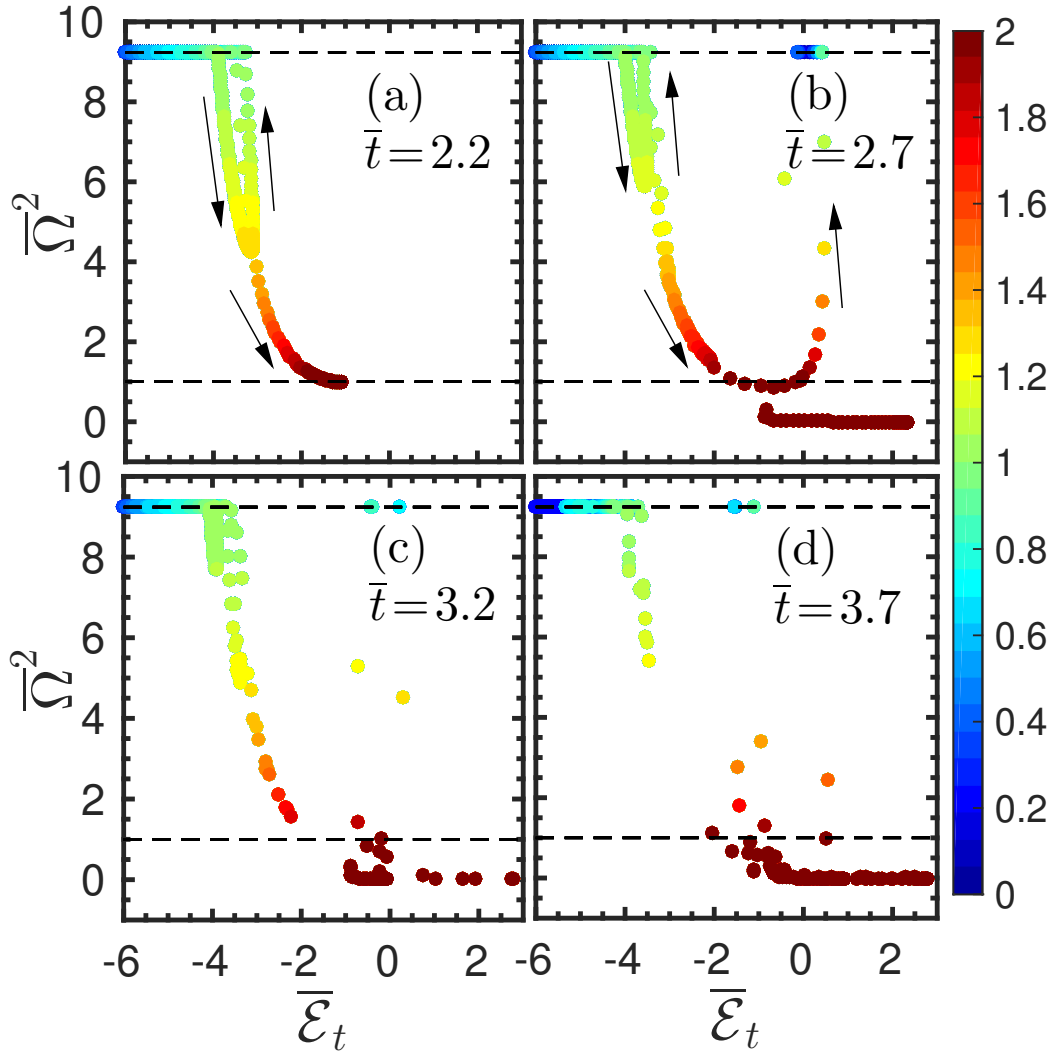


Figure 3.4: Snapshots of $N = 1791$ non-interacting electron spheres in the $(\bar{\mathcal{E}}_t, \bar{\Omega}^2)$ plane at times (a) $\bar{t} = 2.2$, (b) $\bar{t} = 2.7$, (c) $\bar{t} = 3.2$, (d) $\bar{t} = 3.7$ corresponding to Fig.3.3. As the laser field strength increases with time, more and more electrons are drawn towards the line of AHR, i.e, dashed line at $\bar{\Omega}^2 \approx 1$. The parameters of laser and cluster are same as in Fig.3.3.

Chapter 3. Identification of anharmonic resonance absorption

In this model electrons are frozen into a single sphere. Whereas, in reality, electrons in a cluster distinctly move even with a low intensity short laser pulse. Such a multi-electron system with all possible electrostatic interactions will be considered in detail by MD simulations in Sec.3.3. To gain some more physical insight on the dynamics of electrons in a multi-electron cluster and the AHR through the above model, we consider $N = 1791$ non-interacting electron spheres (mimicking the multi-electron system) placed uniformly inside the ion sphere. Each electron sphere mimics a real point size electron.

Figures 3.4(a-d) show snapshots of all non-interacting electron spheres (each dot represents a sphere) in the energy versus effective frequency plane at times $\bar{t} = 2.2, 2.7, 3.2, 3.7$ corresponding to Figs.3.3(a-d). Colors indicate their normalized positions. In an early time $t/T = 2.2$ [in Fig.3.4(a)] a large fraction of electrons are bound in the harmonic part of the potential with frequency $\bar{\Omega}^2 = \omega_M^2/\omega^2 = 9.24$ and excursion $r < 1$ (dark blue to light blue). Some electrons first come out of the harmonic part and continue in the anharmonic part of the potential with a drop in $\bar{\Omega}^2$ (up to 4) and increasing excursion $1 < r < 1.3$ (light green to yellow). But the restoring field on them being higher than the laser field they return to the cluster (see reversal of electrons with change of colors green-yellow-green in the U-shaped lobe) and become bound. At this time a few electrons (dark red to brown) are aligned towards the line of AHR (horizontal dashed line) with excursion $r \approx 2$ and frequency $\bar{\Omega} \approx 1$. At a later time $t/T = 2.7$ [in Figs.3.4(b)], phase of the laser field is reversed with nearly the same strength. Apart from bound and returning electrons [as in Fig.3.4(a)], it is clear that many electrons are now drawn towards the line of resonance, some are already free during this half laser cycles between $t/T = 2.2 - 2.7$ due to change in the field. Beyond $t/T = 2.5$ [in Figs.3.4(b-d)] laser field strength becomes weaker than the restoring field on some quasi-free electrons.

Those electrons (typically having low energies) are dragged inside the cluster (see their color changes from brown to yellow) even though they were made free via the AHR earlier.

Thus a simple nonlinear oscillator model brings out most of the physics of AHR phenomena for a laser driven cluster in the temporal domain (Fig.3.3) as well as in the energy versus frequency domain (Fig.3.4). The identification of the effective dynamical frequency $\Omega[r(t)]$ of the driven oscillator in the numerical model and the liberation of particles from the cluster potential only when Ω matches the resonance condition $\Omega \approx \omega$, clearly justifies the robustness of the formal approximation in Eq.(3.8) and permits its application in the self-consistent MD simulations in Sec.3.3.

3.3 Anharmonic resonance absorption using molecular dynamics simulation

It is mentioned that in the above model electrons are frozen in a sphere which moves in a predefined attractive potential due to the ion sphere. In reality, the potential of the ionized cluster varies with the time to time redistribution of charges. In the initial time, when cluster is charge neutral, potential must start from a zero value. Electrons may also face repulsive potential due to concentrated electron cloud in some part of the cluster. In the model, the electron sphere either stays inside (0% outer ionization) the cluster or completely goes out of the cluster (100% outer ionization) for a given laser intensity. However, there is always a certain fraction of outer ionized electrons even at an intensity just above the inner ionization threshold. These shortcomings of the model can be addressed by MD simulation. In this section we present results obtained from three-dimensional MD simulations.

3.3.1 Required details of molecular dynamics simulation

Extensive details of the new MD simulation code is given in chapter 2 for the study of laser-cluster interaction. Here we again highlight the initial configuration of the cluster, governing EOM, expression for interacting force and potential. Particular attention is given to the identification of AHR process using MD simulation. Cluster is assumed to be pre-ionized. $N_i = N_e = 1791$ number of ions and electrons are uniformly distributed in fixed cluster radius $R = 2.05$ nm. This may be regarded as a situation where ionization has already taken place by a pump pulse and subsequent interaction of a probe pulse is studied. Electron-electron, ion-electron and ion-ion interactions through the Coulomb field are taken into account. Binary collisions among particles are neglected since we are interested in collisionless processes. We recall the EOM of i -th particle of charge q_i due to all j -th particles each of charge q_j in the system in a linear polarized laser field, polarized in x and propagating in z (in the dipole approximation) from chapter 2,

$$m_i \frac{d\vec{v}_i}{dt} = \vec{F}_i(r_i, v_i, t) + \hat{x} q_i E_l(t) + q_i \vec{v}_i \times \hat{y} B_l(t), \quad (3.9)$$

Force and potential are modified with a smoothing parameter $r_0 = r_\omega$, added with r_{ij} to soften the potential and corresponding force. The modified Coulomb force on i -th particle and the corresponding potential at its location are

$$\vec{F}_i = \sum_{j=1, i \neq j}^{N_p} \frac{q_i q_j \vec{r}_{ij}}{(r_{ij}^2 + r_0^2)^{3/2}}, \quad \phi_i = \sum_{j=1, i \neq j}^{N_p} \frac{q_j}{(r_{ij}^2 + r_0^2)^{1/2}}. \quad (3.10)$$

Equation (3.9) is solved using the velocity Verlet time integration scheme [123] (discussed in chapter 2) with a uniform time step $\Delta t = 0.01$ a.u..

3.3.2 Laser energy absorption and outer ionization

The MD code is now used to study interaction of $n = 5$ -cycle laser pulse of duration $nT = 13.5$ fs with the deuterium cluster as in Sec.3.2. Initially, cluster has equal number of uniformly distributed ions and electrons (i.e., $N_i = N_e = N$) so that it is macroscopically charge neutral.

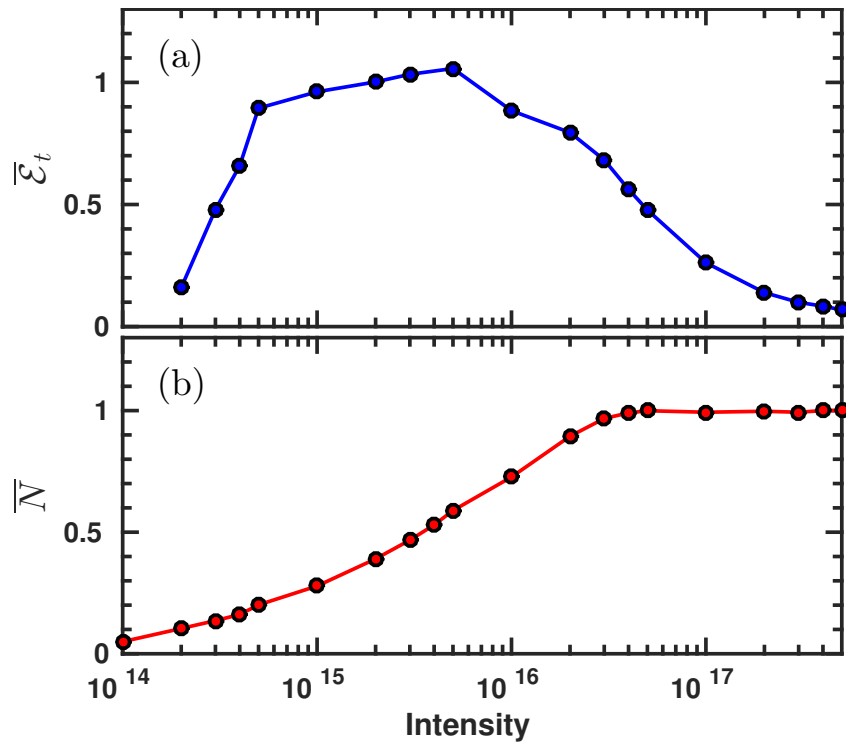


Figure 3.5: Total absorbed energy per electron in units of U_p (top) and fractional outer ionization (bottom) versus the laser intensity for a deuterium cluster of radius $R = 2.05$ nm, and number of atoms $N = 1791$, density $\rho \approx 27.3\rho_c$ and $\omega_M^2/\omega^2 \approx 9.24$. Cluster is illuminated by a $n = 5$ -cycle laser pulse of wavelength 800 nm and various peak intensity.

Figure 3.5 shows total absorbed energy per electron normalized by of U_p and corresponding degree of outer ionization at the end of the laser pulse as the peak intensity is varied. Normalized absorption per electron [in Fig.3.5(a)] attains a maximum between intensities $5 \times 10^{15} - 10^{16} \text{ Wcm}^{-2}$. This nonlinear variation of absorbed energy with

intensity is similar to that reported earlier using PIC simulations [14] of xenon clusters. The outer ionized fraction [in Fig.3.5(b)] of electrons, on the other hand, increases gradually with the peak intensity and saturates at unity (%100 outer ionization) at some higher intensity even for this short 5-cycle pulse. At an intensity $5 \times 10^{15} \text{ Wcm}^{-2}$, it is inferred that almost 60% electrons are outer ionized ($\bar{N} \approx 0.6$) which contribute to the total absorbed energy of $\approx 2000 U_p$.

3.3.3 Analysis of electron trajectory and finding the AHR

The high level of absorption and outer ionization shown in Fig.3.5 with a short 13.5 fs laser pulse is certainly not due to the linear resonance process. Figures 3.6(a-b) show normalized space charge field $\bar{E}_x^{sc} = E_x^{sc}(t)/E_0$ and the total field $\bar{E}_x^t = E_x^t(t)/E_0$ versus excursion $\bar{x}(t)$ of a few selected outer ionized electrons (only 29 electrons are plotted) at the peak intensity $5 \times 10^{15} \text{ Wcm}^{-2}$ of Fig.3.5. Corresponding $\bar{x}(t)$ versus \bar{t} are shown in Fig.3.6(c). The crossing of trajectories of MD electrons [in Fig.3.6(c)] emitted from the cluster at different times, their non-laminar motion in time, the uncompensated laser field by the space charge field [in Fig.3.6(a)] and the corresponding non-zero total field [in Fig.3.6(b)] inside the cluster ($-1 \leq \bar{x} \leq 1$) clearly suggest that absorption is not due the celebrated Brunel effect [89]. The underlying mechanism can be understood by analyzing trajectories of those MD electrons and finding the corresponding effective frequency as shown by the model in Sec.3.2.2. We write the time dependent frequency of the i -th MD electron (in analogy with Eq.(3.8)) as

$$\Omega^2[r_i(t)] = \frac{\vec{E}_i^{sc}(\mathbf{r}_i, t) \cdot \mathbf{r}_i}{r_i^2} = \frac{\text{restoring field}}{\text{excursion}} \quad (3.11)$$

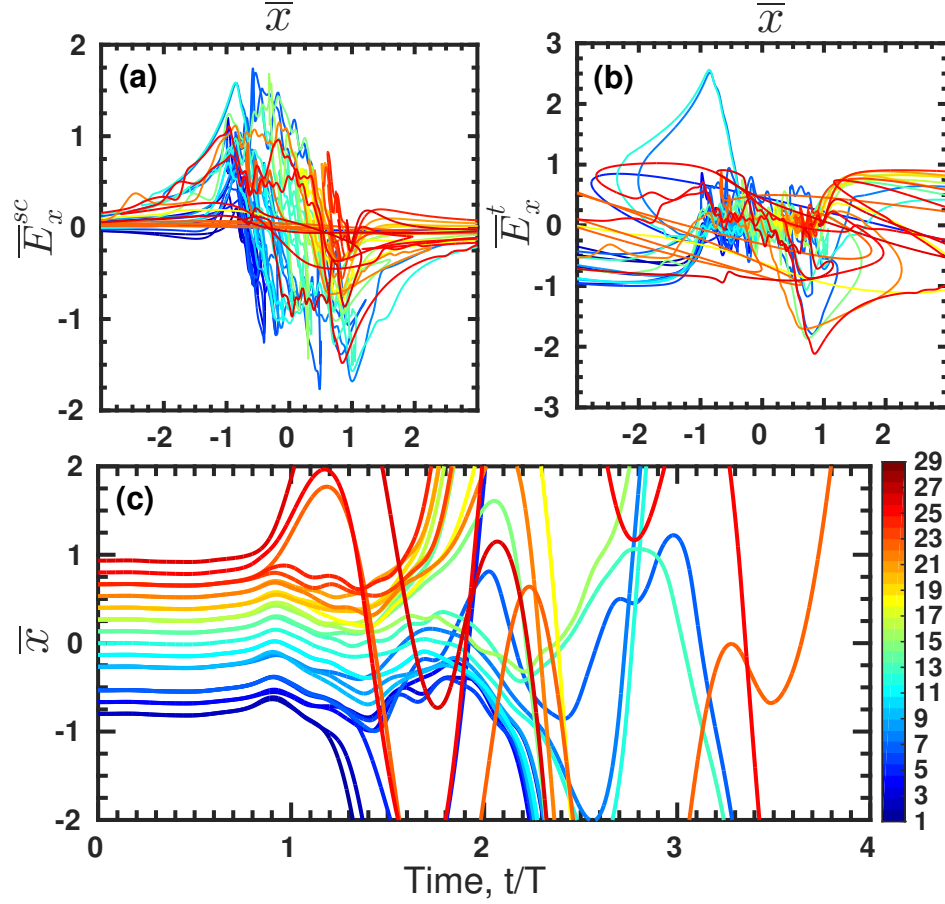


Figure 3.6: (a) Normalized self-generated space-charge field ($E^{sc}(t)/E_0$) and (b) normalized total field ($E_t(t)/E_0$) versus normalized excursion $x(t)/R$ of a few selected outer ionized electrons (only 29 electrons out of $N = 1791$ are plotted, color bar indicates their index $i = 1 - 29$) at a peak intensity of $5 \times 10^{15} \text{ Wcm}^{-2}$. Corresponding trajectories $x(t)/R$ versus t/T are shown in (c). All other the parameters of cluster and the laser are same as in Fig 3.5.

where $\vec{E}_i^{sc} = \vec{F}_i/q_i$ is the electrostatic field on the i -th MD electron obtained from Eq. (3.10).

Figures 3.7(a-b) show different normalized quantities, i.e., frequency squared $\overline{\Omega}^2$, excursion \overline{x} , total energy $\overline{\mathcal{E}}_t$, laser field \overline{E}_l versus normalized time \bar{t} for selected MD electrons which are outer ionized at times: (a) $\bar{t} = 1.1$ and (b) $\bar{t} = 2.2$ from the cluster irradiated by the same 5-cycle laser pulse of peak intensity $5 \times 10^{15} \text{ Wcm}^{-2}$. Initially,

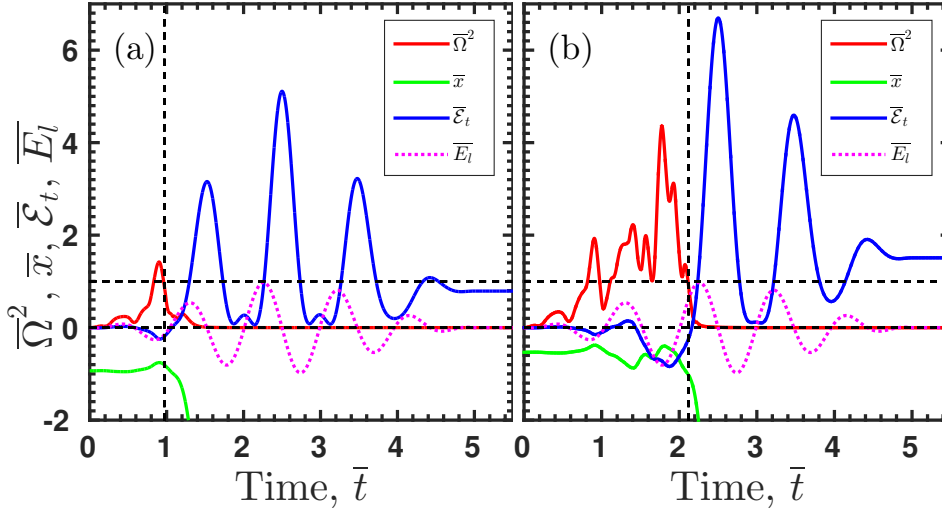


Figure 3.7: Normalized value of the square of the effective frequency $\bar{\Omega}^2(r)$, excursion \bar{x} , total energy $\bar{\mathcal{E}}_t$ and the laser field \bar{E}_l versus the normalized time \bar{t} for different MD electrons undergoing AHR and outer ionization at times (a) $\bar{t} = 1.1$, (b) $\bar{t} = 2.2$. The cluster is irradiated by a $n = 5$ -cycle pulse of peak intensity $5 \times 10^{15} \text{ W/cm}^2$. These results resemble with the results of model analysis in Fig. 3.3.

the cluster is charge neutral, electrostatic field is zero inside the cluster and all particles are at rest. As a result, the effective frequency $\Omega([r(t)])$ and total energy $\bar{\mathcal{E}}_t$ of each electron is zero. As the laser field is switched on, the charge separation potential and the corresponding field are dynamically created due to the movement of more mobile electrons than the slow moving ions. The MD electron in Fig. 3.7(a) is first attracted inside such potential by the restoring force due to ions (see its excursion $|\bar{x}|$ decreases towards the center of the cluster and total energy starts becoming negative) where its effective frequency $\Omega[r(t)]$ after increasing from zero exceeds the laser frequency ω and goes to a maximum value when its total energy reaches a minimum negative value (i.e, it becomes more bound in the potential). From this point onwards the dynamics of the MD electron is very similar to the electron sphere in the model. As the laser field changes further, electron is pulled towards the negative x -direction, $|\bar{x}|$ increases beyond unity, $\bar{\Omega}^2$ drops from its maximum and crosses the line of AHR (horizontal dashed line

where $\bar{\Omega}^2 = 1$) near $t/T \approx 0.95$ with the corresponding increase in $\bar{\mathcal{E}}_t$ from negative to positive value (bound to free motion) similar to that shown in Fig.3.3 using the model. After the AHR, electron leaves the cluster forever with a total energy of $0.8U_p$ in the end of the pulse. In this early time of interaction, the laser field being very weak, only the loosely bound outer most electrons as compared to the core electrons leave the cluster. Such early leaving electrons which experience AHR in a shallower potential with a low laser field strength generally carry low kinetic energies. As the laser field increases to its peak value, more electrons are outer ionized from the core of the cluster [as in Fig.3.7(b)]. They experience a relatively deeper potential. Electrons while moving in deep potentials have relatively higher $\Omega[r(t)]$ [clear from 3.7(b)] and they require higher field strengths for their liberation. Indeed, MD electron in Fig.3.7(b) becomes free when its $\bar{\Omega}^2$ passes the resonance line $\bar{\Omega}^2 = 1$ after dropping from its maximum value and its energy $\bar{\mathcal{E}}_t$ becomes positive at $\bar{t} \approx 2.2$ as the peak of the pulse is approached.

The occurrence of AHR for MD electrons in Fig.3.7 resemble with Fig.3.3 in the model in Sec.3.2 except that frequency and potential start from zero and self-consistently generated in the case of MD while those are predefined in the model.

3.3.4 AHR in the frequency vs energy plane

To prove that all MD electrons essentially pass through AHR during their outer ionization, Figures 3.8(a-d) show snapshots of all electrons in the $(\bar{\Omega}^2, \bar{\mathcal{E}}_t)$ plane at different times $\bar{t} = 1.1, 1.7, 2.2, 3.2$ respectively. Colors indicate normalized positions (r) of those electrons as in the Fig.3.4. From Fig. 3.8 it is clear that each electron leaves the cluster ($r > 1$, green to dark red) and its energy becomes positive *only* when it crosses the line of AHR (dashed horizontal line at $\bar{\Omega}^2 = 1$). After becoming free, electrons have zero effective frequency as they are beyond the influence of the electrostatic field.

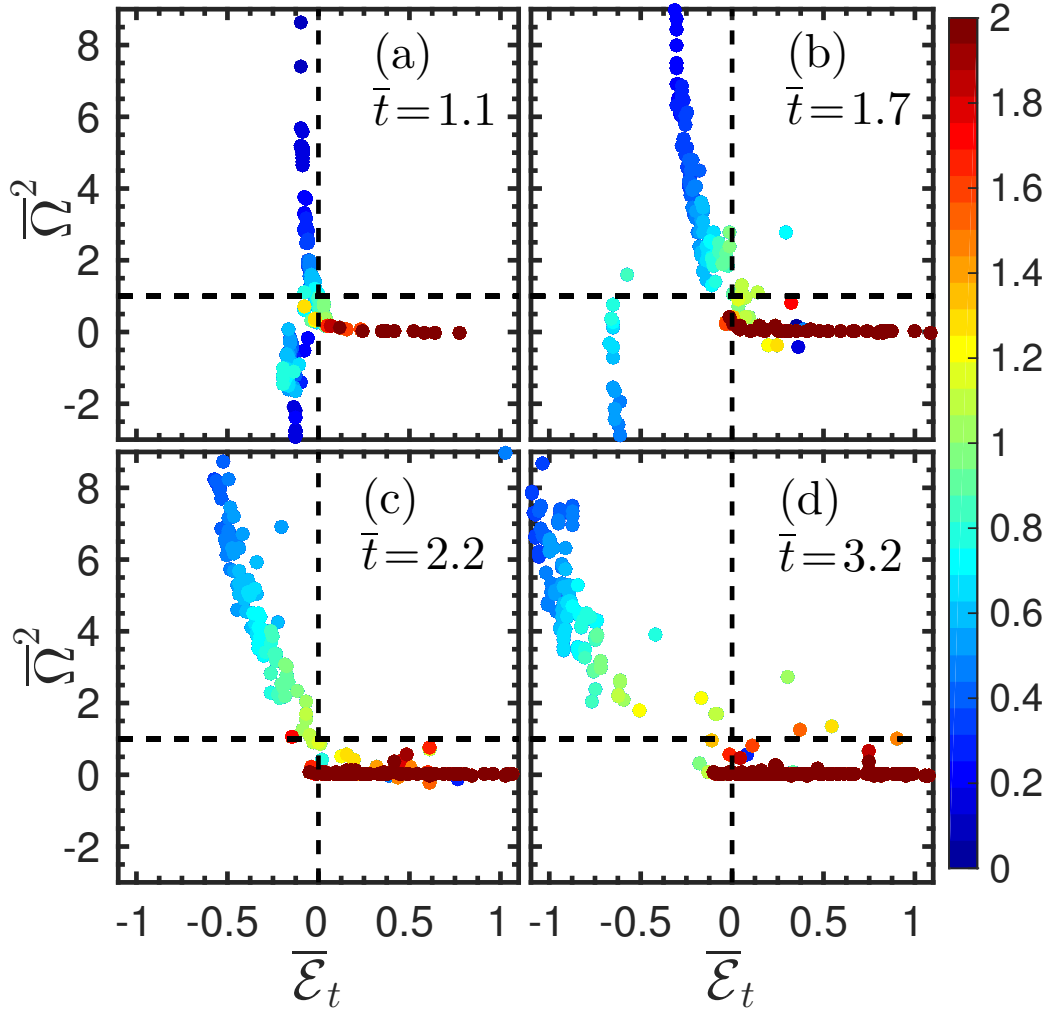


Figure 3.8: Snapshots all MD electrons in the $(\bar{\mathcal{E}}_t, \bar{\Omega}^2)$ plane at times (a) $\bar{t} = 1.1$, (b) $\bar{t} = 1.7$, (c) $\bar{t} = 2.2$, (d) $\bar{t} = 3.2$. As the laser field strength increases with time, more and more electrons are drawn towards the line of AHR, i.e, dashed line at $\bar{\Omega}^2 \approx 1$. The parameters of laser and cluster are same as in Fig.3.7.

In the early time $\bar{t} = 1.1$, in Fig.3.8(a), only few electrons are outer ionized from the cluster and the resulting potential is shallow. As a result energies $(\bar{\mathcal{E}}_t)$ of the bound electrons are very close to zero but negative. Some of the bound electrons have negative $\bar{\Omega}^2$ due to the repulsion of the compressed electron cloud in their vicinity at this early time.

At later times $\bar{t} = 1.7, 2.2$, in Figs.3.8(b)-(c), as the laser field approaches its peak value, an increasing number of electrons are outer ionized via the AHR channel. As a result the potential depth gradually increases, remaining bound electrons move to a deeper potential due to the gradually stronger attractive force of the uncompensated bare ionic background, the population of negative $\bar{\Omega}^2$ valued electrons moves gradually to the attractive potential (repulsion vanishes with increasing potential depth) and becomes almost negligible in Fig.3.8(c) where all bound electrons are aligned to pass the AHR in the next time interval.

After the peak of the laser pulse, e.g., at $\bar{t} = 3.2$ in Fig.3.8(d), since outer ionization is mostly saturated and the potential has already reached to its near maximum depth at the pulse peak before (i.e., near $\bar{t} = 2.5$), many bound electrons are dragged into the potential (they have more negative energies) due to the weakening of the laser field compared to the attractive force due to ions. Some of the quasi-free electrons (electrons with positive $\bar{\Omega}^2$ and positive $\bar{\mathcal{E}}_t$) near the cluster boundary also return inside due to such attraction.

The feature of AHR shown in Fig.3.8 in the frequency versus energy plane resembles Fig.3.4 obtained by the model, except that some MD electrons in Fig.3.8 experience negative frequencies due to repulsion of the neighbouring electrons.

Above analysis of trajectories of MD electrons in the self-generated, time-varying potential clearly indicates that the passage of AHR is must during their outer ionization. The fact that large amount of energy absorption by an electron and its simultaneous liberation from the dynamical potential happening at the same time *only* when AHR condition is met, clearly proves the AHR as a responsible mechanism behind this efficient laser absorption in a cluster.

3.4 Summary

The goal of the work presented in this chapter is to re-examine the AHR absorption mechanism of intense infrared laser pulses in a over-dense cluster using MD simulations. Although, AHR was proved earlier by a rigid sphere model and particle-in-cell (PIC) simulations [14] of clusters, it still remains obscure in many-body plasma simulations. To prove AHR on a firm footing a three dimensional MD simulation code with soft-core Coulomb interactions among charge particles has been developed. By following the trajectory of each individual MD electron and identifying its time-dependent frequency $\Omega[r(t)]$ in the self-consistent anharmonic potential (as in Ref.[14]) it is found that electron leaves the potential and becomes free only when AHR condition $\Omega[r(t)] = \omega$ is met. Thus, for the first time, our MD simulation clearly identifies AHR process in the laser cluster interaction. A simple anharmonic oscillator model (Sec. 3.2) is introduced to understand MD results better. The model brings out most of the features of MD electrons while passing the AHR. Thus, we not only bridge the gap between PIC simulations, analytical models and MD calculations but also unequivocally prove that AHR processes is a universal dominant collisionless mechanism of absorption in the short pulse regime or in the early time of longer pulses in clusters.

We believe that AHR mechanism works irrespective of the target size at least in the first few nano-layer of the sharp over-dense plasma (zero density scale-length) where laser interacts first and the analysis of electron trajectories (Sec. 3.3) presented here may be useful to identify AHR in such targets. The prompt generation of electrons via AHR within a time much shorter than a laser period, the crossing of electron trajectories [in Fig.3.6(c)] demonstrated by MD simulations and the breaking of laminar flow of electrons may lead to plasma wave-breaking and subsequent mixing of wave-phases [88] even at sub-relativistic laser intensities in an extended plasma.

4

Dynamical resonance shift and unification of resonances

*The objective of this chapter * is to examine the role of linear resonance (LR) in the short pulse regime and to find out the optimal regime of laser wavelengths in the entire regime of intensities $\sim 10^{15} \text{Wcm}^{-2} - 10^{17} \text{Wcm}^{-2}$ for an argon cluster so that maximum conversion of laser energy into charged particle energy is obtained. Further goal is also to look for the possibility to unify all kinds of LR i.e., (i) during initial cluster charging, (ii) during Coulomb explosion phase in the later time, and (iii) AHR in the marginal over-dense regime in a single short laser pulse for an argon cluster for maximum absorption of laser energy. Present study uses the improved MD code, where self-consistent inner ionization mechanism for atoms/ions is included via "OBI" model. MD results are also corroborated by the simple RSM of the cluster.*

* **S. S. Mahalik** and M. Kundu, “Dynamical resonance shift and unification of resonances in short-pulse laser-cluster interaction”, [Physical Review A \(97\), 063406 \(2018\)](#)

4.1 Introduction

For a short laser pulse duration < 5 fs, background ions remain relatively frozen and Mie-plasma frequency ω_M (corresponding to wavelength λ_M) remains much above the laser frequency ω for $\lambda > 400$ nm. In this regime linear resonance (LR) can not happen. However, in this regime, an electron may pass through anharmonic resonance (AHR) when its dynamical frequency $\Omega[r(t)]$ in the anharmonic potential gradually decreases and finally meets the driving ω . The role of AHR as a dominant collisionless process in laser cluster interaction is discussed in chapter 3 also in Ref. [13, 21, 87, 100]. Assuming collective motion of electrons as a driven harmonic oscillator, $\ddot{x} + \omega_M^2 x = -E_0 \cos(\omega t)$, which may be satisfied by those bound electrons in the bottom of the potential; one finds the excursion as $x = -E_0 \cos(\omega t) / (\omega_M^2 - \omega^2)$ and average energy $\langle \epsilon \rangle = \langle (\omega_M^2 x^2 + \dot{x}^2) / 2 \rangle = E_0^2 (\omega_M^2 + \omega^2) / 4 (\omega_M^2 - \omega^2)^2$. In this collective oscillation model, pronounced and maximum absorption of laser in a cluster-plasma is expected when the LR condition $\omega_M = \omega$ (or $\lambda_M = \lambda$) is satisfied. Such a LR can be met in different ways, when (i) ω_M rises towards ω during the cluster charging (from the neutral condition) in the initial time, (ii) ω_M drops towards ω during the Coulomb expanding (CE) phase, and (iii) ω approaches ω_M by varying λ of a tunable laser, in the sense that, λ is changed from one experiment to the other. Amongst these possibilities, the LR in the CE phase [option (ii)] has been demonstrated in experiments [9–11, 36, 37, 128, 129] with longer pulses > 50 fs. Due to non-availability of tunable lasers of any desired λ , the option (iii) can not be explored experimentally (always) for a cluster and one has to rely on models or numerical simulations. However, in previous simulations by Petrov *et al.* [19] and in subsequent studies [22, 23, 117] on laser heated clusters with pulses > 75 fs, no enhancement in the laser absorption and cluster charging were found while

passing through the LR by λ variation. Therefore, role of above LR was denied and the controversy *still* persists. For longer wavelengths, typically, $\lambda > 400$ nm, the ω_M rises so sharply (due to faster ionization) that the LR condition is met instantaneously *only* for an infinitesimal time compared to the laser period, thus making this LR [option (i)] in the early time *very inefficient* for which no serious attention is paid to it by experimentalists.

Here, in this chapter, we study laser-cluster interaction in the fascinating regime of 5-fs (fwhm) short laser pulses. The complex interplay between laser absorption, cluster charging, Coulomb expansion and electrons' outer-ionization depending upon laser and cluster parameters inhibits to predict an optimal condition for maximum laser absorption. One hardly thinks of unifying all possible options [(i)-(iii)] in a single experiment. The goal here is to look for the possibility to *unify* all kinds of LR [options (i)-(iii)] and also AHR in this short pulse regime, *particularly* making above options (i) and (iii) very efficient in a single laser pulse, and find out the optimal regime of laser wavelengths in the entire regime of intensities $\sim 10^{15} \text{ Wcm}^{-2} - 10^{17} \text{ Wcm}^{-2}$ for an argon cluster so that maximum conversion of laser energy into charged particle energy is obtained.

The interaction of 5-fs (fwhm) laser pulses (of fixed energy but different $\lambda = 100 - 800$ nm) with an argon cluster is studied by our three dimensional MD simulation [21]. It is found that, for a given pulse energy and a cluster, at each peak intensity there exists a wavelength Λ_d – shifted from the expected wavelength of Mie-resonance λ_M – that corresponds to a *unified dynamical* LR (we call it UDLR) at which evolution of the argon cluster happens through very efficient unification of possible resonances in various stages, including (i) the LR in the initial time of plasma creation, (ii) the LR in the CE phase in the later time and (iii) AHR in the marginally over-dense regime [nearly satisfying $\Lambda_d \approx (1 - 1.5)\lambda_M$] for a relatively longer pulse duration leading to maximum laser

Chapter 4. Dynamical resonance shift and unification of resonances

absorption accompanied by maximum outer-ionization and also maximum charging for the argon cluster. At this Λ_d (typically in the UV regime), respective LR is found to be more efficient not only in the early cycles of laser interaction [option (i)] than the LR in the CE phase [option (ii)] but also it becomes very efficient than a longer $\lambda > 400$ nm, due to significant time elapsed by the system near the LR during the rise of ω_M , thus making options (i) and (iii) more viable for short 5-fs (fwhm) pulse. The dynamical unification of all possible options (i)-(iii) of LR and AHR within a single 5-fs (fwhm) pulse at the shifted wavelength Λ_d of UDLR leading to maximum absorption (as shown here) is also rarely possible with a longer pulse and a longer $\lambda > 400$ nm.

In the conventional notion of LR, the absorption maxima should occur at $\lambda = \lambda_M$ irrespective of the laser intensity. However, as the laser peak intensity increases, the maxima in the absorption and outer-ionization are found to grow together but gradually shift towards higher wavelengths in the band of $\Lambda_d \approx (1 - 1.5)\lambda_M$ for the argon cluster instead of absorption peaking at the expected λ_M . It means that observed redshift of the absorption maxima $\Delta\Lambda_d = \Lambda_d - \lambda_M$ can be as large as 40-50% of λ_M depending upon the laser intensity, cluster size and atomic constituents of the cluster. MD results for the wavelength shift of resonance absorption peak are also justified by a simple rigid sphere model (RSM) [21] of cluster given in chapter 3 (see Sec. 3.2). Thus MD and RSM un-equivocally prove that maximum laser absorption in a cluster happens at a shifted wavelength in the marginally over-dense regime of $\Lambda_d \approx (1 - 1.5)\lambda_M$ due to UDLR instead of $\lambda = \lambda_M$ of LR. Based on above findings, we envisage that this study may serve as a guideline to perform an optimal condition experiment for maximum laser absorption in a cluster at different intensities in the short pulse regime. It also (possibly) explains why Petrov *et al.* [19, 22, 23, 117] could not find maximum absorption at the expected λ_M and removes some of the controversies.

Organization of the chapter is as follows. Section 4.2 illustrates laser absorption in an uniformly charged argon cluster by RSM for the basic understanding of the shifting of the absorption peak from $\lambda = \lambda_M$ of LR. Section 4.3 gives its further detail and possible unification of resonances (LR and AHR, i.e., UDLR) through various stages of evolution of argon cluster by rigorous MD simulations. Summary is given in Sec.4.4.

4.2 Wavelength shift of resonance absorption using RSM

Before studying the absorption of laser pulses in an argon cluster by MD simulation in Sec.4.3, here we first study the same by a RSM. The details of RSM with governing EOM, electrostatic restoring force $g(r)$, corresponding potential $\phi(r)$ and the expression for laser pulse $E_l(t) = -dA/dt$ (in dipole approximation) are discussed in chapter 3 (see Sec. 3.2). Here, in this chapter, a pre-ionized argon cluster of radius R_0 is assumed which consists of uniformly charged spheres of argon ions and electrons of equal radii $R_i = R_e = R_0$. The motion of massive ion sphere is neglected for short laser pulse < 15 fs and also the laser magnetic field for intensities $< 10^{18} \text{ Wcm}^{-2}$ as considered here. From the expression of potential $\phi(r)$ (see Eq.(3.3)), we can infer that as long as the excursion r of the center of the electron sphere remains inside the ion sphere, it executes a harmonic motion with a constant eigen-frequency $\Omega[r(t)] = \omega_M$, where $\Omega[r(t)]$ stands for the anharmonic frequency of electrons as introduced in chapter 3. After crossing the boundary of the ion sphere, it experiences the Coulomb force and its motion becomes anharmonic [21] with gradual decrease in $\Omega[r(t)]$ for increasing $r > 1$ (see chapter 3, Sec. 3.2.1). When the irradiating laser wavelength is such that $\Omega[r(t)] = \omega_M = \omega$, then LR absorption happens for the electron sphere with its center at $r \leq 1$. Otherwise, AHR absorption happens in the over-dense cluster plasma when $\Omega[r(t)] = \omega$ is met by the electron sphere at a location $r > 1$. Thus, RSM can be used to understand both LR and

Chapter 4. Dynamical resonance shift and unification of resonances

AHR processes for laser absorption in a cluster.

In the RSM we need to assign a uniform (an average) charge state \bar{Z} to define ω_M , where $\omega_M = \sqrt{4\pi\rho_i/3}$, $\rho_i = 3N\bar{Z}/4\pi R_0^3$ is the charge density of ion background and N is the number of atoms in the cluster. For an arbitrary value of \bar{Z} irrespective of the laser intensity I_0 , the ω_M may be over-estimated or under-estimated. Therefore, in the RSM, \bar{Z} must be at least the value of the corresponding optical field ionization (OFI) of argon atoms/ions for a given I_0 . To obtain \bar{Z} , we first create a table of Z vs $I_0(Z)$ obeying the critical field $E_c(Z) = I_p^2(Z)/4Z$ of OFI [130, 146, 147], where $I_p(Z)$ is the ionization potential (IP) corresponding to the integer charge state Z of an argon atom/ion. Then from the table look-up (or interpolation from the Z vs $I_0(Z)$ OFI curve) we find a value of Z (and call it average \bar{Z}) for the given intensity of $I_0(\bar{Z})$. Thus $I_0(\bar{Z})$ is regarded as the OFI intensity corresponding to an average \bar{Z} which may be non-integer. In the case of MD simulation (in Sec.4.3), however, each atom/ion is self-consistently ionized to different integer Z only, but the final average charge \bar{Z} per atom/ion may not be an integer.

We consider an argon cluster of $R_0 = 2.91$ nm and $N = 1791$. It is illuminated by respective peak intensities $I_0(\bar{Z}) \approx 5 \times 10^{15}, 10^{16}, 5 \times 10^{16}, 10^{17}$ Wcm⁻² of OFI yielding different $\bar{Z} \approx 2.61, 3.42, 6.2, 6.94$ from the OFI curve, and take different number of non-interacting electron spheres $N_e = N\bar{Z} = 4675, 6125, 11105, 12429$ in the RSM, with centers of electron spheres placed uniformly inside the ion sphere. The center of each electron sphere mimics a real point size electron. For $\bar{Z} = 1$, one obtains an uniform charge density $\rho_i = 3N\bar{Z}/4\pi R_0^3 \approx 2.7 \times 10^{-3}$ a.u. and $\omega_M = \sqrt{4\pi\rho_i/3} \approx 0.104$ a.u. At $\lambda = 800$ nm, it corresponds to an over-dense plasma of $\rho_i/\rho_c \approx 9.95$ and $\omega_M/\omega \approx 1.82$, where $\rho_c \approx 1.75 \times 10^{27}$ m⁻³ is the critical density. With $\bar{Z} = 1 - 8$, the LR wavelengths are found to be in the range of $\lambda_M \approx 440 - 156$ nm.

Above multi-electron systems are now simulated in RSM. Dynamics of an electron sphere and corresponding laser energy absorption are studied with laser pulses of respective $I_0(\bar{Z})$ by solving the EOM (3.1). For a given I_0 and \bar{Z} , λ is varied from 100 nm to 800 nm; while keeping the total pulse duration τ and the pulse energy density $\varepsilon_p = \int_0^\tau I(t)dt$ constant. Throughout this chapter, we keep $\tau \approx 13.5$ fs (fwhm ≈ 5 fs) which corresponds to $n = 5$ periods at $\lambda = 800$ nm. As λ changes from 800 nm to 100 nm, the number of cycles in a pulse (for a fixed τ) increases, electron spheres oscillate more, the nano-plasma passes from the over-dense to the under-dense regime, and the dominant absorption process should exhibit its signature.

4.2.1 RSM results with intensity variation for different \bar{Z}

Figure 4.1(a) shows the average total absorbed energy $\bar{\mathcal{E}}_t = \sum_1^{N_e} (m_s v_i^2 / 2 + q_s \phi_i) / N$ by the electron spheres scaled by number of atoms N (after subtracting the initial energy) at the end of the pulses (after $\tau = 13.5$ fs) versus λ for different $I_0 \leq 10^{17}$ Wcm $^{-2}$ and \bar{Z} . Figure 4.1(b) is the corresponding fraction of outer ionized electrons $\bar{N} = N_e^{out} / N_e$, where N_e^{out} is the total outer ionized electrons (out of R_0) after $\tau = 13.5$ fs. Vertical dashed lines indicate different $\lambda_M \approx 274, 239, 178, 167$ nm (for respective $\bar{Z} \approx 2.61, 3.42, 6.2, 6.94$ above) where absorption maxima are strictly expected by LR. For a combination of I_0 and \bar{Z} (e.g., $I_0(\bar{Z}) \approx 5 \times 10^{15}$ Wcm $^{-2}$), it is found that $\bar{\mathcal{E}}_t$ and \bar{N} increase with increasing λ , attain a maximum at a wavelength Λ_d (e.g., $\Lambda_d \approx 290$ nm for 5×10^{15} Wcm $^{-2}$), then drop as λ is increased beyond Λ_d . Although the pulse energy is kept constant for all λ for a given $I_0(\bar{Z})$, the occurrence of distinct maxima in the $\bar{\mathcal{E}}_t$ and \bar{N} for all $I_0(\bar{Z}) \lesssim 10^{17}$ Wcm $^{-2}$ suggests the clear effect of λ . It also signifies more collective behavior of the electron system at Λ_d . However, absorption peaks are consistently found to be red-shifted from the respective λ_M of LR for all $I_0(\bar{Z})$ which is a new

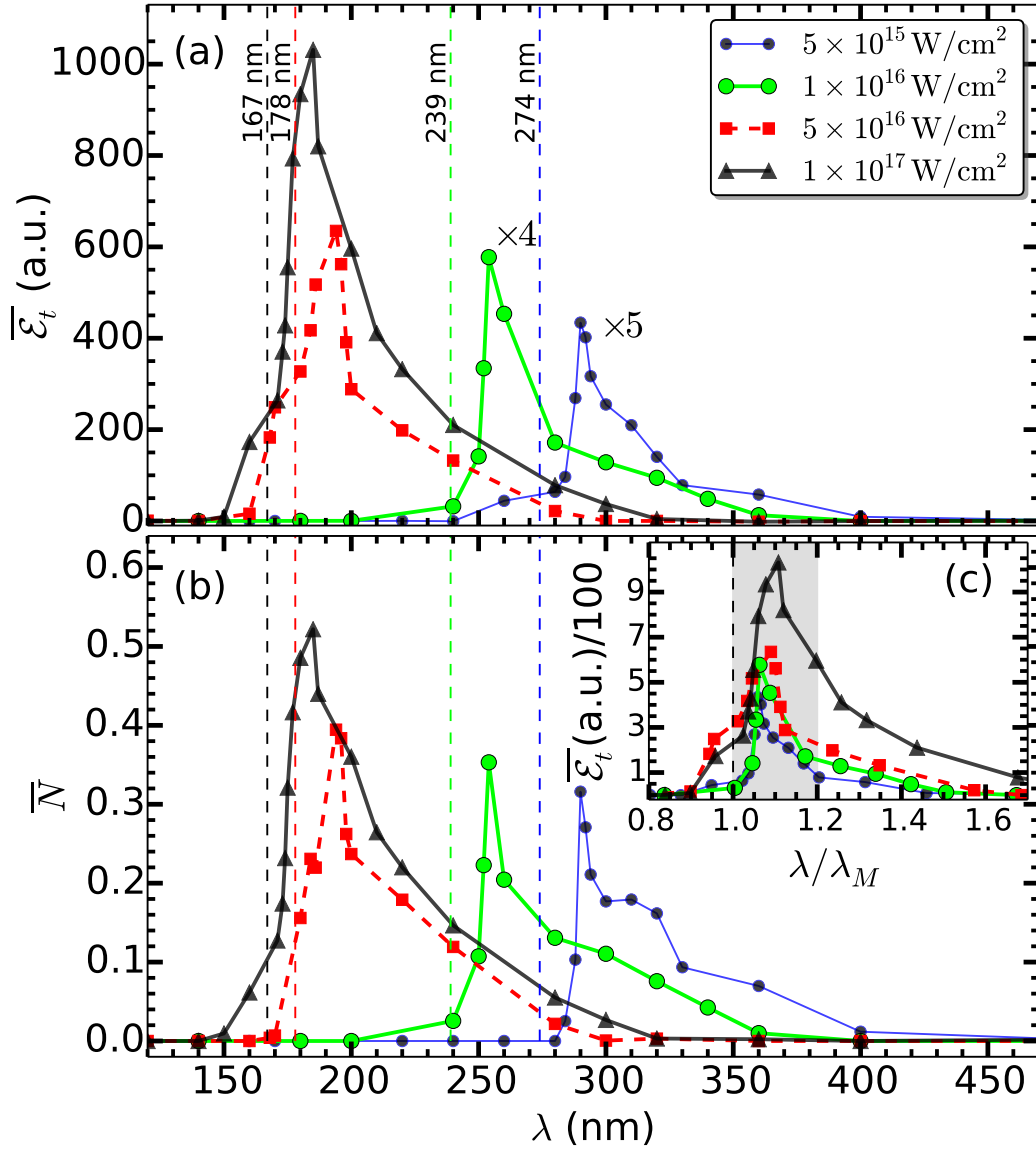


Figure 4.1: Normalized total absorbed energy $\overline{\mathcal{E}}_t$ of electron spheres (a) and corresponding fractional outer ionization \overline{N} (b) versus λ for an argon cluster (radius $R_0 = 2.91 \text{ nm}$, number of atoms $N = 1791$ with various $\overline{Z} \approx 2.61, 3.42, 6.2, 6.94$) irradiated by laser pulses of respective OFI intensities $I_0(\overline{Z}) \approx 5 \times 10^{15}, 10^{16}, 5 \times 10^{16}, 10^{17} \text{ Wcm}^{-2}$. For a given $I_0(\overline{Z})$, pulses of different λ are chosen by keeping pulse duration $\tau \approx 13.5 \text{ fs}$ (fwhm $\approx 5 \text{ fs}$) as constant. Vertical dashed lines indicate different $\lambda_M \approx 274, 239, 178, 167 \text{ nm}$ for respective $\overline{Z} = 2.61, 3.42, 6.2, 6.94$ where absorption maxima are strictly expected by LR. Inset (c) shows that absorption maxima are shifted in the marginally over-dense regime of $\lambda/\lambda_M \approx 1 - 1.2$.

finding by the RSM. Plotting $\overline{\mathcal{E}}_t$ against λ/λ_M in Fig.4.1(c) it is revealed that maxima in the absorption lie in the marginally over-dense regime of $\lambda/\lambda_M \approx 1 - 1.2$ for all OFI intensities.

In the RSM, since ionic sphere charge density does not vary, the ω_M and λ_M remain unchanged. We term the conventional condition $\lambda_M = \lambda$ (or $\omega_M = \omega$) as *static* LR and $\lambda = \lambda_M$ as the wavelength of static LR, to distinguish from the *unified dynamical* LR (we call it UDLR where LR and AHR are indistinguishable, more to be discussed later) in the marginally over-dense regime in presence of outer ionization (as already shown by the RSM), inner ionization and cluster expansion.

4.2.2 RSM results with intensity variation for fixed \overline{Z}

Increasing the peak intensity for a fixed \overline{Z} (e.g., for $\overline{Z} = 3$, this situation may arise when no more inner-ionization happens after the OFI) from the OFI intensity [e.g., $I_0(\overline{Z} = 3) \approx 6.7 \times 10^{15} \text{ Wcm}^{-2}$] as shown in Figs.[4.2(a)-4.2(b)], the maxima of $\overline{\mathcal{E}}_t$ and \overline{N} increase in magnitude but gradually shift towards higher λ from the expected static LR wavelength of $\lambda_M \approx 254 \text{ nm}$ (vertical dashed line). Approaching towards $\lambda_M \approx 254 \text{ nm}$ from 100 nm, higher intensity pulse expels more electrons from the cluster than at a lower intensity. When electrons move far from the cluster, the laser field dominates the restoring field of background ions acting on those free/quasi-free (outer-ionized) electrons. Since the average energy of a laser-driven free electron scales as $\approx E_0^2 \lambda^2 / 4$ and electrons are liberated at different times with different energy, the redshift of absorption maxima from λ_M depends on the population of free electrons during the interaction. As the free population of electrons increases with increasing intensity when \overline{Z} is saturated, absorption peak gradually shifts towards higher λ from the λ_M . Results presented in Fig.4.2 just represent a scenario for the redshift of the absorption peak if I_0 is increased

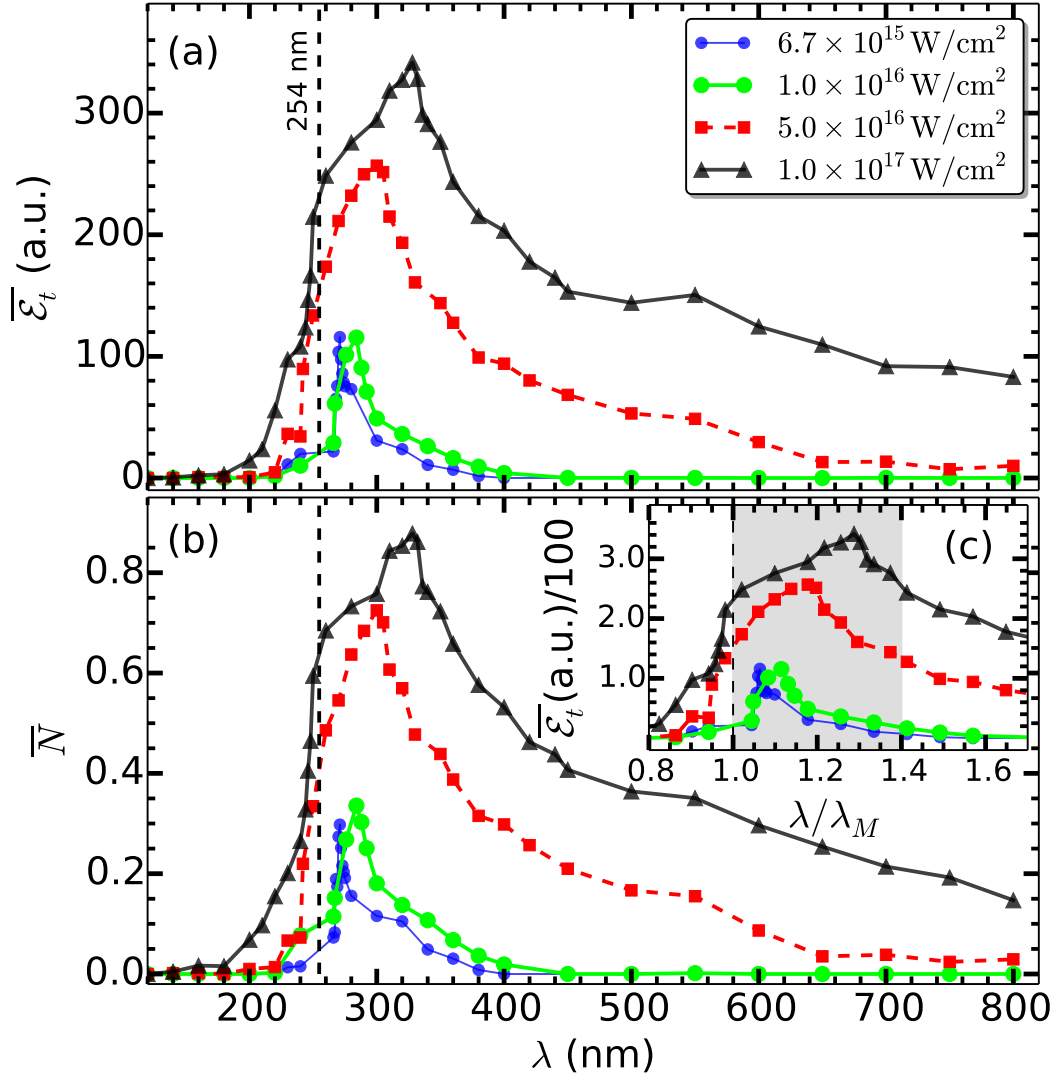


Figure 4.2: Normalized total absorbed energy $\bar{\mathcal{E}}_t$ of electron spheres (a) and corresponding fractional outer ionization \bar{N} (b) versus λ for the argon cluster ($R_0 = 2.91$ nm, $N = 1791$, with fixed $\bar{Z} = 3$ and $N_e = N\bar{Z} = 5373$) irradiated by laser pulses with different I_0 starting from $I_0(\bar{Z}) \approx 6.7 \times 10^{15} \text{ Wcm}^{-2}$ of OFI for $\bar{Z} = 3$. For a given I_0 , pulses of different λ are chosen by keeping pulse duration $\tau \approx 13.5$ fs (fwhm ≈ 5 fs) as constant. Vertical dashed line indicates corresponding $\lambda_M \approx 254$ nm where absorption maxima is strictly expected by LR. Inset (c) shows that absorption maxima are shifted in the marginally over-dense regime of $\lambda/\lambda_M \approx 1 - 1.4$. Other parameters are same as in Fig.4.1.

when there is a saturation of \bar{Z} . So, in this case with increasing I_0 , where \bar{Z} is quickly saturated at $\bar{Z} = 1$ in beginning of the laser pulse and remaining part of the pulse is utilized for increasing outer ionization of electrons and gradual redshift of the absorption peak from the corresponding λ_M . Certainly, an under-estimated \bar{Z} for an intensity will give more redshift than the actual. However, a better and a self-consistent estimation of \bar{Z} at a given I_0 can only be obtained by MD simulations.

At 400 nm wavelength, the argon cluster in Fig.4.2 is ≈ 7.46 times over-dense with $\omega_M/\omega \approx 1.58$. For a low intensity $< 10^{16} \text{ Wcm}^{-2}$, almost all electrons remain bound in the harmonic part of the potential (3.3) with nearly the same energy as the initial energy and negligible fractional outer ionization occurs after the pulse [see Figs.4.2(a)-4.2(b)]. Clearly, LR has no role beyond $\lambda = 400$ nm. *Still*, significant absorption and outer ionization persists for $I_0 > 10^{16} \text{ Wcm}^{-2}$. In this regime, as I_0 is increased, excursions of electron spheres increase beyond $r = 1$, dynamical frequency $\Omega[r(t)]$ of each electron sphere drop from its initial value of ω_M and may meet the laser ω , i.e., the AHR absorption condition $\Omega[r(t)] = \omega$ is met for those electron spheres [14, 21, 99]. In the intermediate regime of $\omega_M/\omega = \lambda/\lambda_M \approx 1 - 1.5$, effects of LR and AHR often become indistinguishable (the UDLR regime) with dominant contribution due to LR (and/or near LR fields) as evident from the occurrence of the absorption peak. Note that the approximate effective field $E_{eff} \approx |E_0/(\omega_M^2/\omega^2 - 1)|$ inside the cluster is greatly enhanced (both in the under-dense and over-dense regime, e.g., $1/2 \lesssim (\lambda/\lambda_M)^2 \lesssim 2$) near the LR and symmetric about $\lambda = \lambda_M$ where it has a peak. Whereas AHR can work *only* in the over-dense regime of $\lambda > \lambda_M$, absorption due to AHR monotonically decreases with increasing $\lambda > \lambda_M$ at a given laser intensity, and AHR can not solely produce an absorption peak without the dominant contribution of near LR enhanced fields. Here, near-the-LR augmented fields $E_{eff} > E_0$ (for $1 \lesssim (\lambda/\lambda_M)^2 \lesssim 2$) help some/many

electrons to undergo AHR at ease. For higher intensity of 10^{17} Wcm^{-2} , the absorption and outer ionization maxima are found at $\lambda = \Lambda_d \approx 330 \text{ nm}$ with $\lambda/\lambda_M \approx 1.3$ [see inset Fig.4.2(c)]. In reality, however, at 10^{17} Wcm^{-2} , charge states $\bar{Z} > 3$ are possible by OFI, leading to increasing restoring force on electrons, reducing fractional outer ionization and possible shifting of the absorption peak somewhere in the marginally over-dense regime of $\Lambda_d \approx (1 - 1.5)\lambda_M$ as predicted in Fig.4.1.

From the simple RSM analysis we find that UDLR has a prominent role on maximum laser absorption and outer ionization. The absorption peak is justified to be red-shifted from the static LR wavelength λ_M (in the absence of further inner-ionization), since there is always a fraction of free population of electrons with positive energy (for $I_0 > 10^{15} \text{ Wcm}^{-2}$) which causes this shift. Therefore, *even if* ω_M remains fixed, the absorption maxima will *never* be found at the pre-calculated static LR wavelength of λ_M . Instead, it occurs at an un-predictable value in the shifted band of wavelengths $\Lambda_d \approx (1 - 1.5)\lambda_M$ that depends upon the level of outer ionization which in turn depends upon the laser intensity. In this shifted band of Λ_d , evolution of the cluster happens in the marginally over-dense regime – the UDLR regime – where AHR and influence of LR become indistinct and maximum absorption and outer ionization occur taking the benefit of the both.

4.3 Unified resonance absorption by MD simulation

Although RSM brings out basic features of laser-cluster interaction during the LR and AHR, many important aspects: (i) cluster expansion due to ion motion, (ii) cluster charging via polarization, and (iii) creation of enhanced charge states beyond OFI via ionization ignition can not be addressed by the RSM. Moreover, a fixed ion-potential is presumed in the RSM. In reality, potential should evolve in time, starting from zero,

depending upon the spatial distribution of charges.

Previously, Petrov *et al.* [19, 22] performed MD simulations for a xenon cluster *only* at three laser wavelengths of 100 nm, 248 nm, and 800 nm at an intensity of 10^{16} Wcm^{-2} and concluded that, (i) cluster charging, (ii) average charge per atom, (iii) number of electrons, and (iv) peak electron density do not depend on laser wavelengths [22]. At $\lambda = 248 \text{ nm}$ of KrF laser, maximum laser absorption was expected due to the static LR. However, they *failed* to find any enhancement in the absorbed energy at $\lambda = 248 \text{ nm}$ compared to 100 nm and 800 nm; and *discarded* the role of LR. The “null effect” of LR was vaguely argued due to the “non-uniform electron density” in the cluster [19]. Note that electron density is always non-uniform in an ionized cluster and in its vicinity which can not explain non-existence of resonance peak at $\lambda = \lambda_M$. On the contrary, RSM results in Sec.4.2 clearly demonstrate an indispensable and combined role of LR and AHR for maximum absorption. The most important outcome of the RSM is that, the maximum absorption in a cluster *hardly* occurs at the static LR wavelength (as expected by Petrov *et al.* [19, 22] and almost all in this field). Instead, it occurs in a shifted wavelength band of $\Lambda_d \approx (1 - 1.5)\lambda_M$ due to outer ionization depending upon the laser intensity. In order to gain deeper insight for the absorption peak shift and to demonstrate the unified role of possible LR and AHR (the UDLR) on a strong footing, we perform more realistic three dimensional MD simulation [21] which is free from above mentioned short-comings of the RSM.

4.3.1 Details of MD simulation

To study high Z clusters (e.g., argon) by MD simulation, we have incorporated self consistent inner ionization process of atoms/ions. Ionization of atoms/ions is treated by “over the barrier” ionization (OBI) model. Details of initial configuration of neu-

tral atoms atoms, inner ionization mechanism are already described in chapter 2 (see Sec. 2.9). $N = 1791$ Number of neutral atoms are put randomly inside the cluster radius $R_0 = r_w N^{1/3} \approx 2.91$ nm, where $r_w \approx 0.24$ nm is the Wigner-seitz radius for argon cluster. The thermal velocity assignment of neutral atoms in the cluster is done by Gaussian random distribution generated by the Box-Muller transformation (see Sec. 2.9). We apply the dipole approximation and neglect binary collisions between electrons and ions, as in chapter 3. Ion motion and laser magnetic field is taken into consideration. In many works, ion dynamics is often neglected assuming it to be important only after tens of femtoseconds. We find that ion dynamics is important *even* for the short 5-fs (fwhm) pulses consider here, since it determines the cluster expansion and the Mie-frequency ω_M which in turn determines LR and AHR.

4.3.2 Calculation of Mie-plasma frequency in MD simulation

In MD simulations, charge states of ions are dynamically created depending upon the laser intensity, wavelength, and self-consistent plasma field. Since ion charge density is inhomogeneous due to variation of degree of ionization of ions at different locations at different times and due to the anisotropic cluster expansion [147]; the exact calculation of dynamical $\omega_M(t)$ is difficult. To this end, we have tried the relation $\omega_M^2(t) = Q_T(t)/R(t)^3$, where $Q_T(t)$ is the total ionic charge inside the dynamical cluster $R(t)$ which is the distance of the outermost ion in the expanding cluster at time t . Due to higher Coulomb expansion energy of outermost cluster ions than the ions in the cluster interior, the outer ion-layer dis-integrates much faster radially outward than the nearly homogeneously distributed, slowly moving interior ions. Therefore, when this $R(t)$ is taken into account, the dynamical $\omega_M(t)$ using above definition of $\omega_M(t)$ greatly underestimates the actual $\omega_M(t)$ in the CE phase of the cluster and can not explain results in

Fig.4.5. Hence, we calculate $\omega_M(t)$ from the relation $\omega_M^2(t) = Q_0(t)/R_0^3$ by assuming instantaneous total positive charge $Q_0(t) = N_i(t)\bar{Z}(t)$ inside the initial cluster radius R_0 having $N_i(t)$ number of ions with average charge $\bar{Z}(t)$ as in Refs.[130, 146, 147].

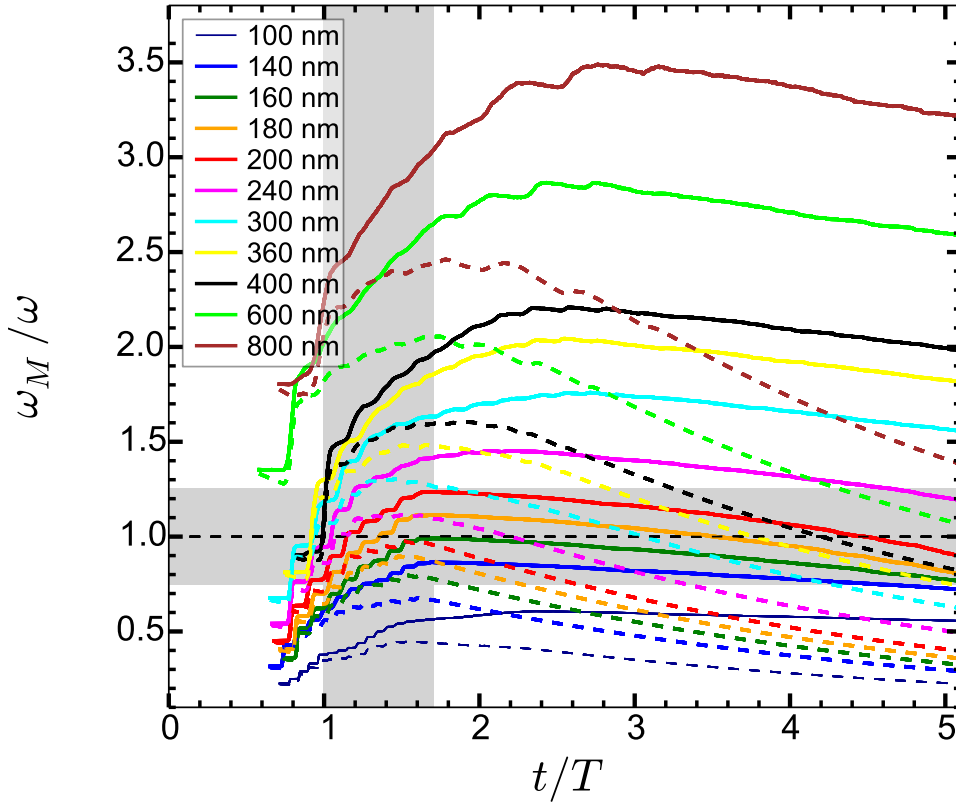


Figure 4.3: Temporal variation of normalized Mie-frequency $\omega_M(t)/\omega$, for the argon cluster when irradiated by 13.5 fs [5-fs (fwhm)] laser pulses of peak intensity $5 \times 10^{16} \text{ Wcm}^{-2}$ and different $\lambda = 100 - 800 \text{ nm}$. Time is normalized by the period T of $\lambda = 800 \text{ nm}$. Two different expressions of ω_M have been used here for comparison, namely, (i) $\omega_M = \omega_{M2} = \sqrt{Q_T(t)/R(t)^3}$ where $Q(t)$ is the total ionic charge inside the dynamical cluster radius $R(t)$ (dashed lines) and (ii) $\omega_M = \omega_{M1}(t) = \sqrt{Q_0(t)/R_0^3}$ where $Q_0(t)$ is the total ionic charge inside the initial radius R_0 at time t (solid lines). The expression $\omega_M = \omega_{M2} = \sqrt{Q_T(t)/R(t)^3}$ greatly under-estimates the actual $\omega_M(t)$ in the Coulomb expanding phase of the cluster.

To justify our argument, we now define two different expressions for ω_M calcula-

tion as $\omega_M = \omega_{M2} = \sqrt{Q_T(t)/R(t)^3}$ and $\omega_M = \omega_{M1}(t) = \sqrt{Q_0(t)/R_0^3}$. Fig. 4.3 shows the direct comparison of these above mentioned two different estimates of ω_M at different λ . Solid lines for each wavelengths refer to the ω_{M1} calculation and dashed lines are for ω_{M2} calculation. Clearly, “the latter” is more under-estimated for all $\lambda = 100 - 800$ nm as time increases. To understand it, in a simple way, in Fig. 4.4 we plot typical Coulomb explosion scenario of the cluster ions at different times at some λ (e.g., 200 nm) corresponding to Fig. 4.3, i.e., projections of ion co-ordinates ($\bar{X}_i, \bar{Y}_i, \bar{Z}_i$ normalized by R_0) in X-Y and X-Z plane. Inner circle (dashed red) represents cluster of initial radius R_0 and outer circle (dashed blue) represents a sphere of radius $R(t) = \max \left(R_0 \sqrt{\bar{X}_i^2(t) + \bar{Y}_i^2(t) + \bar{Z}_i^2(t)} \right)$ which the maximum distance of an ion from the center of the cluster at time t , called as dynamical cluster radius as considered in the expression of $\omega_M = \omega_{M2} = \sqrt{Q_T(t)/R(t)^3}$. Note that instantaneous total positive charge $Q_T(t)$ of the cluster is enclosed within this $R(t)$. As time increases, due to Coulomb explosion, some of the ions cross initial R_0 and only one (or a few) reaches at the maximum radial distance $R(t)$ (see Fig. 4.4). Now, if seen carefully, charge distribution is inhomogeneous and anisotropic which increase with time. The ions which are relatively at a larger distance from the center, after crossing R_0 , quickly disintegrate (due to their higher Coulomb repulsion energy) from the rest of the slowly moving ions within the initial cluster radius R_0 . These disintegrated, inhomogeneously and anisotropically distributed ions beyond R_0 when considered in the expression $\omega_M = \omega_{M2} = \sqrt{Q_T(t)/R(t)^3}$, certainly can not give the correct estimate of the harmonic frequency ω_M which can be uniquely calculated only from a homogeneous or nearly homogeneous ion charge distribution. On the other hand we find that charge distribution is maintained nearly homogeneous inside initial R_0 or much less inhomogeneous compared to that within $R(t)$ due to slow outward motion of interior

ions. Due to many ions inside R_0 at a given instant, an averaging yields almost homogeneous charge density $\rho_i(t)$. The latter enables us to find the approximate harmonic frequency $\omega_M = \omega_{M1}(t) = \sqrt{Q_0(t)/R_0^3}$, which we consider more accurate than the expression $\omega_M = \omega_{M2} = \sqrt{Q_T(t)/R(t)^3}$. Now, as Coulomb explosion continues, the radial distance $R(t) - R_0$ increases for the outermost ion and the volume $V_d = 4\pi(R^3(t) - R_0^3)/3$ between outer sphere and inner sphere increases. However, only a few percent of ions (which are disintegrated, in-homogeneously and anisotropically distributed) occupies the volume V_d and most of space in this volume is empty (see Fig.4.4). Therefore, when dynamical radius $R(t)$ or the dynamical volume $V(t) = 4\pi R^3(t)/3$ is considered, the charge density $\rho_i(t) = Q_T(t)/V(t)$ is greatly under-estimated. As a result, the expression of $\omega_M = \omega_{M2} = \sqrt{Q_T(t)/R(t)^3} = \sqrt{4\pi\rho_i(t)/3}$ greatly under-estimates the actual $\omega_M(t)$ which we have shown in Fig.4.3.

In the initial time (in Fig.4.3) just after the ionization, the dynamical radius $R(t) = R_0$, and both ω_{M1} and ω_{M2} start at the same value. As time goes on, ionization tries to increase both ω_{M1} and ω_{M2} which go hand in hand up to some time (e.g., $t/T < 1$ for 200 nm, red and red-dashed line) and Coulomb explosion (which starts little late just after initial ionization and after few electrons have left the system) tries to reduce the charge density. Even if, only one ion (of some average charge $\bar{Z}_0 < 8$) moves little beyond R_0 , say $R(t) = 1.1R_0$ in the initial time $t/T < 1.5$, the $\omega_{M2} = \sqrt{Q_T(t)/R(t)^3}$ would more underestimate the actual ω_M than the estimate of $\omega_M = \omega_{M1} = \sqrt{(Q_0(t) - \bar{Z}_0)/R_0^3} \approx \sqrt{Q_0(t)/R_0^3} \approx \omega_{M0}$ (since $Q_0 \gg 1000$, $Q_0 - \bar{Z}_0 \approx Q_0$ holds in the initial time) which is physically more acceptable.

To be more explicit, let us consider the data in Fig.4.4 at time $t/T = 3.0$ and corresponding $R(t)/R(0) \approx 1.5$ from Fig.4.4(c) for $R(t)/R(0)$ versus t/T . In this case, at time $t/T = 3$, $Q_T(t) = N\bar{Z}(t) \approx 1791 \times 8$ (with $N = 1791$ and $\bar{Z}(t) = 8$) and $V(t) =$

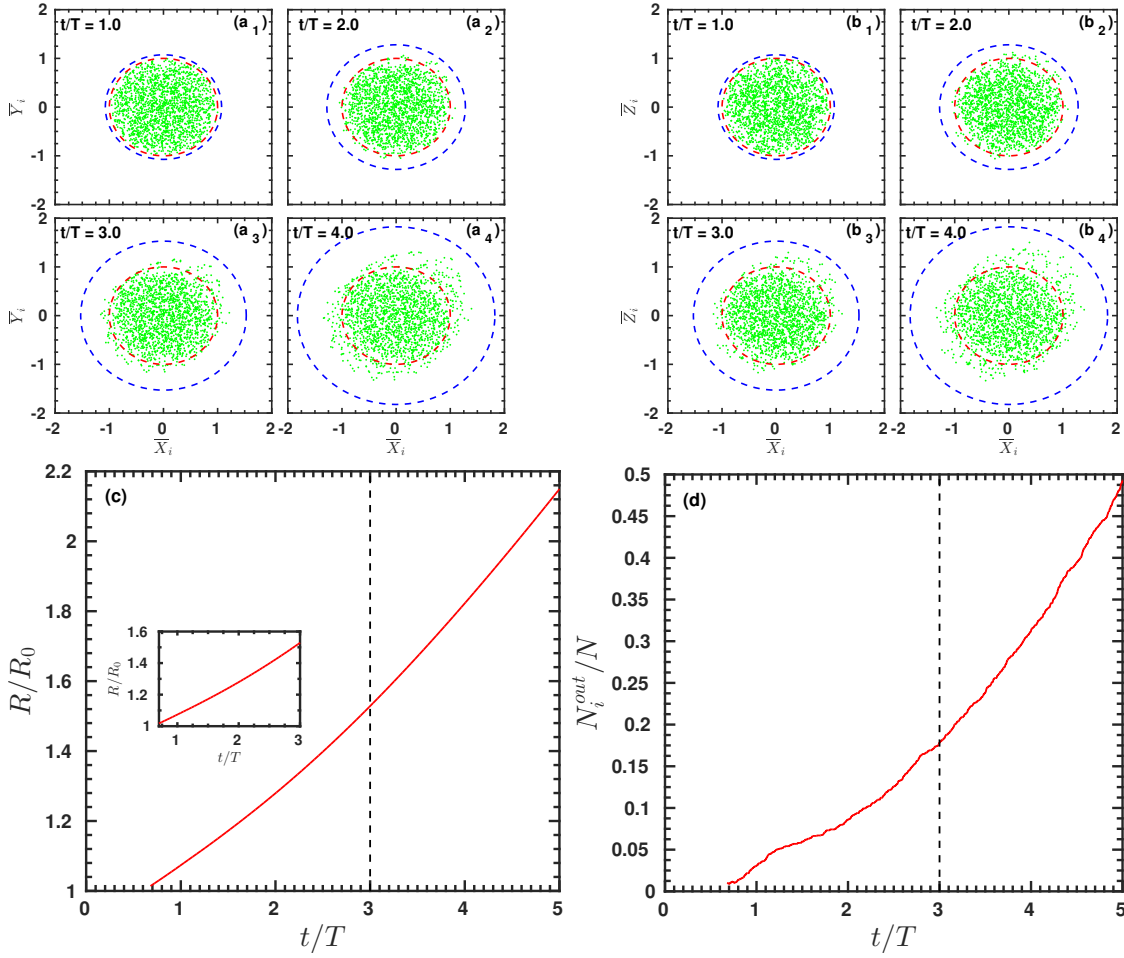


Figure 4.4: Typical Coulomb explosion scenario for the Argon cluster corresponding to MD results in Fig. 4.6 and Fig.4.3 at $\lambda = 200$ nm. Top panels are snapshot of cluster ions at different times corresponding to Fig.4.3, i.e., projections of ion co-ordinates $(\bar{X}_i, \bar{Y}_i, \bar{Z}_i)$ normalized by R_0 in X-Y and X-Z plane. The dynamical cluster radius $R(t)/R_0$ (left bottom) and number of argon ions N_i^{out} (right bottom) versus time are also plotted.

$(4\pi R_0^3/3) \times (1.5)^3 = 3.375V_0$ where $V_0 = (4\pi R_0^3/3)$. It gives us $\omega_{M1} \approx 0.27$ a.u. and $\omega_{M2} \approx 0.16$ a.u with $Q_0(t) = 1471 \times 8$ and number of ions outside R_0 being $N_i^{out} = 320$ (obtained from the MD calculation, Fig.4.4(d) for N_i^{out}/N versus t/T) which only occupies the outer volume $V_d = 4\pi(R^3(t) - R_0^3)/3 = 2.375V_0$. Note that outer volume V_d is more than two times the inner volume V_0 , but it occupies only $N_i^{out}/N \approx 18\%$ of ions [see Fig.4.4(d) at time $t/T = 3$]. Clearly, $\omega_{M2} \approx 0.16$ a.u. gives more under-estimated

value of ω_M than the estimate of $\omega_M = \omega_{M1} \approx 0.27$ a.u. Therefore, we discarded ω_{M2} to the benefit of ω_{M1} which is more accurate. In normalized units (for $\lambda = 200$ nm, red and red-dashed) these two values are $\omega_{M1}/\omega \approx 1.2$ and $\omega_{M2}/\omega \approx 0.7$ which precisely match the respective values in Fig.4.3 for $\omega_M/\omega = \omega_{M1}/\omega$ vs t/T at time $t/T = 3$. Therefore, we can conclude ω_{M1} is perfectly compatible for the calculation of actual ω_M .

4.3.3 Dynamical resonance shift and unification of resonances

The shift of the absorption peak as shown by the RSM becomes more un-predictable when there is cluster expansion and simultaneous creation of multiply charged ions during the laser interaction. Figures 4.5(a)-4.5(d) show total absorbed energy $\overline{\mathcal{E}}_t = \sum_1^{N_p} (m_i v_i^2/2 + q_i \phi_i)/N$ per atom, fractional outer ionization $\overline{N} = N_e^{out}/N_e$ of electrons, average charge state $\overline{Z} = N_e/N$ of ions (number of electrons produced N_e divided by number of atoms N) and an approximate $(\lambda/\lambda_M)^2 = (\omega_M/\omega)^2$ versus λ at the end of laser pulses (i.e., after 13.5 fs) of different peak intensities as in Fig.4.1 with RSM. Here λ_M is calculated from the simple estimate of $\omega_M = (N\overline{Z}/R_0^3)^{1/2}$ [130, 146, 147]. As in the RSM (Figs.4.1,4.2), $\overline{\mathcal{E}}_t$ and the corresponding \overline{N} for an intensity [Figs.4.5(a)-4.5(b)] increase with increasing λ , reach a maximum in the band of $\lambda \approx 196 \pm 40$ nm and then decrease with further increase of λ . In addition, average \overline{Z} also exhibit a peak [Fig.4.5(c)] in the above band of λ at lower intensities $\leq 10^{16}$ Wcm $^{-2}$. For higher intensities $> 10^{16}$ Wcm $^{-2}$, due to higher absorption and outer ionization even at lower wavelengths < 150 nm, the average \overline{Z} saturates at $\overline{Z} = 8$ due to removal of all electrons from the $3s^2 3p^6$ shell of all argon atoms. Considering the OFI (2.24), only average $\overline{Z} \approx 2.61, 3.42, 6.2, 6.94$ are expected (as used in Fig.4.1) at the respective peak intensities of $\approx 5 \times 10^{15}, 10^{16}, 5 \times 10^{16}, 10^{17}$ Wcm $^{-2}$ for an isolated argon atom. However, for the *argon cluster*, the average \overline{Z} exceeding the respective OFI values [Fig.4.5(c)]

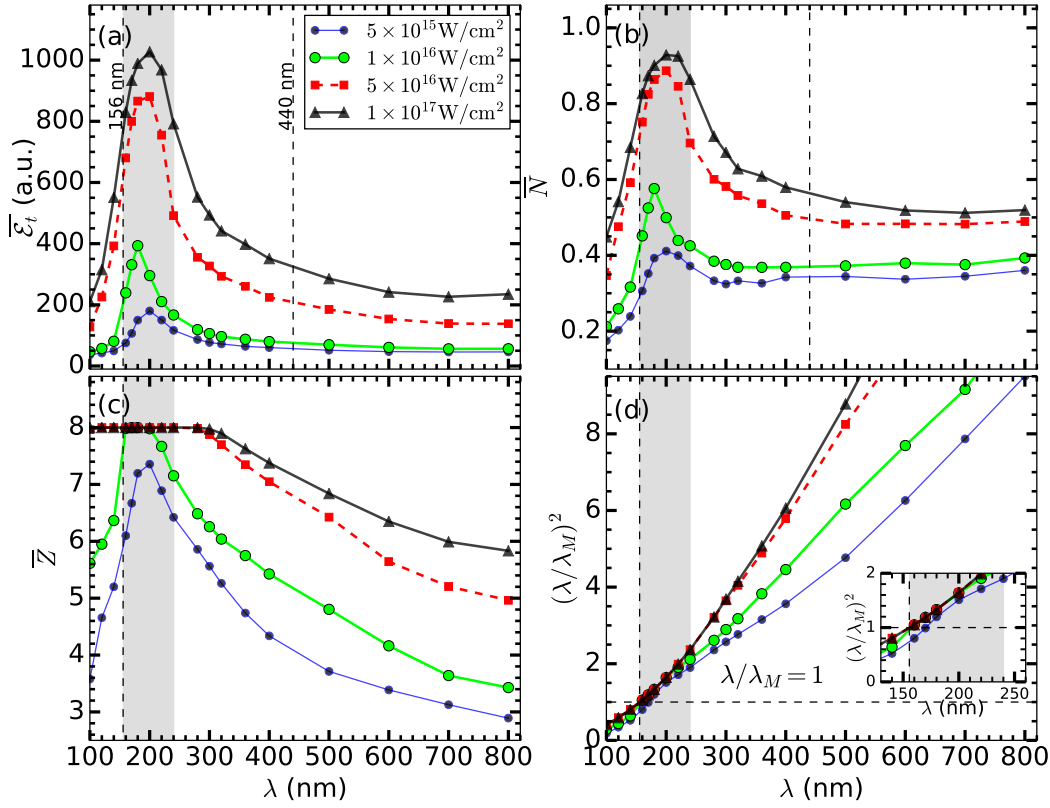


Figure 4.5: Average total absorbed energy $\bar{\mathcal{E}}_t$ per atom (a), corresponding fractional outer ionization \bar{N} of electrons (b), average \bar{Z} of argon ions (c), and an approximate $(\lambda/\lambda_M)^2 = (\omega_M/\omega)^2$ (d) versus λ for the argon cluster (radius $R_0 = 2.91$ nm, number of atoms $N = 1791$) after the laser pulses of peak intensities $I_0 \approx 5 \times 10^{15}, 10^{16}, 5 \times 10^{16}, 10^{17} \text{ Wcm}^{-2}$ as in Fig.4.1. For a given I_0 , pulses of different λ are chosen by keeping pulse duration $\tau \approx 13.5$ fs (fwhm ≈ 5 fs) as constant. Vertical dashed lines indicate λ_M where absorption maxima are strictly expected by LR for respective $\bar{Z} = 1, 8$. Shaded bar highlights that absorption maxima are red-shifted in the marginally over-dense regime of $\lambda/\lambda_M \approx 1 - 1.5$, which is more clear in the inset of (d).

signifies the role of “ionization ignition” (by plasma space-charge fields \vec{E}_{sc}) which is found to be more efficient at lower intensities for the creation of higher \bar{Z} than expected by OFI. As more electrons are removed from the $3s^23p^6$ shell, the ionization ignition becomes gradually weaker [an “ionization depletion” may also happen where \bar{Z} falls below the OFI expected value [147] for some I_0 and λ as evident in Fig.4.5(c)] due to

higher restoring force of ions on electrons. The field enhancement due to ionization ignition is not sufficient for the removal of next inner shell ($2s^22p^6$) electrons of argon atoms which require an intensity $> 10^{18} \text{Wcm}^{-2}$.

For the argon cluster the static LR wavelength for $\bar{Z} = 1$ is $\lambda_{M1} = \lambda_M \approx 440 \text{ nm}$. Since \bar{Z} varies between 1 – 8, the static LR wavelengths vary from $\lambda_{M1} \approx 440 \text{ nm}$ to $\lambda_{M8} \approx 440/\sqrt{8} \approx 156 \text{ nm}$ for $\bar{Z} = 8$ [shown by vertical dashed lines in Figs.4.5(a)-4.5(b)]. However, the maxima in the absorption and outer ionization occur at shifted wavelengths (in spite of the saturation of inner-ionization at $\bar{Z} = 8$) which lie in the band of $\lambda \approx 196 \pm 40 \text{ nm}$ because of UDLR (i.e., combined dynamical LR and AHR) those are met differently for different peak intensities. Here, the dynamical LR, unlike the static LR, is decided self-consistently by the inner ionization, outer ionization and cluster expansion during the temporal evolution of a laser pulse and can not be decided *a priori*. At an intensity, the UDLR establishes an optimized competition between outer ionization, cluster expansion and inner ionization: the increasing outer ionization and cluster expansion momentarily try to push the absorption peak right-ward (not visible) from the static LR wavelength of $\lambda_{M1} = 440 \text{ nm}$ in the initial time of OFI, while rapid creation of higher $\bar{Z} = 2 - 8$ soon nullifies the expected red-shift and pushes the absorption peak opposite (ionization induced blue-shift towards $\lambda_{M8} \approx 156 \text{ nm}$, left vertical dashed line) during the laser pulse driving. Finally, due to simultaneous outer ionization and cluster expansion, absorption peaks gradually shift right-ward in the band of wavelength $\Lambda_d \approx 196 \pm 40 \text{ nm}$ from the expected $\lambda_{M8} \approx 156 \text{ nm}$ with increasing intensity similar to the RSM.

Beyond $\lambda \approx 240 \text{ nm}$, argon cluster becomes significantly over-dense as seen from Fig.4.5(d) (and also from its inset) where $(\lambda/\lambda_M)^2 > 2$. In this regime of $\lambda > 240 \text{ nm}$, only AHR plays the dominant role [14, 21] as a collisionless process behind the absorp-

tion, outer ionization and charging of the argon cluster and the approximate effective field $E_{eff} \approx E_0/(\omega_M^2/\omega^2 - 1)$ in the cluster is suppressed below E_0 . In the intermediate (marginally over-dense) regime of $\lambda \approx 156 - 240$ nm [i.e., $\lambda \approx (1 - 1.5)\lambda_M$, or $(\lambda/\lambda_M)^2 \lesssim 1 - 2$, as seen from the inset of Fig.4.5(d)] where AHR and LR become indistinguishable (regime of UDLR), the LR and near LR enhanced field effects play the dominant role as it is understood from the simple estimate of $E_{eff} \approx E_0/(\omega_M^2/\omega^2 - 1)$, e.g., for $(\lambda/\lambda_M)^2 = 1.2, 1.5$, one obtains $E_{eff} = 5E_0, 2E_0$ respectively which may be little over-estimated from the reality. The near-LR enhanced field $E_{eff} \approx E_0/(\omega_M^2/\omega^2 - 1) \gtrsim E_0$, in the marginally over-dense regime of $1 \lesssim (\lambda/\lambda_M)^2 \lesssim 2$, increases efficiency of AHR and helps some/many electrons to undergo AHR at ease. Clearly, MD results with self-consistently determined charge states and cluster expansion (i.e., with variable ω_M) in addition to the absorption and outer ionization as in the RSM, un-equivocally support that maximum absorption in a cluster happens in a shifted band of $\Lambda_d \approx (1 - 1.5)\lambda_M$, but not at the widely expected $\lambda = \lambda_M$ of static LR. The relative red-shifts of absorption peaks are $\Delta\Lambda_d/\lambda_M \approx 6.2\%, 7.5\%, 9.0\%, 9.6\%$ in Fig.4.1, whereas in more realistic MD simulations (Fig.4.5) these are found to be $\Delta\Lambda_d/\lambda_M \approx 19.8\%, 12.8\%, 25\%, 28.2\%$ with increasing I_0 .

Contrary to earlier findings of Petrov *et al.*[19, 22] for a laser driven xenon cluster, we find that cluster charging, average charge per atom, number of electrons, and peak electron density are strong function of λ (see Fig.4.5) depending upon the peak laser intensity. Note that Petrov *et al.*[19, 22] performed MD simulations *only* at three different $\lambda = 100, 248, 800$ nm at a single intensity of 10^{16} Wcm^{-2} . Since the absorption maxima is red-shifted (as shown by MD and RSM) in the regime of $\lambda \approx (1 - 1.5)\lambda_M$, it is possible that they had missed the absorption maxima which they precisely expected at $\lambda = \lambda_M = 248$ nm (for the xenon cluster) according to the conventional notion.

4.3.4 Time domain analysis of the resonance shift

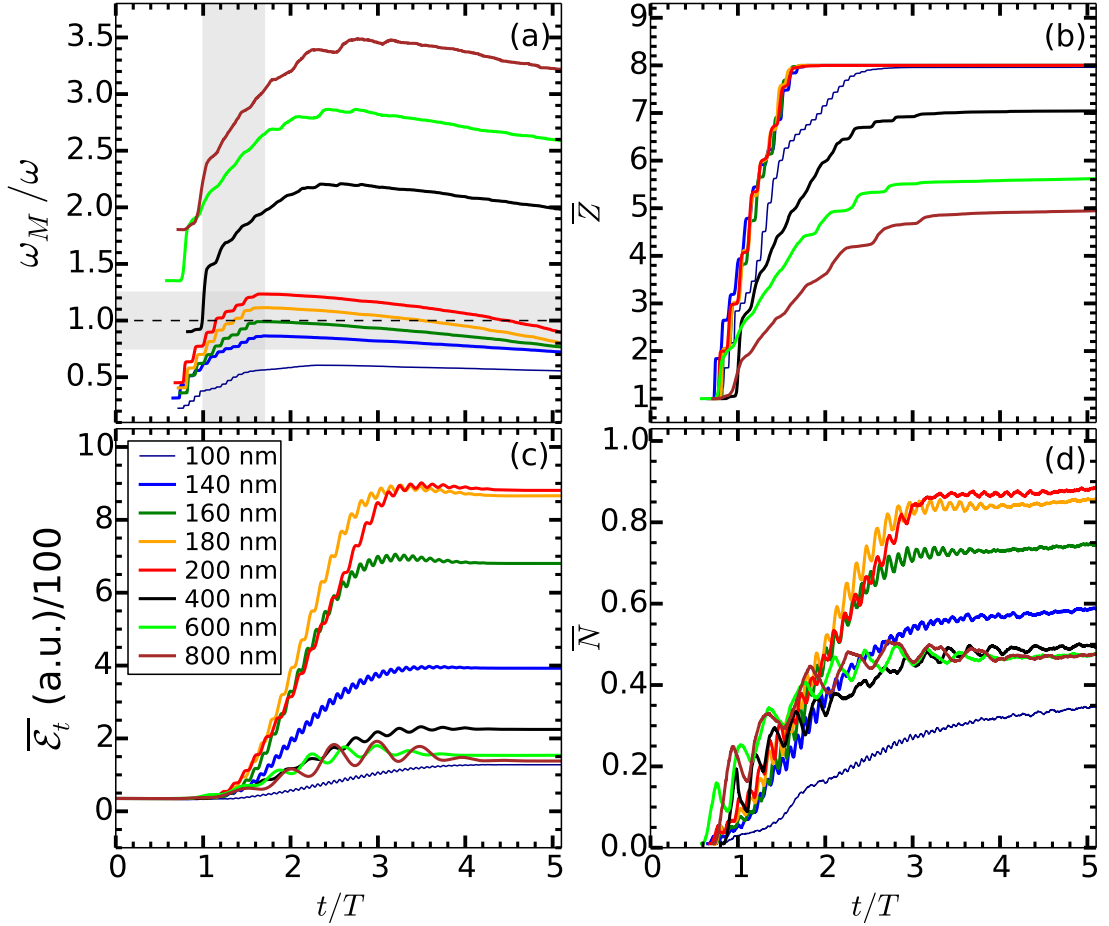


Figure 4.6: Temporal variation of (a) normalized Mie-frequency $\omega_M(t)/\omega$, (b) average charge state $\bar{Z}(t)$, (c) total absorbed energy $\bar{\mathcal{E}}_t(t)$ per atom and (d) fraction of outer electrons $\bar{N}(t)$ for the argon cluster (in Fig. 4.5) when irradiated by 5-fs (fwhm) laser pulses of peak intensity $5 \times 10^{16} \text{ Wcm}^{-2}$ and different $\lambda = 100 - 800 \text{ nm}$. Time is normalized by the period T of $\lambda = 800 \text{ nm}$. Other parameters are same as Fig. 4.5. It is seen that maximum absorption and outer ionization happen at the marginally over-dense $\lambda \approx 200 \text{ nm}$. Shaded regions in (a) highlight efficient regime of interaction where UDLR is prominent.

To further justify the UDLR and the shifting of the absorption maxima, we analyze the evolution of the argon cluster in the time domain. Figures 4.6(a)-4.6(d) show temporal variation of scaled Mie-frequency $\omega_M(t)/\omega = \lambda/\lambda_M(t)$, average charge state $\bar{Z}(t) =$

$N_e(t)/N$ of an argon ion, total absorbed energy $\bar{\mathcal{E}}_t(t)$ per atom and fractional outer ionization $\bar{N}(t) = N_e^{out}(t)/N_e(t)$ of electrons respectively, for different $\lambda = 100 - 800$ nm at the peak intensity of $5 \times 10^{16} \text{ Wcm}^{-2}$ corresponding to the result (red, dashed square) in Fig. 4.5. Time axis is normalized by the laser period T of $\lambda = 800$ nm. The horizontal dashed line in Fig. 4.6(a) indicates the line of static LR condition $\omega_M = \omega$. The charging of the argon cluster starts around $t/T \approx 0.6 - 0.7$ for all wavelengths by the OFI (2.24) when $\bar{Z}(t) = 1$ and the dynamical $\omega_M(t)/\omega$ jumps from zero to a finite value [see Figs. 4.6(a)-4.6(b)]. Successively, laser absorption and outer ionization lead to “ionization ignition” which in turn creates higher $\bar{Z}(t) > 1$ at different ion locations by meeting the condition (2.25) dynamically, thus causing $\bar{Z}(t)$ and corresponding $\omega_M(t)/\omega$ to increase in a step wise manner.

For a shorter $\lambda < 150$ nm, $\omega_M(t)/\omega$ remains below the line of static LR (under-dense) all the time, though respective $\bar{Z}(t)$ increases and saturates at $\bar{Z}(t) \approx 8$ before the peak of the laser pulse at $t/T = 2.5$. In spite of a large number of inner ionized electrons $N_e(t) \approx N\bar{Z}(t)$, absorption and outer ionization is low at 100 nm because of lower ponderomotive energy of electrons at 100 nm compared to 140 nm. Moreover, the $\omega_M(t)/\omega$ at 140 nm being more closer to the LR (from below), electrons experience more enhanced, near-the-LR effective field $E_{eff} \sim E_0/(\omega_M^2/\omega^2 - 1)$ which is responsible for higher absorption and outer ionization than at 100 nm.

For a longer $\lambda > 300$ nm, the line of LR is passed too fast by $\omega_M(t)/\omega$ (see its sharp rise) just after the OFI in the initial time $t/T < 1$ and $\omega_M(t)/\omega$ remains much above the line of LR (over-dense) all the time. This LR in the early time is not effective, due to weaker laser field and negligible time spent during (or near) the LR while crossing the resonance line. Just meeting the frequency matching condition of resonance is not enough for efficient transfer of energy from the driver to an oscillator. The

time spent near the resonance and the strength of the driver are also important. Thus at long wavelengths > 300 nm, absorption and outer ionization are not so much in the early time $t/T < 1.5$. However, as time goes on, $\bar{Z}(t)$ increases and reaches a saturation while corresponding $\omega_M(t)/\omega$ reaches a maximum and drops due to cluster expansion after $t/T \approx 3$. The cluster charging, absorption and outer ionization for $\lambda > 300$ nm are poorer than their respective values at the near-the-LR under-dense wavelength of $\lambda \approx 140$ nm. In this over-dense regime of $\lambda > 300$ nm, clearly LR does not play *any role* but cluster charging, absorption and outer ionization still happen [Figs.4.6(b)-4.6(d)] due to the *dominant* AHR process [14, 21, 99].

In the intermediate band of $\lambda \approx 196 \pm 40$ nm, respective dynamical $\omega_M(t)/\omega$ just cross the line of static LR during $t/T \approx 1 - 1.6$ (vertical shaded bar) and elapse different times to its vicinity (in the marginally over-dense region, horizontal shaded bar) as compared to the other wavelengths outside this band. The slow passage of different $\omega_M(t)/\omega$ through the line of LR (i.e., more time elapsed near the LR) in the initial time $t/T < 1.6$ couples laser energy so efficiently (in spite of laser field not being at its maximum) that inner-ionization is saturated due to the liberation of all electrons from $3s^23p^6$ shells of argon atoms while absorption and outer ionization start at a greater pace as evident from change of their respective slopes. At 160 nm, which is close to the static LR condition of $\lambda_M \approx 156$ nm for $\bar{Z} \approx 8$, the $\omega_M(t)/\omega$ just meets the line of LR for a while $t/T \approx 1.5 - 2.0$, but absorption and outer ionization are *still* not at their maximum which is often expected according to LR. Since $\omega_M(t)/\omega$ does not exceed unity, AHR is not possible. Instead, for 200 nm, the $\omega_M(t)/\omega$ slowly passes the line of LR during $t/T \approx 1 - 1.4$, reaches a maximum value of $\omega_M/\omega \approx 1.25$ at $t/T \approx 1.6$ and remains marginally above the line of LR for almost the entire pulse duration with a slow fall towards the under-dense regime due to Coulomb expansion. Here, resonances are

efficiently and dynamically met at different stages, e.g., (i) LR during the initial time $t/T \approx 1 - 1.4$, (ii) combined LR and AHR in the marginally over-dense regime during $t/T \approx 1.2 - 4.5$, and (iii) LR in the Coulomb expansion phase around $t/T \approx 4.5$. The absorption and outer ionization are almost indistinguishable and remain almost equally efficient up to $t/T \lesssim 2.5$ for both 160 nm and 200 nm, but they begin to separate after the pulse peak at $t/T \approx 2.5$ where $\omega_M(t)/\omega$ quickly falls to the under-dense regime (where AHR is not possible) for 160 nm whereas it continues in the marginally over-dense regime (where both AHR and near-LR field effects contribute) for 200 nm until the end of the pulse. The case of 180 nm is very similar to the case of 200 nm, i.e., passage of $\omega_M(t)/\omega$ through LR during $t/T \approx 1 - 1.2$, reaching a maximum value of $\omega_M(t)/\omega \approx 1.1$ at $t/T \approx 1.6$, traversal of $\omega_M(t)/\omega$ in the marginally over-dense regime during $t/T \approx 1 - 3.6$, meeting the LR in the CE phase at $t/T \approx 3.6$, and finally dropping to the under-dense regime for $t/T > 3.6$. It is noticed that for 180 nm, $\bar{\mathcal{E}}_t(t)$ and $\bar{N}(t)$ grow in faster pace than those at 200 nm upto $t/T \approx 3$. However, the longer time spent by the system while passing through the LR and in the marginally over-dense regime justifies maximum absorption and outer ionization at the *shifted* wavelength of $\lambda = 200$ nm (from the static LR wavelength of $\lambda_M \approx 156$ nm) than 160 nm and 180 nm as well. The average charge state, laser absorption and outer ionization of electrons [Figs. 4.6(b)-4.6(d)] are greatly enhanced at the end of the pulse of 200 nm due to the above unified dynamical LR which explains the maximum charging, absorption and outer ionization in Fig.4.5 at different intensities as well as shifting of absorption peaks from the expected LR condition of $\lambda = \lambda_M$.

Clearly, an effective unification of the early time LR [option(i)] along with the wavelength variation [option (iii)] in the band of $\Lambda_d \approx 196 \pm 40$, the LR in the Coulomb expanding phase [option(ii)] and the AHR in the marginally over-dense regime have been

self-consistently decided by the system to work unitedly here (at 200 nm) for the maximum laser absorption in the argon cluster with a short 5-fs (fwhm) pulse which is rarely possible with long wavelength > 400 nm and longer pulses. Thus we find that unified dynamical LR (UDLR) leads to maximum laser absorption in a cluster in a shifted band of wavelength $\Lambda_d \approx (1 - 1.5)\lambda_M$ in presence of outer ionization.

4.3.5 Resonance shift with continuous short laser pulses

One may surmise that whether redshifts of absorption peaks in Fig.4.5 are due to the frequency broadening of short pulses used here. Note that pulse duration is fixed at $\tau \approx 13.5$ fs which corresponds $n = 5$ laser cycles at $\lambda = 800$ nm and $n = 40$ laser cycles at $\lambda = 100$ nm. So the uncertainties $\Delta\omega = \omega/n$ in frequencies $\omega_{2,3} = (1 \pm 1/n)\omega$ [see below Eq.(3.4) for $\omega_{2,3}$] are greatly reduced from 0.2ω to 0.025ω as λ is changed from 800 nm to 100 nm. Corresponding to peak values of $\bar{Z} \approx 7 - 8$ in Fig.4.5(c), for intensities $I_0 \approx 5 \times 10^{15} - 10^{17} \text{ Wcm}^{-2}$ near the absorption peak, Mie-resonance wavelengths lie in the range of $\lambda_M \approx 166 - 156$ nm. The uncertainties in frequencies at these laser wavelengths λ are $\Delta\omega \approx (800 \times 5/166)^{-1}\omega \approx 0.0415\omega$ and $\Delta\omega \approx (800 \times 5/156)^{-1}\omega \approx 0.04\omega$ where $(800 \times 5/\lambda)$ is the n for λ ; and corresponding redshifts of $\Delta\lambda \approx 0.0415 \times 166 \approx 7$ nm and $\Delta\lambda \approx 0.04 \times 156 \approx 6$ nm may be expected in absorption peaks. However, if we see MD results in Fig.4.5, absorption peaks occur near $\lambda = \Lambda_d \approx 200$ nm and estimated redshifts of Λ_d from λ_M range from $\Delta\Lambda_d \approx 30$ nm to $\Delta\Lambda_d \approx 45$ nm (depending on the laser intensity). The expected redshifts of $\Delta\lambda \approx 6 - 7$ nm (obtained above) due to the uncertainties in laser frequencies of shorter pulses are significantly small and insufficient to explain estimated redshifts $\Delta\Lambda_d \approx 30 - 45$ nm of Λ_d from respective $\lambda_M = 166 - 156$ nm.

To establish the argument that redshifts of absorption peaks in Fig.4.5 (also in Figs.4.1,4.2

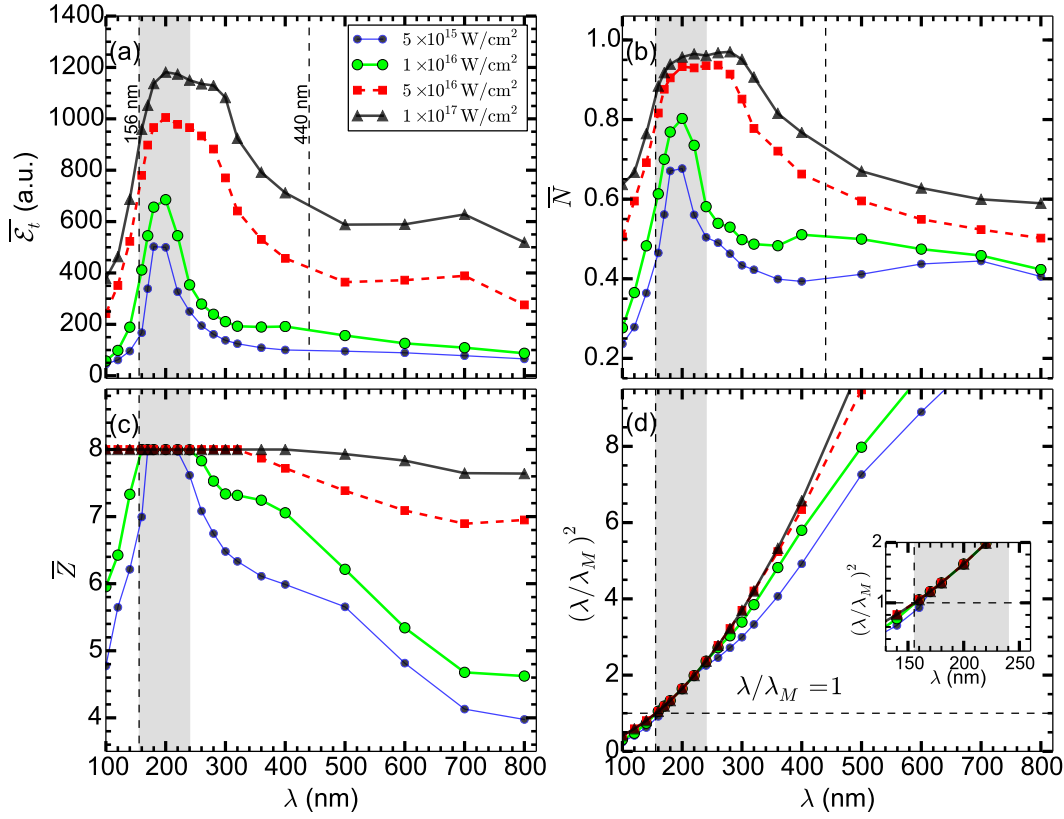


Figure 4.7: (color online) Average total absorbed energy $\bar{\mathcal{E}}_t$ per atom (a), corresponding fractional outer ionization \bar{N} of electrons (b), average \bar{Z} of argon ions (c), and $(\lambda/\lambda_M)^2$ (d) versus λ for the same argon cluster ($R_0 = 2.91$ nm, $N = 1791$) at the end of 13.5 fs continuous pulses $E_I(t) = E_0 \sin(\omega t)$ (with no uncertainty in ω) of same $I_0 \approx 5 \times 10^{15}, 10^{16}, 5 \times 10^{16}, 10^{17} \text{ Wcm}^{-2}$ as in Fig.4.5. For a given I_0 , continuous pulses of different λ are chosen by keeping pulse duration $\tau \approx 13.5$ fs as constant. Vertical dashed lines indicate λ_M where absorption maxima are strictly expected by LR for respective $\bar{Z} = 1, 8$. Shaded bar highlights that absorption maxima are red-shifted in the marginally over-dense regime of $\lambda/\lambda_M \approx 1 - 1.5$, which is more clear in the inset of (d). Clearly, redshifts in absorption peaks are not due to uncertainties in frequencies of shorter pulses.

in the model), are not only due to the frequency broadening of short pulses, we now simulate the argon cluster of Fig.4.5 with continuous laser pulses $E_I(t) = E_0 \sin(\omega t)$ (having no uncertainty in ω) of same $I_0 \approx 5 \times 10^{15}, 10^{16}, 5 \times 10^{16}, 10^{17} \text{ Wcm}^{-2}$ and $\lambda = 100 - 800$ nm as in Fig.4.5, and stop the pulses after $\tau = 13.5$ fs (for 5-cycles at

800 nm). In this case, pulse-envelops may be regarded as rectangular, each having a duration of $\tau = 13.5$ fs. Corresponding results are displayed in Figs.4.7(a)-4.7(d) which bear same meaning of respective Figs.4.5(a)-4.5(d) (see also caption of Fig.4.7). Compared to Fig.4.5, for a given I_0 and λ , absorbed energy $\overline{\mathcal{E}}_t$ per atom, and fractional outer ionization \overline{N} of electrons systematically increase (average \overline{Z} also systematically increase except near the closed shell of argon atoms, where $\overline{Z} = 8$ is saturated) due to more energy carried by a continuous pulse than a \sin^2 -enveloped pulse (3.4) (used in Fig.4.5) of same duration $\tau = 13.5$ fs. Even, at the lowest intensity $I_0 \approx 5 \times 10^{15} \text{ Wcm}^{-2}$, average \overline{Z} now reaches a saturation at $\overline{Z} = 8$ within the band of $\lambda \approx 156 - 240$ nm. For a given I_0 , however, redshifts of peaks of $\overline{\mathcal{E}}_t$ and \overline{N} in Figs.4.7(a)-4.7(b) are either nearly the same as those of Figs.4.5(a)-4.5(b) or have the tendency to be more red-shifted from the static Mie-resonance wavelength $\lambda_M = 156$ nm (dashed vertical line). Nevertheless, redshifts of absorption peaks also occur with continuous pulses (in Fig.4.7) and the uncertainty in the frequency broadening of a shorter pulse of $\tau = 13.5$ fs is insufficient to explain the estimated redshift of Λ_d from λ_M in this work.

4.3.6 Resonance shift with cluster size variation

So far it is not known how the redshift of the absorption peak changes with the cluster size variation. For completeness, we now study argon clusters of four different sizes of $R_0 \approx 2.2, 2.5, 2.9, 3.7$ nm (including the cluster of Fig.4.5) with respective number of atoms $N = 739, 1189, 1791, 3695$ while keeping the peak intensity fixed at $I_0 \approx 5 \times 10^{16} \text{ Wcm}^{-2}$ and the same laser pulse conditions of Fig.4.5 with $\tau = 13.5$ fs.

As in Figs.4.5(a)-4.5(c), $\overline{\mathcal{E}}_t$, \overline{N} and \overline{Z} versus λ for different R_0 are shown in respective Figs. 4.8(a)-4.8(c) where different \overline{Z} do not differ much for $\lambda < 500$ nm and saturate at $\overline{Z} = 8$ irrespective of cluster sizes in the marginally over-dense band of

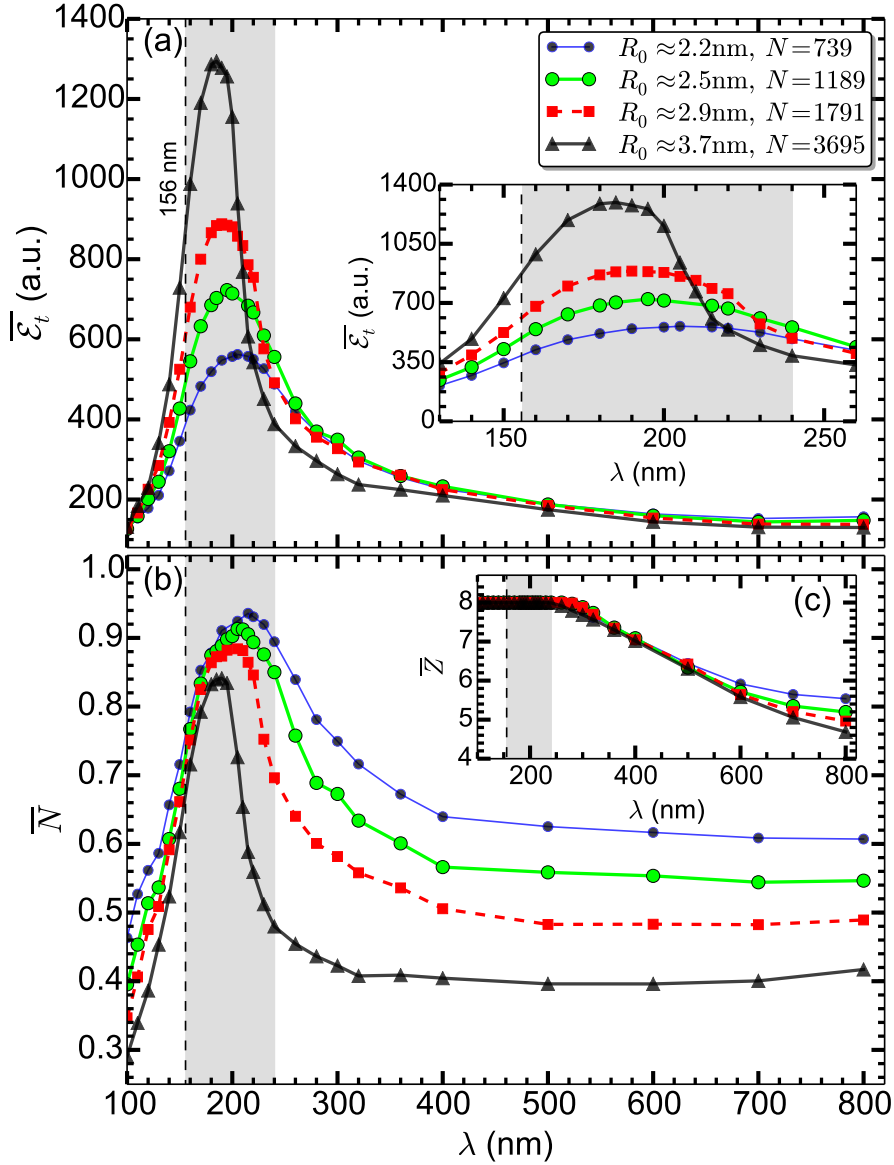


Figure 4.8: (color online) Average total absorbed energy $\bar{\mathcal{E}}_t$ per atom (a), fractional outer ionization \bar{N} of electrons (b) and average \bar{Z} of argon ions (c) versus λ for different argon clusters of radii $R_0 \approx 2.2, 2.5, 2.9, 3.7$ nm with respective number of atoms $N = 739, 1189, 1791, 3695$ (including cluster of Fig.4.5) after the laser pulse of fixed $I_0 \approx 5 \times 10^{16} \text{ Wcm}^{-2}$ as in Fig.4.5 and fixed $\tau \approx 13.5$ fs. Other conditions are same as Fig.4.5. Vertical dashed line indicate λ_M where absorption peak is expected by LR for $\bar{Z} = 8$. Shaded bar highlights that absorption maxima are red-shifted in the marginally over-dense regime of $\lambda/\lambda_M \approx 1 - 1.5$ [more clear in the inset of (a)]. Redshift in absorption peak decreases as cluster size increases.

$\lambda = 156 - 240$ nm. The maximum number of electrons created in the largest and the smallest cluster are respectively $N_e \approx N\bar{Z} = 29560, 5912$, corresponding maximum outer ionized electrons are $N_e^{om} \approx 24535, 5498$ with $\bar{N} \approx 0.83, 0.93$ [from Fig. 4.8(b)], and number of outer ionized electrons per atom can be estimated to be $N_e^{om}/N \approx 6.64, 7.44$ respectively. It means that a bigger cluster retains more electrons per atom by exerting relatively higher restoring force than a smaller cluster for the same laser intensity, although absolute outer ionization of electrons from a bigger cluster may exceed a small cluster. Thus, for the same I_0 and τ , as the cluster size increases, the higher restoring of ions on the electrons in a bigger cluster reduces \bar{N} , reduces the redshift of the peak of $\bar{\mathcal{E}}_t$ and \bar{N} towards $\lambda_M = 156$ nm (dashed vertical line), *but* redshift *still* persists in the marginally over-dense band of $\Lambda_d = (1 - 1.5)\lambda_M$.

4.3.7 Resonance shift with different CEPs

It may be questioned that laser absorption is affected due to carrier envelope phase (CEP) effects of short 13.5 fs pulses and consequently the red-shift of the absorption peak may differ for different CEPs. We have checked this by MD simulations for all wavelengths of $\lambda = 100 - 800$ nm at two values of CEPs i.e., $\Phi = 0$ and $\Phi = \pi/2$ for a peak laser intensity of $5 \times 10^{16} \text{ Wcm}^{-2}$ and for the same laser pulse duration of 13.5 fs with same argon cluster ($R_0 = 2.91$ nm, $N = 1791$) of Fig. 4.5 in chapter 4. We can get the temporal nature of the instantaneous electric field for these different phases ($\Phi = 0$ and $\Phi = \pi/2$) from the equation of laser vector potential (Eq. 2.2) described in chapter 2 as $E_l(t) = -dA/dt$.

Figs. 4.9(a)-4.9(c) show average total absorbed energy $\bar{\mathcal{E}}_t$ per atom, fractional outer ionization \bar{N} of electrons and average \bar{Z} of argon ions versus λ for the argon cluster corresponding to $\Phi = 0$ (red, dashed line with square) and $\Phi = \pi/2$ (green, solid line with

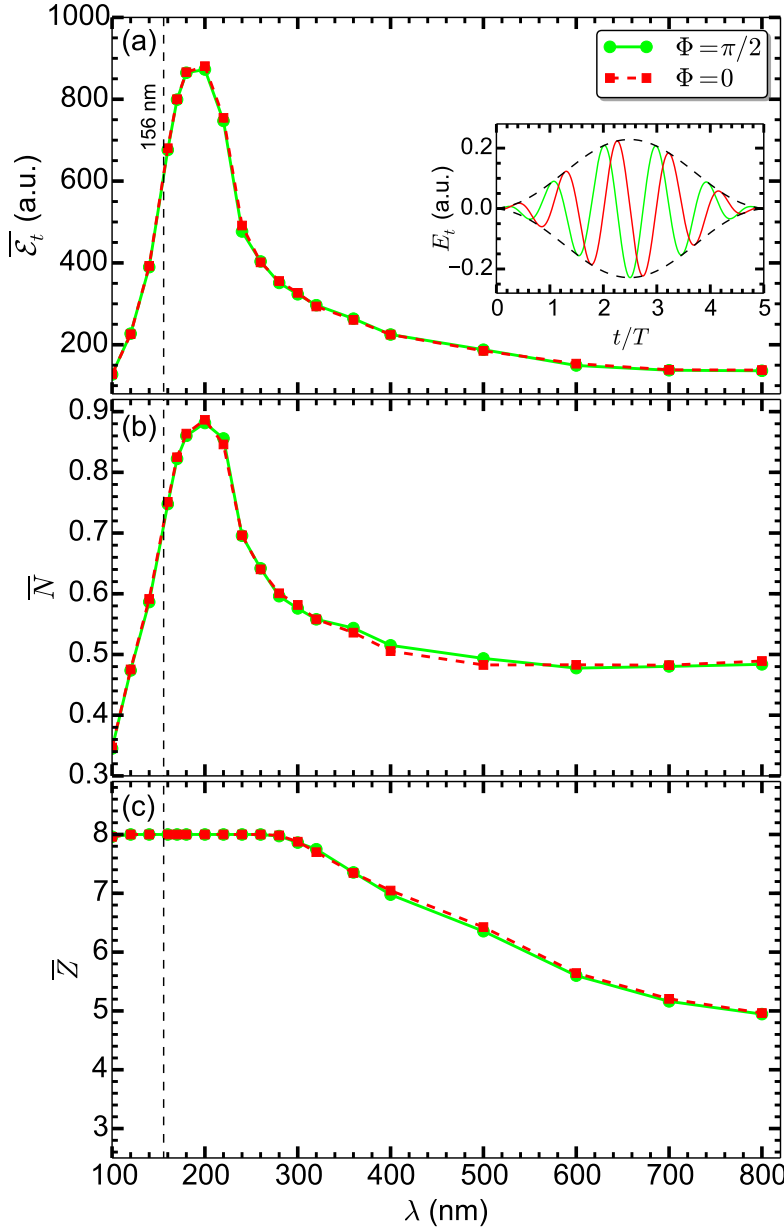


Figure 4.9: Average total absorbed energy $\overline{\mathcal{E}}_t$ per atom (a), corresponding fractional outer ionization \overline{N} of electrons (b) and average \overline{Z} of argon ions (c) versus λ for the argon cluster ($R_0 = 2.91$ nm, $N = 1791$) when irradiated by 13.5 fs (5-fs, fwhm) laser pulses of $I_0 = 5 \times 10^{16} \text{ Wcm}^{-2}$ for CEPs $\Phi = 0$ (red, dashed line with square) and $\Phi = \pi/2$ (green, solid line with circle). The inset in (a) shows typical variation of $E_t(t)$ with same parameters for $\Phi = 0$ (red) and $\Phi = \pi/2$ (green) at 800 nm. Results are overlapped and indistinguishable which clearly show CEP has insignificant role.

circle). Typical nature of $E_I(t)$ for $\Phi = 0, \pi/2$ are shown in the inset of Fig.4.9(a) for 800 nm. From these results (Fig.4.9), we confirm that there is no significant difference in $\overline{\mathcal{E}}_t$, \overline{N} and \overline{Z} if we change the CEP and the effect of CEP is not important at all for the 13.5 fs pulse-duration and hence, the red-shift of an absorption peak is hardly affected by different CEPs.

4.4 Summary

In this chapter, we study interaction of short 5-fs (fwhm) laser pulses with an argon cluster using MD simulation and RSM to find out the wavelength regime where laser absorption in argon cluster is maximized for a given intensity and pulse energy. It seems trivial for many researchers (in the field of laser-plasma interaction) to answer immediately that maximum absorption should occur at the wavelength λ_M of linear resonance (LR) irrespective of laser intensity, as in the nano-plasma model [9] or in the collective oscillation model. However we find that, for a given laser pulse energy and a cluster, at each peak intensity there exists a λ – shifted from the expected LR wavelength of λ_M – that corresponds to a *unified dynamical* LR (coined as UDLR) at which evolution of the cluster happens through very efficient unification of possible resonances in various stages, including (i) the LR in the initial time of plasma creation, (ii) the LR in the Coulomb expanding phase in the later time and (iii) anharmonic resonance in the marginally over-dense regime for a relatively longer pulse duration below 5-fs (fwhm), leading to maximum laser absorption accompanied by maximum removal of electrons from cluster and also maximum allowed average charge states \overline{Z} of argon atoms in the cluster. Increasing the laser intensity, the absorption maxima is found to shift to a higher wavelength in the band of $\Lambda_d \approx (1 - 1.5)\lambda_M$ than staying permanently at the expected λ_M , e.g., $\lambda_M \approx 156$ nm for $\overline{Z} = 8$ [see Fig.4.5]. The simple RSM

also corroborates the wavelength shift of the absorption peak (in spite of the absence of cluster charging and expansion) as found in MD. Thus RSM and MD un-equivocally prove that maximum absorption in a laser driven cluster happens at a shifted λ in the marginally over-dense regime of $\lambda \approx (1 - 1.5)\lambda_M$ instead of λ_M of LR for all intensities $10^{15} \text{ Wcm}^{-2} - 5 \times 10^{17} \text{ Wcm}^{-2}$. The redshift of resonance with respect to the Mie-wavelength (λ_M) may be attributed to spill out of electrons beyond the ion background as in the case of typical laser-solid interaction.

Therefore, if an experiment or a simulation is performed at the static LR wavelength which is *often* decided *a priori*, the absorption will not be maximum and may lead to a conclusion that resonance has no role [19, 22] for laser absorption. Instead, at a given intensity, an efficient unification of resonances (i.e., UDLR) happens at a shifted wavelength in the band of $\Lambda_d \approx (1 - 1.5)\lambda_M$ that leads to maximum laser absorption. Our results may be useful to guide an optimal condition experiment with argon cluster in the short pulse regime where maximum conversion of energy from laser to particles is required.

5

Dependence of red-shift of absorption peak on laser polarization, intensity, and wavelength for a deuterium cluster

*In the previous chapter (4), we have restricted the study of unified dynamical linear resonance (UDLR) for one type of atom (e.g., argon) and also for one degree of polarization, e.g., linear polarization. To justify and validate the UDLR in the wavelength band of $\Lambda_d = (1 - 1.5)\lambda_M$, in this chapter *, we have further extended our study for a different cluster type, i.e., deuterium (other than argon) for its universal acceptance. We also explore the effect of laser polarization on the UDLR and the red-shift of the resonance absorption peak using the MD simulation and by the RSM analysis.*

* **S. S. Mahalik** and M. Kundu, “Collisionless absorption of short laser pulses in a deuterium cluster: dependence of redshift of resonance absorption peak on laser polarization, intensity and wavelength”, [arXiv:1812.10046](https://arxiv.org/abs/1812.10046) (2018)

5.1 Introduction

Several experimental, theoretical and particle-simulation works on laser-cluster interaction have reported the effect of various parameters of laser and cluster (i.e., peak intensity, wavelength, pulse duration, polarization of laser pulse, cluster size and type etc.) on average charge per atom, mean electron and ion energies and also total absorbed energy. In chapter 4, we reported dependence of energy absorption on laser wavelength (λ) by MD simulation for an argon clusters of different sizes (2-4 nm) irradiated by LP laser fields with different peak intensities and wavelengths $\lambda = 100 - 800$ nm. MD results were also supported by RSM. We showed that for a given pulse energy, maximum laser absorption in a cluster happens *not* at the well-known static Mie-resonance wavelength of λ_M , but at a red-shifted λ which lies in the marginally over-dense band of wavelength $\Lambda_d \approx (1 - 1.5)\lambda_M$. Note that linear Mie-theory (as in the case of nano-plasma model [2, 9]) is valid only at lower intensities where static Mie-resonance at $\lambda = \lambda_M$ is possible which is often identified as a sharp peak in the absorption curve. However, with increasing laser intensity, linear Mie-theory fails and resonance absorption peak is gradually red-shifted from λ_M . At this shifted $\Lambda_d \approx (1 - 1.5)\lambda_M$ all the possible resonances, i.e., dynamical linear resonance (LR) and anharmonic resonance (AHR) are unified [24] to yield maximum laser absorption. We termed this combined resonance as the unified dynamical linear resonance (UDLR) and strongly concluded that there is always a redshift of the absorption peak with respect to λ_M in the band of $\Lambda_d \approx (1 - 1.5)\lambda_M$ irrespective of the laser intensity, cluster size and laser pulse type.

However, for different types of clusters, it is still unknown how the redshift of the absorption peak changes with laser intensity. This is particularly very important to justify and validate the above mentioned UDLR [24] in the wavelength band of

$\Lambda_d \approx (1 - 1.5)\lambda_M$ with a different cluster type (other than the argon cluster) for its universal acceptance. Further, the degree of polarization of the impinging laser pulse is also an important parameter that changes the dynamics of the cluster electrons, hence it *might* effect the UDLR and the redshift of the absorption peak which remains to be *explored*. An electron under the influence of a circularly polarized (CP) laser moves spirally, whereas in LP laser it executes oscillatory motion perpendicular to the direction of the laser propagation. The spiral motion of electron in CP prevents the electron-rescattering from the cluster boundary, whereas the probability of rescattering is more for LP. Particle-in-cell (PIC) simulations [99] performed for a xenon cluster at different intensities and cluster charge densities but at a *fixed* $\lambda = 1056$ nm (with immobile ions) concluded that energy absorption and outer ionization in CP and LP laser field are almost equally efficient. However, it is not known (i) how absorbed energies compare with LP and CP laser fields with the variation of λ and (ii) how UDLR (in the marginally overdense regime) helps in the redshift of absorption peaks from the λ_M in LP and CP fields. Note that, even if laser intensity is kept fixed, ponderomotive energy $U_p = E_0^2 \lambda^2 / 4$ of electron and its dynamics is affected by varying λ which is expected to contribute to the redshift of the absorption peak. We thus present energy absorption and outer ionization for a deuterium cluster (as a different cluster type other than argon) with CP and LP lasers. Particularly, we show the effect of laser polarization on the redshift of the absorption peak in the collisionless regime.

We consider a deuterium cluster of radius $R_0 \approx 2.05$ nm (charge state $Z = 1$) which is irradiated by LP and CP laser pulses of different peak intensities $I_0 = 5 \times 10^{15} - 5 \times 10^{17} \text{ Wcm}^{-2}$ and $\lambda = 100 - 800$ nm. For a given intensity and polarization we vary λ . Similar to previous studies with argon clusters in chapter 4, here we find that, for both LP and CP, redshifts of the absorption peaks from the static Mie-resonance wave-

length $\lambda_M = 263$ nm (for deuterium cluster) still persist, which also lie in the marginally over-dense band of wavelength $\Lambda_d \approx (1 - 1.5)\lambda_M$ as long as outer-ionization is below 100%. Redshift of the absorption peak monotonically increases with increasing I_0 . Additionally, above a certain I_0 , absorption peak is found to disappear with further increase in $I_0 \geq 10^{17} \text{Wcm}^{-2}$ as outer ionization saturates at 100%. It is also found that before the absorption peak in the band of $\Lambda_d \approx (1 - 1.5)\lambda_M$, laser absorption due to LP and CP lasers are almost equally efficient (CP case being inappreciably higher than LP) for all intensities and λ . However, after the absorption peak, at lower intensities $\leq 10^{17} \text{Wcm}^{-2}$, absorption due to LP inappreciably dominates absorption due to CP with increasing λ which gradually reverses at higher intensities $\geq 10^{17} \text{Wcm}^{-2}$.

Organization of the chapter is as follows: Section 5.2 illustrates laser absorption and the role of laser polarization on the redshift of the absorption peak in the deuterium cluster by a MD simulation. Section 5.3 gives justification of MD results by RSM analysis. Summary of this chapter is given in Section 5.4.

5.2 Resonance absorption by MD simulation

In this section, we report a comparative study of laser absorption and outer ionization and the dependence of the red-shift of absorption maxima in the UDLR regime with a deuterium cluster for different polarization states of laser pulses by MD simulation.

We consider a deuterium cluster of radius $R_0 \approx 2.05$ nm and $N = 1791$ number of neutral atoms. Ionization of deuterium atoms is treated by “over the barrier” ionization (OBI) model (2.24) of optical field ionization (OFI) as described in chapter 2. When all atoms are ionized initially, it gives a charge density $\rho_i \approx 7 \times 10^{-3}$ a.u. and $\omega_M = \sqrt{4\pi\rho_i/3} = 0.1735$ a.u.. For 800 nm, it represents an over-dense plasma with $\rho_i/\rho_c \approx 27.87$ and $\omega_M/\omega \approx 3.05$, where $\rho_c \approx 1.75 \times 10^{27} \text{m}^{-3}$ is the critical density.

The deuterium cluster is irradiated by short laser pulses of duration 13.5 fs (FWHM of 5-fs) at different $I_0 = 5 \times 10^{15} \text{ Wcm}^{-2} - 5 \times 10^{17} \text{ Wcm}^{-2}$. The pulse energy is also kept fixed for a particular I_0 and wavelength is varied in the range of $\lambda = 100 - 800 \text{ nm}$ for both LP and CP laser light (see Sec. 2.4 for laser pulses of different polarization).

5.2.1 Absorption and outer ionization with LP laser

Figs. 5.1(a)-(b) depicts average total absorbed energy $\overline{\mathcal{E}}_t = \sum_1^{N_p} (v_i^2/2 + q_i\phi_i)/N$ per atom and corresponding fractional outer ionization $\overline{N} = N_e^{\text{out}}/N$ of electrons at the end of 13.5 fs LP laser pulses versus λ for different I_0 , where N_e^{out} is the number of electrons outside the initial radius R_0 . At lower $I_0 \lesssim 5 \times 10^{16} \text{ Wcm}^{-2}$, $\overline{\mathcal{E}}_t$ and \overline{N} initially increase with increasing λ , attain different maximum values at different λ between $263 - 400 \text{ nm}$, i.e., in the band of $\lambda = \Lambda_d \approx 330 \pm 67 \text{ nm}$ which is equivalent to $\Lambda_d \approx (1 - 1.5)\lambda_M$, then drop as λ is increased further. For the deuterium cluster, the static Mie-resonance (or the static LR) with a sharp absorption maxima is often conventionally expected at $\lambda = \lambda_M \approx 263 \text{ nm}$ (marked by vertical dashed line) according to the nano-plasma model. In stead, it is seen that $\overline{\mathcal{E}}_t$ and \overline{N} attain maximum values in the band of $\Lambda_d \approx (1 - 1.5)\lambda_M$ which are red-shifted from the expected $\lambda_M \approx 263 \text{ nm}$, and the red-shift increases with increasing values of $\overline{\mathcal{E}}_t$ and \overline{N} for increasing $I_0 \lesssim 5 \times 10^{16} \text{ Wcm}^{-2}$. For higher $I_0 > 5 \times 10^{16} \text{ Wcm}^{-2}$, absorption peaks gradually disappear due to faster saturation of outer ionization of electrons to 100%. Approaching towards $\lambda_M \approx 263 \text{ nm}$ from 100 nm , higher intensity pulse expels more electrons from the cluster at a much faster rate than at a lower intensity [see Figs.5.1(a)-(b)]. As electrons move far from the cluster, the laser field dominates over the restoring field of background ions acting on those free/quasi-free electrons. Therefore, after the 100% outer ionization for an intensity, the average $\overline{\mathcal{E}}_t$ may also grow [see Fig.5.1(a) for $I_0 \geq 10^{17} \text{ Wcm}^{-2}$] with increasing

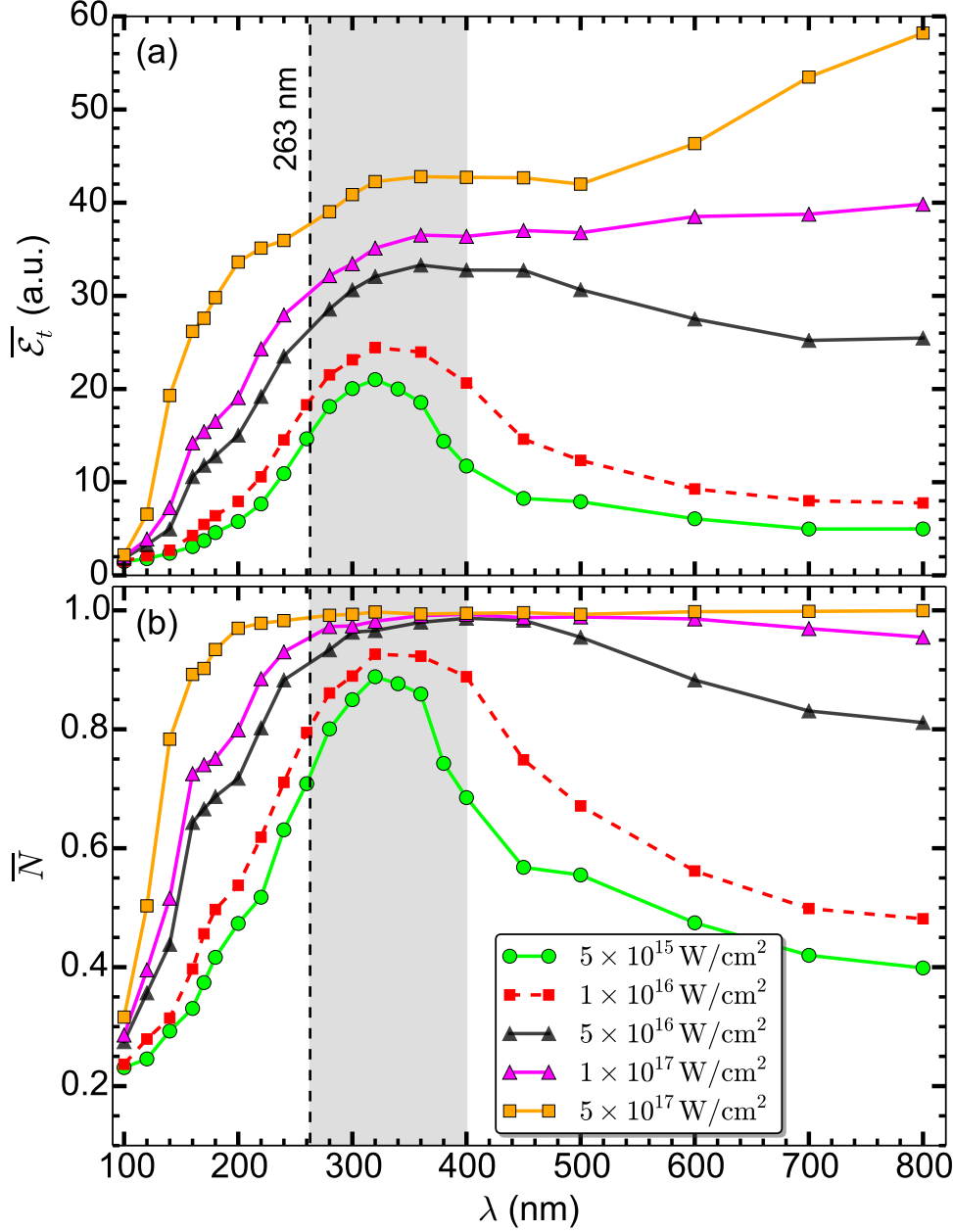


Figure 5.1: MD results showing average total absorbed energy $\overline{\mathcal{E}}_t$ per atom (a) and corresponding fractional outer ionization of electrons \overline{N} versus λ for deuterium cluster ($R_0 = 2.05 \text{ nm}$, $N = 1791$) at different peak intensities $I_0 = 5 \times 10^{15} \text{ Wcm}^{-2} - 5 \times 10^{17} \text{ Wcm}^{-2}$. At a particular I_0 , pulse energy for all λ is kept constant with constant pulse duration $\tau = 13.5 \text{ fs}$ (fwhm $\approx 5\text{-fs}$). Vertical dashed line indicates λ_M that corresponds to LR wavelength for $\overline{Z} = 1$. The shaded bar highlights that absorption maxima are red-shifted in the marginally overdense regime of $\lambda = (1 - 1.5)\lambda_M$.

λ since the average energy of a laser-driven free electron scales as $\approx U_p \propto E_0^2 \lambda^2 / 4$. Because electrons (free or bound) do not have same energy and liberated at different times, the growth of $\overline{\mathcal{E}}_t$ is slower than the scaling of $\approx U_p$. In this regime of 100% outer ionization, absorption maxima does not show up and the absorption curve does not bend down with increasing λ . So, the survival of the absorption peak (and its red-shift from the static LR wavelength $\lambda_M \approx 263$ nm) depends on the population of bound and free electrons during the interaction. As the free population of electrons increases with increasing I_0 , absorption peak gradually shifts towards higher λ in the band of $\Lambda_d \approx (1 - 1.5)\lambda_M$ from λ_M , and finally it disappears with the free population eventually reaching to 100%.

To understand the growth of average energy with increasing I_0 and disappearance of the absorption peak when outer ionization is 100% saturated for some higher I_0 , we look into the kinetic energy scaling of free/quasi-free electrons which are far from the cluster. We extract the average total kinetic energy of the electrons $\overline{\mathcal{E}}_k = \sum_1^N m_e v_i^2 / 2 / N$ for the highest intensity of $5 \times 10^{17} \text{ Wcm}^{-2}$ corresponding to Fig. 5.1 and compared with the ponderomotive energy scaling $U_p \propto E_0^2 \lambda^2 / 4$. Fig. 5.2 shows $\overline{\mathcal{E}}_k$ for those electrons which are beyond different radii $3R_0, 5R_0, 10R_0, 20R_0$ for $I_0 = 5 \times 10^{17} \text{ Wcm}^{-2}$. The solid (blue) line with circle represents $U_p/5$ for different λ . It is found that the growth of $\overline{\mathcal{E}}_k$ is $\propto U_p$, but it is slower than U_p scaling as different electrons are liberated from the cluster potential at different times by experiencing different laser fields and restoring forces of background ions. Moreover, the scaling $U_p \propto E_0^2 \lambda^2 / 4$ is an over-estimation for a short pulsed light, i.e., shorter the pulses more is the over-estimation. Thus Fig. 5.2 justifies that growth of absorption beyond some intensity and wavelength (when outer ionization reaches 100% in Fig. 5.1) is due to increasing population of free electrons.

The redshifts of absorption peaks in the case of deuterium cluster for lower intensi-

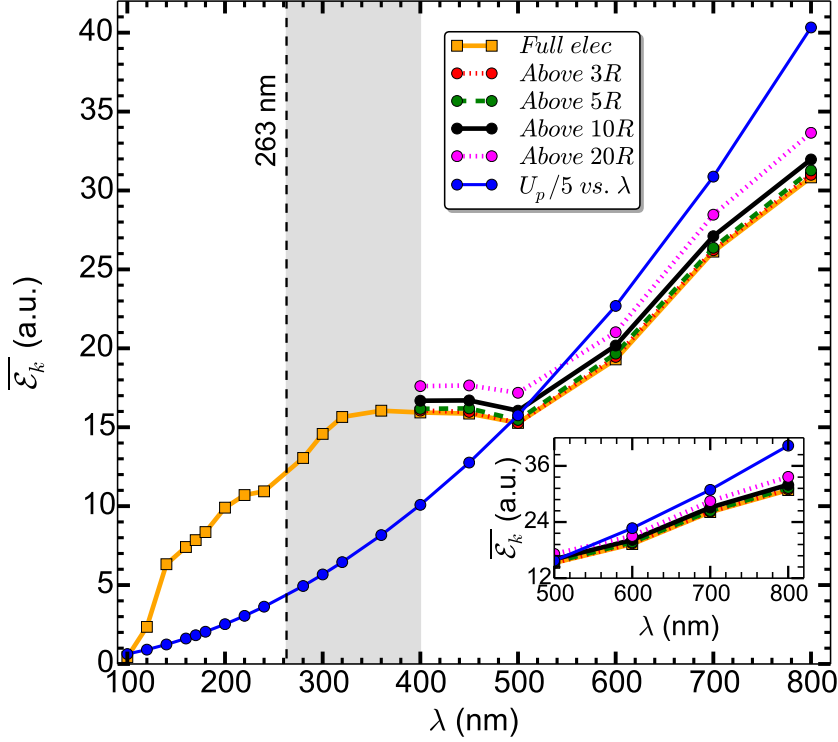


Figure 5.2: MD results showing average kinetic energy $\overline{\mathcal{E}}_k$ per electron versus λ at $I_0 = 5 \times 10^{17} \text{ Wcm}^{-2}$, corresponding to Fig. 5.1 (orange curve). Red, green, black, and magenta curves are the average $\overline{\mathcal{E}}_k$ of those electrons which are beyond $3R_0$, $5R_0$, $10R_0$ and $20R_0$ respectively for $\lambda \geq 400$ nm. Blue curve represents $U_p/5$ for different λ . Thus growth of $\overline{\mathcal{E}}_k$ and $\overline{\mathcal{E}}_t$ (in Fig. 5.1) are due to free electrons.

ties in the band of $\Lambda_d \approx (1 - 1.5)\lambda_M$ also resembles redshifts in the case of argon cluster as described in the chapter 4, which justifies red-shifting of the absorption maxima irrespective of the atom type of a cluster. However, for an argon cluster, absorption peak does not disappear due to supply of electrons via inner ionization and unsaturated outer ionization $< 100\%$ for the same laser intensity $\leq 5 \times 10^{17} \text{ Wcm}^{-2}$ (see chapter 4). For deuterium cluster, in Fig. 5.1, the red-shifted absorption peaks for $I_0 = 5 \times 10^{15} \text{ Wcm}^{-2}$ and $5 \times 10^{16} \text{ Wcm}^{-2}$ are located at $\Lambda_d = 320, 360$ nm respectively and the corresponding free electron's population are 88.8%, 98.6%. With increasing I_0 , for the deuterium cluster, average charge state is quickly saturated at $\overline{Z} = 1$ in the early time of the laser

pulse and remaining pulse energy helps in increasing the absorption, outer ionization of electrons (also early Coulomb explosion of cluster) and gradual increase of redshift of the absorption peak from the expected $\lambda_M \approx 263$ nm. Note that Coulomb explosion of background ions also contributes to the redshift of the absorption peak in the band of $\Lambda_d \approx (1 - 1.5)\lambda_M$ from the λ_M . Therefore larger the peak intensity, larger will be the redshift in the absorption peak from the expected $\lambda_M = 263$ nm when $\bar{Z} = 1$ is saturated as compared to argon cluster [24].

The occurrence of distinct maxima in the absorption and outer ionization in the red-shifted band of $\Lambda_d \approx (1 - 1.5)\lambda_M$ for lower intensities and also dis-appearance of absorption maxima after the 100% saturation of outer ionization for some higher intensities clearly shows the effect of λ variation. Our results in Figs.5.1 contradicts earlier MD simulation works by Petrov et al.[19, 22] where they considered only three wavelengths $\lambda = 100, 248, 800$ nm at a fixed intensity of $I_0 = 5 \times 10^{16} \text{ Wcm}^{-2}$. They could not find any maxima in the absorption while passing through Mie-resonance and nullified any role of Mie-resonance for laser absorption. They further argued that “non-uniform electron density” inside the cluster is responsible for the “null effect” of Mie-resonance [19, 22]. Firstly, we point out that, electron density is always non-uniform within the cluster and its surroundings (during the laser pulse driving; also by birth due to the random distribution of parent atoms in the position and velocity space) that does not explain the absence of Mie-resonance absorption peak. Secondly, only three well-separated wavelengths $\lambda = 100, 248, 800$ nm chosen by Petrov et al. [19, 117] can not resolve the absorption maxima which is evident from Fig.5.1. Thirdly, due to high intensity, resonance absorption maxima is *actually red-shifted* in the band of $\Lambda_d \approx (1 - 1.5)\lambda_M$ from the commonly expected λ_M of Mie-resonance as shown in Fig.5.1 and linear Mie-resonance theory is invalid here. It is delusive to look for the absorption maxima exactly

Chapter 5. Dependence of red-shift of absorption peak on laser polarization, intensity, and wavelength for a deuterium cluster

at the λ_M in presence of non-zero outer ionization at higher intensities. However, the absence of absorption maxima at the expected λ_M does not mean that Mie-resonance has “null effect” in the absorption and outer ionization [19, 22]. In stead, dynamic LR (dynamic Mie-resonance) and AHR work in unison (i.e., UDLR works) in the band of $\Lambda_d \approx (1 - 1.5)\lambda_M$ very efficiently and the near-the-LR effective field E_{eff} [as understood from the simple estimate of $E_{eff} = E_0/(\omega_M^2 - \omega^2)$] inside the cluster is *so much* enhanced that it forces almost 90% electrons to be outer ionized *even* at the near-resonance (under-dense) values of $\lambda \approx 250 - 260$ nm before the $\lambda_M \approx 263$ nm and responsible for the resonance peak shift towards a higher $\lambda > \lambda_M$ as seen in Fig.5.1. For elaborate discussion on UDLR see Ref.[24] and Sec.5.2.2.1.

5.2.1.1 Resonance peak shift with radius variation of cluster

For a cluster, the static Mie-resonance can be met by a transition from over-dense to under-dense plasma regime (artificially) by increasing the cluster radius (mimicking cluster expansion) for a fixed number of ions/electrons at a fixed λ , e.g., 800 nm as performed by Petrov *et al.* [19] by a MD test simulation where “no enhancement of energy absorption” was found “near the plasmon resonance”. Contrarily, we show by our MD simulation that LR indeed plays a major role for pronounced laser absorption during the variation of cluster radius, but red-shift of absorption peak occurs depending upon laser intensity due to the UDLR in presence of outer ionization.

The deuterium cluster ($N = 1791$ atoms) is irradiated by LP laser pulses of fixed $\lambda = 800$ nm and $\tau = 13.5$ fs. At a given I_0 , cluster radius R is varied from $R = R_0 = 2.05$ nm to $R = 15R_0$ with fixed N and immobile ions. Thus plasma density is successively reduced. For $R = 2.05$ nm, the density is $\rho_i = 27.87\rho_c$, where $\rho_c \approx 1.75 \times 10^{21} \text{ cm}^{-3}$ and $\omega_M/\omega \approx 3.05$. Since $\omega_M^2 \propto 1/R^3$, the static LR condition $\lambda_M = \lambda$ (or $\omega_M = \omega$) is achieved when $R \approx 2.1R_0$.

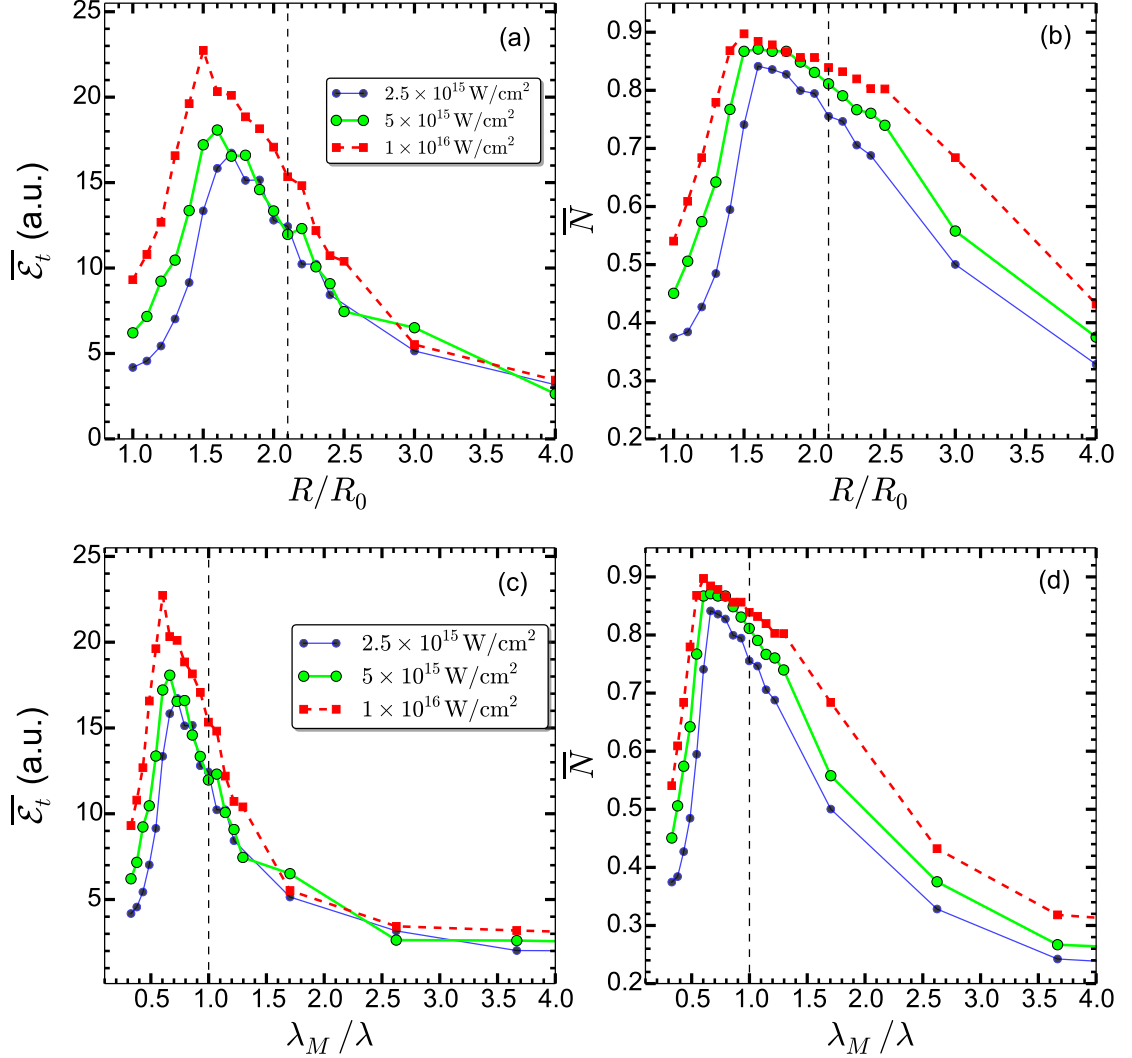


Figure 5.3: Test MD simulation results for total absorbed energy $\overline{\mathcal{E}}_t$ per atom and fractional outer ionization \overline{N} versus R/R_0 (top row) for the deuterium cluster of $N = 1791$ atoms irradiated by $\tau = 13.5$ fs LP laser pulses of different $I_0 = 2.5 \times 10^{15} - 5 \times 10^{16} \text{ Wcm}^{-2}$. For each I_0 , $\tau = 13.5$ fs and $\lambda = 800$ nm are kept fixed while the initial cluster radius R is varied from R_0 to $15R_0$. Same results are shown against λ_M/λ (bottom row). The static LR condition $\lambda_M/\lambda = 1$ is achieved when $R/R_0 \approx 2.1$ (vertical dashed lines). Clearly absorption and outer ionization maxima are red-shifted from the λ_M and our results are different from Petrov *et al.* [19].

Test MD results with above parameters in Figs. 5.3(a)-(b) show the absorbed energy $\overline{\mathcal{E}}_t$ per atom and fractional outer ionization \overline{N} of electrons versus R/R_0 (top row) for

different I_0 at the end of LP laser pulses. Same results are shown in Figs. 5.3(c)-(d) with the corresponding λ_M/λ (bottom row). Our results are different than Petrov *et al.* [19]. It is seen that maximum absorption and outer ionization occur for all three intensities but at red-shifted wavelength ratios of λ_M/λ before meeting the static LR condition at $\lambda_M/\lambda \approx 1$ (or $R/R_0 \approx 2.1$, vertical dashed lines). The gradual red-shifting of absorption and outer ionization maxima with increasing intensity in Fig. 5.3 in the marginally over-dense regime of $0.7 \lesssim \lambda_M/\lambda \leq 1$ (or $1.5 \lesssim R/R_0 \leq 2.1$) is very much consistent with the findings in Figs. 5.1(a)-(b) with varying λ and mobile ions.

5.2.2 Absorption and outer ionization with CP vs LP light

To see the impact of laser polarization on the absorption and outer ionization; and to know how the resonance absorption maxima shifts due to it, we simulate the same deuterium cluster with CP light (Eqn.(2.3),(2.4) with $\delta = 1/\sqrt{2}$) with similar laser parameters as in Fig. 5.1 of the LP case. Laser electric field components being different for LP and CP at a given instant, overall electron dynamics becomes different for a given I_0 and λ which may impact differently (i.e., CP may yield different results than LP) on energy absorption, outer ionization and the redshift of the resonance absorption peak.

Figure 5.4(a)-(b) show the comparison of average total absorbed energy $\overline{\mathcal{E}}_t = \sum_1^{N_p} (v_i^2/2 + q_i\phi_i)/N$ per atom and corresponding fractional outer ionization $\overline{N} = N_e^{out}/N$ of electrons at the end of 13.5 fs LP and CP laser pulses versus λ for different I_0 . The solid lines correspond to LP results from Figs.5.1(a)-(b) and the dashed lines correspond to CP. The vertical dashed line represents the wavelength of static Mie-resonance $\lambda_M = 263 \text{ nm}$. In the case of CP, $\overline{\mathcal{E}}_t$ and \overline{N} initially increase with increasing λ , attain different maximum values in the range of $\lambda \approx 330 \pm 67 \text{ nm}$, then drop as λ is increased further for intensities $< 10^{17} \text{ Wcm}^{-2}$ similar to the case of LP. Surprisingly, for CP, the maxima of $\overline{\mathcal{E}}_t$ and \overline{N} for different intensities are also red-shifted from the expected λ_M for $I_0 \leq 10^{17} \text{ Wcm}^{-2}$

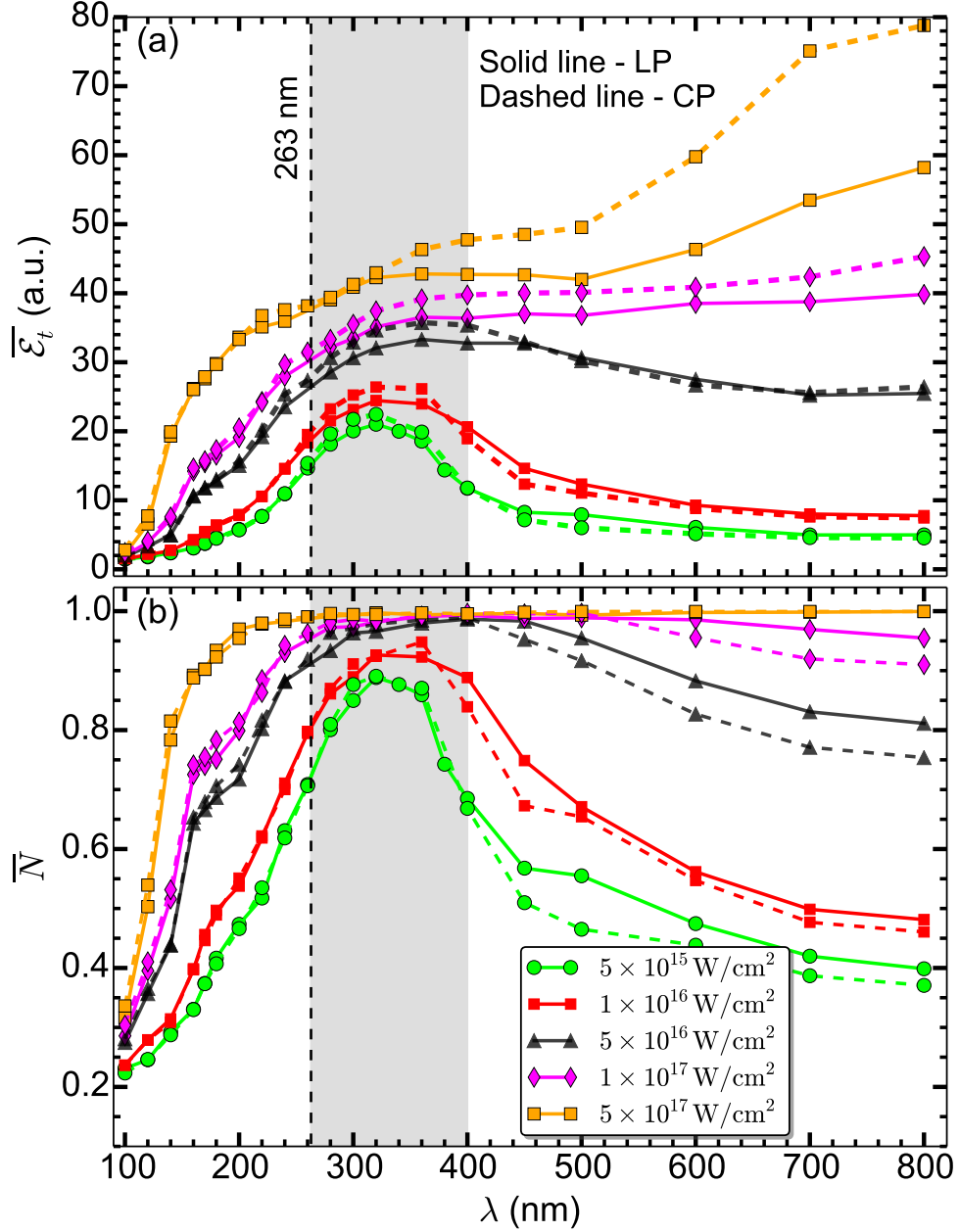


Figure 5.4: Comparison of (a) total absorbed energy $\bar{\mathcal{E}}_t$ per atom and (b) fractional outer ionization of electrons \bar{N} versus λ for the deuterium cluster ($R = 2.05 \text{ nm}$, $N = 1791$) as in Fig. 5.1 with same parameters of LP (solid line) and CP (dashed line) laser pulses.

in the *same* marginally over-dense band of $\Lambda_d \approx (1 - 1.5)\lambda_M$ (shaded region) as in the case of LP, *in spite* of electron dynamics and laser field configuration are different in CP

Chapter 5. Dependence of red-shift of absorption peak on laser polarization, intensity, and wavelength for a deuterium cluster

and LP. In fact, for some intensities (specially for low intensities) CP and LP results for $\overline{\mathcal{E}}_t$ and \overline{N} have only minor differences in the entire range of $\lambda = 100 - 800$ nm; and up to the static Mie-resonance $\lambda = \lambda_M$, $\overline{\mathcal{E}}_t$ and \overline{N} have almost no difference, irrespective of the laser polarization.

In the microscopic level, main difference between CP and LP results is that the magnitude of the maximum of $\overline{\mathcal{E}}_t$ and \overline{N} are little more for CP as compared to LP within the band of $\Lambda_d \approx (1 - 1.5)\lambda_M$. For example, the value of $\max(\overline{\mathcal{E}}_t)$ for LP (CP) case are 21, 24, and 33 a.u. (23, 26, and 36 a.u.) for $I_0 = 5 \times 10^{15}, 10^{16}, 5 \times 10^{16} \text{ Wcm}^{-2}$ respectively; and corresponding percentages of $\max(\overline{N})$ are 88.8%, 92.6%, and 98.6% (89%, 94.8%, and 98.9%) respectively. However, after the absorption maximum, for lower intensities, absorption due to LP either remains almost same as CP or dominates absorption due to CP with increasing λ outside the band of $\Lambda_d \approx (1 - 1.5)\lambda_M$ which gradually reverses its tendency at higher values of $I_0 = 10^{17}, 5 \times 10^{17} \text{ Wcm}^{-2}$ (i.e., CP dominates LP); although \overline{N} remains mostly higher for LP than the CP case except for a very high $I_0 = 5 \times 10^{17} \text{ Wcm}^{-2}$ where absorption peak disappears (outer ionization saturates to 100%) and absorption grows with increasing λ similar to the LP case as seen after 400 nm (explained in Fig.5.2). We shall further justify this findings of MD by the RSM in Sec.5.3.

However, above microscopic differences may not be captured in real laser-cluster experiments using CP and LP pulses. We conclude that the efficiency of laser energy absorption and outer ionization are almost same for LP and CP laser pulses of moderate $I_0 < 10^{17} \text{ Wcm}^{-2}$. We have checked (not presented here) that absorption and outer ionization in Fig.5.4 do not depend on the handedness of the CP laser, i.e., right-handed CP laser and left-handed CP laser yield almost same results, since the components of electric field amplitudes remain unchanged and the cluster is almost spherically symmetric.

5.2.2.1 Time domain analysis of resonance shift with CP vs LP light

By analyzing the results in time domain, we now justify the shifting of absorption maxima from the expected static LR wavelength of $\lambda_M = 263$ nm in Fig.5.4 at some intensity of 10^{16} Wcm^{-2} (red, dashed square line of Fig.5.4) and various λ with LP and CP light. Similar analysis for the redshift of absorption maxima was previously reported in chapter 4 in detail for a argon cluster illuminated by LP light. Figures 5.5(a)-5.5(c) present comparison of scaled Mie-frequency $\omega_M(t)/\omega$, total absorbed energy $\overline{\mathcal{E}}_t(t)$ per atom and fractional outer ionization $\overline{N}(t) = N_e^{out}(t)/N_e(t)$ of electrons respectively with LP (solid line) and CP (dashed line) versus normalized time in units of the laser period T of $\lambda = 800$ nm. The horizontal dashed line in Fig. 5.5(a) indicates the line of static LR condition $\omega_M = \omega$. The dynamical $\omega_M(t)$ is calculated from the relation $\omega_M^2(t) = Q_0(t)/R_0^3$ (for detail see Sec. 4.3.2). At $I_0 = 10^{16} \text{ Wcm}^{-2}$, the only charge state $Z = 1$ of the deuterium ions for all λ is created during $t/T = 0.9 - 1.1$ by the OFI (2.24) and the corresponding dynamical $\omega_M(t)/\omega$ jumps from zero to its maximum for both LP and CP. After the respective maximum values, $\omega_M(t)/\omega$ drops due to Coulomb explosion. For a chosen λ , although there are minor differences in $\overline{\mathcal{E}}_t(t)$ and $\overline{N}(t)$, surprisingly temporal variation of $\omega_M(t)/\omega$ remains indistinguishable until the end of laser pulses for both LP and CP. It is known that the efficient transfer of energy from an oscillatory driver (laser fields) to the oscillators (bound electrons) is possible *not only* by the frequency matching condition $\omega_M = \omega$ of LR, the time spent by the system near the LR and the strength of the driver at that time are also crucial [24]. The longer time spent by the dynamical $\omega_M(t)/\omega$ near the line of LR ($\omega_M/\omega = 1$) and in the marginally over-dense band of $\Lambda_d \approx (1 - 1.5)\lambda_M$, the higher is the absorption and outer ionization due to the combined effect of AHR and dynamical LR [24], coined as unified dynamical LR (UDLR) [24].

Chapter 5. Dependence of red-shift of absorption peak on laser polarization, intensity, and wavelength for a deuterium cluster

For the deuterium cluster also the absorbed energy and outer ionization are enhanced (see Figs. 5.5(b),(c)) for those wavelengths which lie in the marginally over-dense band of $\lambda \approx 330 \pm 67$ nm (e.g., 260 nm, 320 nm and 360 nm), equivalent to $\Lambda_d \approx (1 - 1.5)\lambda_M$, as compared to the other wavelengths which lie outside this band (e.g., 200 nm and 800 nm). Among the three intermediate λ , dynamical $\omega_M(t)/\omega$ for $\lambda = 260$ nm (magenta line) is very close to the static LR, $\omega_M/\omega = 1$ (where $\lambda_M = 263$ nm), but the absorption and outer ionization are not still at their expected maximum. For 260 nm, the dynamical $\omega_M(t)/\omega$ just meet the line of static LR *only* for a very short time during $t/T = 0.9 - 1.2$ and rest of the time it remains in the under-dense regime below the line of static LR (where AHR does not work), so can not absorb energy efficiently. Instead, for $\lambda = 320, 360$ nm (green, red lines), the respective dynamical $\omega_M(t)/\omega$ continues to remain in the marginally over-dense band of $\Lambda_d \approx (1 - 1.5)\lambda_M$ for a prolonged period up to $t/T \approx 4.1, 5.0$, where both AHR and dynamical LR with near-LR enhanced effective field $E_{eff} = E_0/(\omega_M^2(t) - \omega^2)$ contribute unitedly (i.e., UDLR happens) to maximize absorption and outer ionization for both LP and CP. Thus UDLR explains the red-shift of absorption maxima from the static LR wavelength of $\lambda_M = 263$ nm in Fig.5.4 for LP and CP light. It is observed that the maximum of $\overline{\mathcal{E}}_t(t)$ is little enhanced for CP in comparison to LP for those λ which lie in the UDLR regime of $\Lambda_d \approx (1 - 1.5)\lambda_M$. This enhanced energy is partly due to non-zero rotating electric field vector of the CP laser, although $\overline{N}(t)$ for CP light is either less (or nearly equal) compared to LP light in Fig. 5.5(b). The oscillatory nature of $\overline{\mathcal{E}}_t(t)$ and $\overline{N}(t)$ for LP are due to the oscillating electric field vector while for CP they smoothly increase due to non-zero rotating electric field vector.

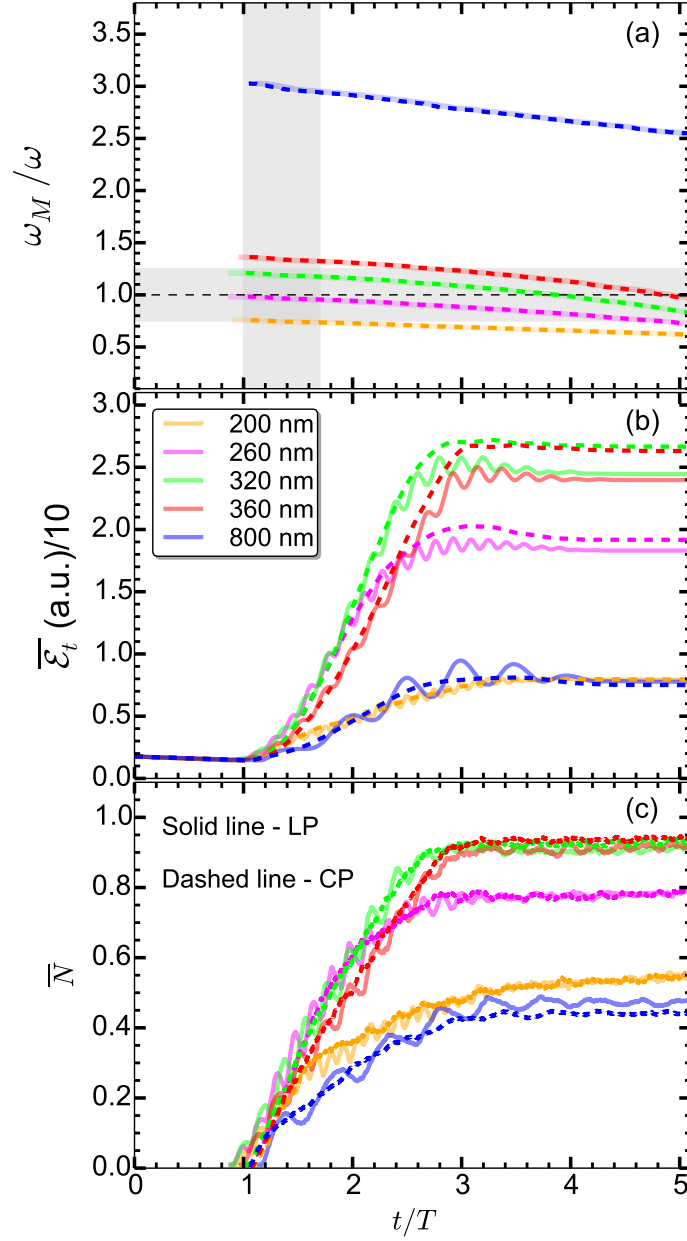


Figure 5.5: Comparison of temporal variation (a) normalized Mie-frequency $\omega_M(t)/\omega$, (b) total absorbed energy $\bar{\mathcal{E}}_t$ per atom, and (c) fractional outer ionization of electrons \bar{N} for two polarization states LP (solid line) and CP (dashed line) for the same deuterium cluster (Fig.5.4) when irradiated by 5-fs (FWHM) laser pulse of $I_0 = 10^{16} \text{ Wcm}^{-2}$ (red, dashed square line in Fig.5.4) and different $\lambda = 100 - 800 \text{ nm}$. Time is scaled by the period T at $\lambda = 800 \text{ nm}$. At $\lambda = 320 \text{ nm}$ (green), $\omega_M(t)/\omega$ spends more time near the $\omega_M/\omega = 1$ line in the marginally over-dense band of $\Lambda_d \approx (1 - 1.5)\lambda_M$, which leads to efficient UDLR and more higher absorption for both LP and CP.

5.3 RSM results : Absorption and outer ionization with CP vs LP laser

We further justify MD results (qualitatively) by a simple rigid sphere model (RSM). We simulate the system with LP and CP laser pulses with same parameters as in Sec. 5.2. The dynamics of each electron sphere is governed by the laser field pulse the electrostatic restoring field in the background potential of positively charged ion sphere. The details of RSM for LP case is described in chapter 3. To study the dynamics of electron spheres with CP light we write EOM in two dimension as [99],

$$\ddot{\vec{r}}_x + \vec{r}_x g(r)/r = \hat{x}(q_e/m_e) E_l^x(t)/R_0 \quad (5.1)$$

$$\ddot{\vec{r}}_y + \vec{r}_y g(r)/r = \hat{y}(q_e/m_e) E_l^y(t)/R_0. \quad (5.2)$$

Here $\vec{r}_x = \vec{x}/R_0$, $\vec{r}_y = \vec{y}/R_0$, $r = \sqrt{r_x^2 + r_y^2}$. The electric field components for CP light are given by Eqn. (2.3) and (2.4) with $\delta = 1/\sqrt{2}$. Similar to MD study in sec. 5.2.2, here also we have same $U_p = E_0^2/4\omega^2$ as in the LP case. Each electron sphere moves spirally in the potential $\phi(r)$ driven by CP light.

Figures 5.6(a)-(b) show comparison of average total absorbed energy $\overline{\mathcal{E}}_t = \sum_1^N (m_s v_i^2/2 + q_s \phi_i)/N$ per electron sphere for LP and CP laser pulses (after $\tau = 13.5$ fs) versus λ for different I_0 . Figure 5.6(c)-(d) are the corresponding fraction of outer ionized electrons $\overline{N} = N_{out}/N$. Results are separated in two regimes of intensities for more clarity. Figures 5.6(a),(c) are for $I_0 \leq 10^{17} \text{ Wcm}^{-2}$ and Figs. 5.6(b),(d) are for $I_0 = 5 \times 10^{17} \text{ Wcm}^{-2}$. It is noted that RSM results (for both LP and CP) resemble the MD results in Fig. 5.4: (i) growth of absorption and outer ionization with increasing λ for $I_0 \lesssim 10^{17} \text{ Wcm}^{-2}$ with distinct maxima located in the band of $\Lambda_d \approx (1 - 1.5)\lambda_M$, i.e., in between 263 – 400 nm

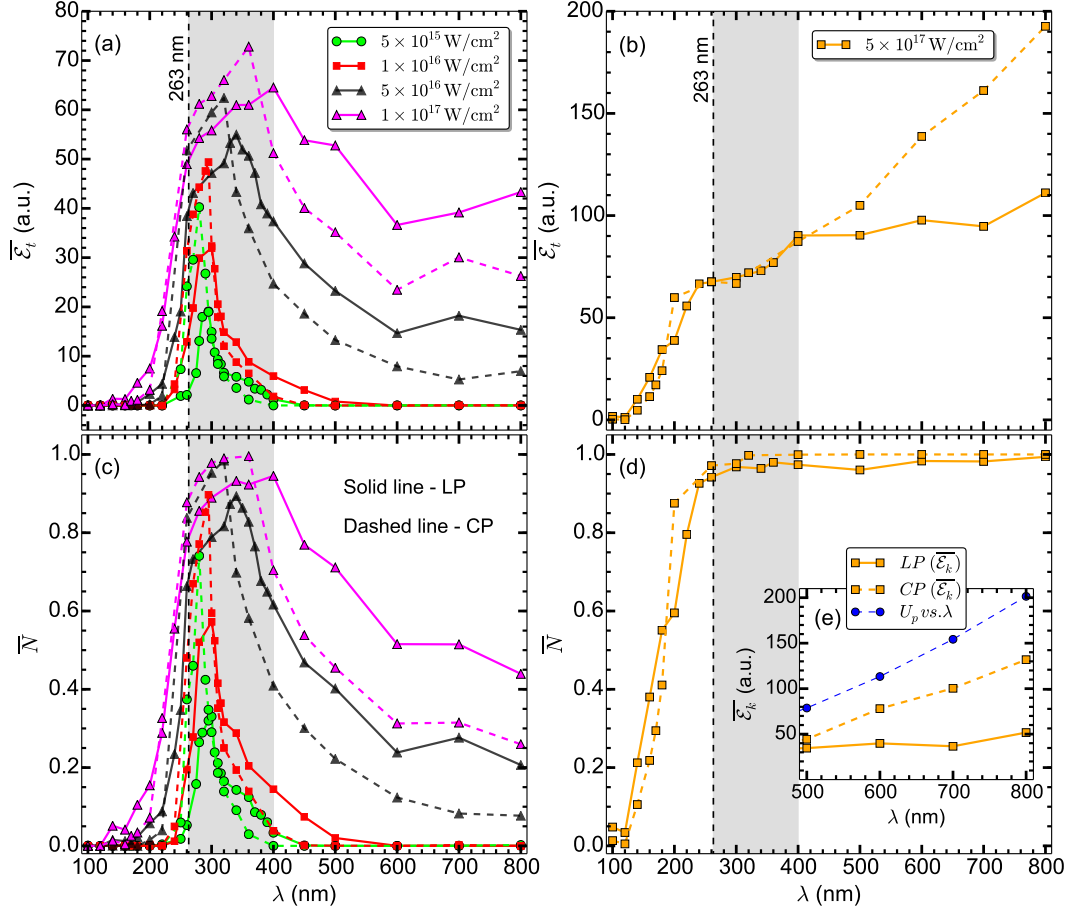


Figure 5.6: RSM results showing wavelength dependence of total absorbed energy $\overline{\mathcal{E}}_t$ [(a),(b)] per electron sphere and the corresponding fraction of outer ionization \overline{N} [(c),(d)] in the deuterium cluster (of Fig. 5.1) irradiated laser pulses with parameters same as in Fig. 5.1. Results show the comparative study for LP (solid line) and CP (dashed line) as in Fig. 5.4. Inset (e) shows the comparison of the average kinetic energy of the electron spheres $\overline{\mathcal{E}}_k$ versus higher $\lambda \geq 500 \text{ nm}$ for LP (solid-squared orange line) and CP (dashed-squared orange line) with the ponderomotive energy U_p (dashed-dotted blue line) at $I_0 = 5 \times 10^{17} \text{ Wcm}^{-2}$ corresponding to subplot (b). Vertical dashed line indicates corresponding $\lambda_M \approx 263 \text{ nm}$ where absorption maximum is strictly expected by LR. The shaded bar highlights that absorption maxima are red-shifted in the marginally overdense band of $\Lambda_d \approx (1 - 1.5)\lambda_M$.

in Figs. 5.6(a),(c); (ii) increasing redshift of the absorption and outer ionization maxima from the static LR wavelength of $\lambda_M \approx 263 \text{ nm}$ (vertical dashed line) with increasing

Chapter 5. Dependence of red-shift of absorption peak on laser polarization, intensity, and wavelength for a deuterium cluster

$I_0 \lesssim 10^{17} \text{ Wcm}^{-2}$ due to increasing outer ionization; and (iii) gradual disappearance of absorption maxima (followed by *even* a growth of $\overline{\mathcal{E}}_t$ for $\lambda > 400 \text{ nm}$) due to 100% saturation of \overline{N} when I_0 exceeds 10^{17} Wcm^{-2} in Figs. 5.6(b),(d).

Similar to the MD results in Fig. 5.4 the magnitude of the maximum value of $\overline{\mathcal{E}}_t$ and \overline{N} are more for CP than LP in the marginally overdense band of $\Lambda_d \approx (1 - 1.5)\lambda_M$. The maxima of $\overline{\mathcal{E}}_t$ for LP (CP) are 19.1, 31.9, 54.9, and 64.5 a.u. (40.3, 49.4, 62.4, and 72.8 a.u.) for $I_0 = 5 \times 10^{15}, 10^{16}, 5 \times 10^{16}, 10^{17} \text{ Wcm}^{-2}$ respectively and corresponding \overline{N} are 33%, 57%, 89%, and 94% (74%, 90%, 98%, and 99%) for respective I_0 in Figs. 5.6(a),(c). Also, after the maxima, for lower intensities, both $\overline{\mathcal{E}}_t$ and \overline{N} with CP light drop below the values with LP light which, on the other hand, gradually reverses at higher intensities (i.e., CP dominates LP as in Figs. 5.6(b),(d)), as λ is increased. At the higher intensity $5 \times 10^{17} \text{ Wcm}^{-2}$, after $\lambda \approx 320 \text{ nm}$, \overline{N} is saturated at 100% for CP and almost 98.5% for LP but $\overline{\mathcal{E}}_t$ gradually grows with increasing $\lambda > 320 \text{ nm}$ for both CP and LP. For higher intensities $\geq 5 \times 10^{17} \text{ Wcm}^{-2}$, when 100% outer ionization is reached (almost all electrons are freed) in the early cycles of a laser pulse due to efficient UDLR, the average absorbed energy $\overline{\mathcal{E}}_t$ per electron sphere may grow (as for MD in Fig. 5.4 at the intensity $5 \times 10^{17} \text{ Wcm}^{-2}$) with increasing λ due to the dominant variation of free electron kinetic energy as $U_p \propto E_0^2 \lambda^2 / 4$. To support this again for the RSM, we look at the free electrons kinetic energy scaling similar to the MD case presented in Fig. 5.2. Inset Fig. 5.6(e) show the comparison of the average kinetic energy $\overline{\mathcal{E}}_k$ per electron sphere versus higher $\lambda \geq 500 \text{ nm}$ for both LP (solid-squared orange line) and CP (dashed-squared orange line) with $U_p \propto E_0^2 \lambda^2 / 4$ (dashed-dotted blue line) at $5 \times 10^{17} \text{ Wcm}^{-2}$ corresponding to Fig. 5.6(b). One can see the growth of $\overline{\mathcal{E}}_k \propto U_p$, but it is slower than the scaling of U_p for both LP and CP since the electrons (free or bound) do not have same kinetic energy and liberated at different times of the laser cycle. Also,

growth $\overline{\mathcal{E}}_k$ is more close to U_p for CP than LP due to more number outer electrons with higher kinetic energies at different λ for CP than LP. This justifies the growth of $\overline{\mathcal{E}}_t$ with λ at a higher $I_0 = 5 \times 10^{17} \text{Wcm}^{-2}$ for CP and LP; and also explains why $\overline{\mathcal{E}}_t$ for CP dominates LP as in Fig. 5.4 for λ beyond the band of $\Lambda_d \approx (1 - 1.5)\lambda_M$.

Thus RSM results (in Fig. 5.6) bring out most of the features of MD results (in Fig. 5.4) which justify the dependence of redshift of absorption maxima on laser polarization and intensity and also disappearance of absorption maxima followed by a growth of absorption at higher intensity of $5 \times 10^{17} \text{Wcm}^{-2}$ for CP and LP, with increasing λ .

5.4 Summary

We demonstrate the effect of laser polarization on the red-shift of the resonance absorption peak for a deuterium cluster irradiated by short 5-fs (fwhm) laser pulses using MD simulation and supported by RSM analysis. For both the polarization cases (LP and CP), we show that for a given intensity $< 10^{17} \text{Wcm}^{-2}$ the optimized wavelength for maximum laser absorption in deuterium cluster lie in the band of wavelengths $\lambda \approx 330 \pm 67 \text{ nm}$ in stead of the commonly expected static LR (Mie-resonance) wavelength of $\lambda_M = 263 \text{ nm}$. MD simulation and the RSM show gradual red-shift of the absorption maxima towards higher wavelengths in the marginally over-dense band of $\Lambda_d \approx (1 - 1.5)\lambda_M$ from λ_M of static LR with increasing laser intensity; and for higher intensities $> 10^{17} \text{Wcm}^{-2}$ absorption peak disappears as outer ionization saturates at 100% for both LP and CP. This disappearance of the resonance absorption peak should not be misinterpreted as the negligible (or no) role of Mie-resonance. In fact, in this marginally over-dense band of $\Lambda_d \approx (1 - 1.5)\lambda_M$, both AHR and dynamical LR with near-LR enhanced effective field $E_{eff} = E_0/(\omega_M^2(t) - \omega^2)$ contribute in unison very efficiently – UDLR happens – to maximize absorption and outer ionization for both LP

Chapter 5. Dependence of red-shift of absorption peak on laser polarization, intensity, and wavelength for a deuterium cluster

and CP. It is also found that before the absorption peak, laser absorption due to LP and CP lasers are almost equally efficient (CP case being inappreciably higher than LP) for all intensities and λ . However, after the absorption peak, at lower intensities, absorption due to LP inappreciably dominates absorption due to CP with increasing λ which gradually reverses at higher intensities. Neglecting marginal differences for LP and CP cases, which may not be differentiated in real experiments, we conclude that laser absorption and outer ionization are almost same irrespective of the states of laser polarization for intensities $< 10^{17} \text{ Wcm}^{-2}$. Analysis (Fig.5.5) of dynamical $\omega_M(t)$ suggests that Coulomb explosion of deuterium cluster is also almost independent of laser polarization. Our results agree with the general observation from the nano-plasma model [9] that absorption peaks exist but red-shifted in the band of $\Lambda_d \approx (1-1.5)\lambda_M$. It is perhaps misleading to look for the absorption maxima *exactly* at the λ_M in presence of non-zero outer ionization at higher intensities since linear Mie-resonance theory is invalid here.

6

Conclusions and future scope

The main focus of this thesis is to study the energy absorption mechanisms in the short-pulse regime for a laser-driven atomic cluster using simple theoretical model and exhaustive 3D molecular dynamics simulation. Particular emphasis has been given to understand various collisionless resonance absorption processes behind the efficient laser energy absorption to cluster electrons, which include both linear resonance (LR) and anharmonic resonance (AHR). We have also examined the dependency of resonance absorption on different laser and cluster parameters (i.e, peak intensity, wavelength, pulse duration, laser polarization, cluster size and atom type etc.). The major outcomes of this thesis have been already mentioned in the preceding chapters. In the following, we briefly summarize those results and also highlight several possible future directions emerging from this thesis work.

6.1 Conclusions

This thesis work has been started with the development of a 3D classical MD code from scratch (see chapter 2 for detail), where interactions among charge particles are taken as soft core Coulomb potential. The code has been benchmarked with various existing results and the numerical accuracy has been compared with the corresponding analytical results. Systematic studies for single-particle dynamics and multi-particle dynamics have been performed. To validate the MD code, energy conservation has also been rigorously checked for both the systems. Mie-plasma frequency (ω_M), which is a *crucial* parameter for resonance phenomena has been verified in a 2D as well as in a 3D system (i.e., pre-ionized deuterium cluster) with analytical results along with the energy conservation under a small perturbation of the electron cloud. To study high Z clusters (e.g., argon), we have further improved the MD code to include self-consistent ionization of atoms/ions assuming “over the barrier ionization (OBI)” model.

Anharmonic resonance (AHR) absorption mechanism of intense laser pulse in an over-dense deuterium cluster has been identified through the newly developed 3D-MD simulation code for the first time (see chapter 3). It has been shown that the individual electrons, which are driven by the laser field in the self-generated anharmonic cluster potential can leave the cluster and become free only when AHR condition $\Omega[r(t)] = \omega$ is met. Various features of AHR obtained through MD simulation were also verified by a simple RSM. Thus, we proved that AHR process is a universal dominant collisionless mechanism in the short-pulse regime behind efficient laser energy absorption.

We have shown the existence of an optimal laser wavelength λ for an argon cluster at a given laser intensity and pulse energy, which has led to efficient laser energy absorption accompanied by maximum average ion charge states and maximum outer ionization (see

chapter 4). MD results reveal that, for a given peak intensity and a plasma density ρ , the efficient coupling of laser energy to cluster electrons does not happen at the well-known wavelength of linear resonance $\lambda_M = \lambda$; instead it happens at a red-shifted wavelength in the marginally over-dense regime of wavelength $\Lambda_d \approx (1 - 1.5)\lambda_M$ depending upon the percentage of the outer ionization that in turn depends on the field strength of the laser. At this shifted band of Λ_d (typically lies in the ultra-violet regime), different resonances (both LR and AHR) are dynamically unified in various stages, including (i) the LR in the initial time of plasma creation, (ii) the LR in the Coulomb expanding phase in the later time and (iii) anharmonic resonance (AHR) in the marginally over-dense regime for a relatively longer pulse duration below 5-fs (fwhm) leading to maximum absorption. This regime is termed as unified dynamical linear resonance (UDLR). Also, it has been confirmed by the MD simulation that the redshift is hardly affected by different carrier-envelope phase (CEP) for this short duration of the laser pulse.

We have further demonstrated the effect laser polarization (by considering linear polarized and circularly polarized laser in chapter 5) on the redshift of the resonance absorption peak for a deuterium cluster for its universal acceptance. Our results have confirmed that there is always a redshift of the absorption peak with respect to λ_M in the marginally over-dense band of $\Lambda_d \approx (1 - 1.5)\lambda_M$ irrespective of laser intensity, cluster type, and laser polarization. In addition to these findings, we have also observed that the absorption peak gradually disappears for both LP and CP cases at higher intensities $> 10^{17} \text{ Wcm}^{-2}$ due to quick saturation of outer ionization at 100%. Also, it has been found that for lower intensities, laser absorption due to different polarization of the laser pulse (both LP and CP) are almost equally efficient. However, after absorption peak, at lower laser intensities, absorption due to LP inappreciably dominates absorption due to CP with increasing λ which gradually reverses its character at higher intensities.

6.2 Future scope

In the following, we mention some of the possible future directions based on the work presented in this thesis:

- In this thesis, we restrict ourselves in the non-relativistic regime, i.e., the laser intensity is kept below 10^{18} Wcm^{-2} . One can extend the laser intensity beyond 10^{18} Wcm^{-2} to include the relativistic effect and study the additional effect on absorption mechanisms with this intense laser field.
- We have only considered the “OBI” mechanism for the inner ionization of atoms/ions, which is valid for longer wavelengths and higher intensities. However, for shorter wavelengths and lower intensities additional ionization mechanism called as “electron impact ionization” can also be included considering the electron-ion inelastic collision to see the effect of wavelength on resonance absorption processes. Moreover, multi-photon and tunnelling ionization can be included to include ionization by the low intensity foot of the laser pulse.
- The effect of external magnetic field on the dynamics of cluster electrons as well as on the resonance absorption mechanism can be studied. By magnetic field control, electro-cyclotron resonance may be excited which may possibly increase laser energy coupling.
- In this thesis we have considered the interaction of laser pulses with a single cluster without the effect of low density background plasma in the laser focus. In reality, however, there are many clusters in the laser focus in the presence of low density background plasma. These more realistic scenarios may be taken into account in the future studies of laser-cluster interaction to see effects on ionization, absorption and coulomb explosion.



Appendix

A.1 Atomic units and SI units conversion

Throughout the work in the thesis we have used atomic units. In atomic units $m_e = -e = 4\pi\epsilon_0 = \hbar = 1$. Here ϵ_0 is the permittivity of vacuum, $-e$ and m_e are the charge and the mass of the electron, and \hbar is the Planck constant. Speed of light in atomic unit is taken as $c = 1/\alpha = 137$. The conversion relation between SI units and atomic units for the fundamental physical quantities are:

$$1 \text{ atomic mass unit} = m_e = 9.11 \times 10^{-31} \text{ kg},$$

$$1 \text{ atomic charge unit} = e = 1.602 \times 10^{-19} \text{ C},$$

$$1 \text{ atomic action unit} = \hbar = 1.05 \times 10^{-34} \text{ J s}.$$

In table [A.1](#) we provide a list of important physical quantities, with their units and their values on SI units.

Appendix A. Appendix

Physical quantity	Definition atomic unit	SI unit
Length	$a_0 = \hbar^2 4\pi\epsilon_0 / e^2 m_e$	$5.3 \times 10^{-11} \text{ m}$
Electric field	$E_0 = e / 4\pi\epsilon_0 a_0^2$	$5.14 \times 10^{11} \text{ V/m}$
Intensity	$I_0 = c\epsilon_0 E_0^2 / 2$	$3.51 \times 10^{16} \text{ Wcm}^{-2}$
Energy	$\mathcal{E}_0 = eE_0 a_0$	27.21 eV
Time	$t_0 = \hbar / \mathcal{E}_0$	$2.4 \times 10^{-17} \text{ sec} = 0.024 \text{ fs}$
Velocity	$v_0 = a_0 / t_0$	$2.18 \times 10^6 \text{ m/sec}$
Frequency	$\omega_0 = \mathcal{E}_0 / \hbar$	$4.134 \times 10^{16} \text{ sec}^{-1}$

Table A.1: SI units of various physical quantities, which is related to 1 atomic unit of the corresponding quantity.

A.2 Comparison between different parameters for a deuterium cluster and an argon cluster

Cluster type	Atomic weight	Wigner Seitz radius r_ω (nm)	Number of atoms N	Cluster radius $R_0 = r_\omega N^{1/3}$ (nm)	Atomic density $\rho = \frac{3N}{4\pi R_0^3} (m^{-3})$	ρ/ρ_c	$\omega_M/\omega = \sqrt{\rho/3\rho_c}$
Deuterium	2.014	0.17	1791	2.05	4.87×10^{28}	27.87	3.05
Argon	39.948	0.24	1791	2.91	1.73×10^{28}	9.9	1.82

Table A.2: Comparison between different parameters for a deuterium cluster and an argon cluster containing the same number of atom $N = 1791$. For laser pulse of wavelength $\lambda = 800 \text{ nm}$, the critical density is defined as $\rho_c = 1.75 \times 10^{27} \text{ m}^{-3}$.

Bibliography

- [1] T. Ditmire, R. A. Smith, J. W. G. Tisch, and M. H. R. Hutchinson. High intensity laser absorption by gases of atomic clusters. *Phys. Rev. Lett.*, 78:3121–3124, Apr 1997.
- [2] T. Ditmire, E. Springate, J. W. G. Tisch, Y. L. Shao, M. B. Mason, N. Hay, J. P. Marangos, and M. H. R. Hutchinson. Explosion of atomic clusters heated by high-intensity femtosecond laser pulses. *Phys. Rev. A*, 57:369–382, Jan 1998.
- [3] Y. L. Shao, T. Ditmire, J. W. G. Tisch, E. Springate, J. P. Marangos, and M. H. R. Hutchinson. Multi-keV electron generation in the interaction of intense laser pulses with Xe clusters. *Phys. Rev. Lett.*, 77:3343–3346, Oct 1996.
- [4] L. M. Chen, J. J. Park, K. H. Hong, I. W. Choi, J. L. Kim, J. Zhang, and C. H. Nam. Measurement of energetic electrons from atomic clusters irradiated by intense femtosecond laser pulses. *Physics of Plasmas*, 9(8):3595–3599, 2002.
- [5] T. Ditmire, J. W. G. Tish, E. Springate, M. B. Mason, N. Hay, J. Marangos, and M. H. R. Hutchinson. High-energy ions produced in explosions of superheated atomic clusters. *Nature (London)*, 386:54–56, March 1997.
- [6] M. Lezius, S. Dobosz, D. Normand, and M. Schmidt. Explosion dynamics of rare gas clusters in strong laser fields. *Phys. Rev. Lett.*, 80:261–264, Jan 1998.
- [7] A. McPherson, B. D. Thompson, A. B. Borisov, K. Boyer, , and C. K. Rhodes. Multiphoton-induced x-ray emission at 4–5 keV from Xe atoms with multiple core vacancies. *Nature*, 370:631–634, August 1994.

Bibliography

- [8] R. Rajeev, T. Madhu Trivikram, K. P. M. Rishad, V. Narayanan, E. Krishnakumar, and M. Krishnamurthy. A compact laser-driven plasma accelerator for megaelectronvolt-energy neutral atoms. *Nat Phys.*, 9:185–190, March 2013.
- [9] T. Ditmire, T. Donnelly, A. M. Rubenchik, R. W. Falcone, and M. D. Perry. Interaction of intense laser pulses with atomic clusters. *Phys. Rev. A*, 53:3379–3402, May 1996.
- [10] J. Zweiback, T. Ditmire, and M. D. Perry. Femtosecond time-resolved studies of the dynamics of noble-gas cluster explosions. *Phys. Rev. A*, 59:R3166–R3169, May 1999.
- [11] L. Köller, M. Schumacher, J. Köhn, S. Teuber, J. Tiggesbäumker, and K. H. Meiwes-Broer. Plasmon-enhanced multi-ionization of small metal clusters in strong femtosecond laser fields. *Phys. Rev. Lett.*, 82:3783–3786, May 1999.
- [12] Toshihiro Taguchi, Thomas M. Antonsen, and Howard M. Milchberg. Resonant heating of a cluster plasma by intense laser light. *Phys. Rev. Lett.*, 92:205003, May 2004.
- [13] P. Mulser, M. Kanopathipillai, and D. H. H. Hoffmann. Two very efficient nonlinear laser absorption mechanisms in clusters. *Phys. Rev. Lett.*, 95:103401, Sep 2005.
- [14] M. Kundu and D. Bauer. Nonlinear resonance absorption in the laser-cluster interaction. *Phys. Rev. Lett.*, 96:123401, Mar 2006.
- [15] C. Rose-Petruck, K. J. Schafer, K. R. Wilson, and C. P. J. Barty. Ultrafast electron dynamics and inner-shell ionization in laser driven clusters. *Phys. Rev. A*, 55:1182–1190, Feb 1997.

- [16] Isidore Last and Joshua Jortner. Quasiresonance ionization of large multicharged clusters in a strong laser field. *Phys. Rev. A*, 60:2215–2221, Sep 1999.
- [17] Kenichi Ishikawa and Thomas Blenski. Explosion dynamics of rare-gas clusters in an intense laser field. *Phys. Rev. A*, 62:063204, Nov 2000.
- [18] Ulf Saalmann and Jan-Michael Rost. Ionization of clusters in intense laser pulses through collective electron dynamics. *Phys. Rev. Lett.*, 91:223401, Nov 2003.
- [19] G. M. Petrov, J. Davis, A. L. Velikovich, P. C. Kepple, A. Dasgupta, R. W. Clark, A. B. Borisov, K. Boyer, and C. K. Rhodes. Modeling of clusters in a strong 248-nm laser field by a three-dimensional relativistic molecular dynamic model. *Phys. Rev. E*, 71:036411, Mar 2005.
- [20] Mathias Arbeiter and Thomas Fennel. Ionization heating in rare-gas clusters under intense xuv laser pulses. *Phys. Rev. A*, 82:013201, Jul 2010.
- [21] S. S. Mahalik and M. Kundu. Anharmonic resonance absorption of short laser pulses in clusters: A molecular dynamics simulation study. *Physics of Plasmas*, 23, 2016.
- [22] G. M. Petrov and J. Davis. Impact of the laser wavelength on the dynamics of xe cluster plasma produced by an intense ultrashort laser pulse. *Physics of Plasmas*, 13(3), 2006.
- [23] J. Davis, G. M. Petrov, and A. Velikovich. Nonlinear energy absorption of rare gas clusters in intense laser field. *Physics of Plasmas*, 14(6), 2007.
- [24] S. S. Mahalik and M. Kundu. Dynamical resonance shift and unification of resonances in short-pulse laser-cluster interaction. *Phys. Rev. A*, 97:063406, Jun 2018.

Bibliography

- [25] Gerard A. Mourou, Toshiki Tajima, and Sergei V. Bulanov. Optics in the relativistic regime. *Rev. Mod. Phys.*, 78:309–371, Apr 2006.
- [26] Thomas Brabec and Ferenc Krausz. Intense few-cycle laser fields: Frontiers of nonlinear optics. *Rev. Mod. Phys.*, 72:545–591, Apr 2000.
- [27] Ferenc Krausz and Misha Ivanov. Attosecond physics. *Rev. Mod. Phys.*, 81:163–234, Feb 2009.
- [28] G Mainfray and G Manus. Multiphoton ionization of atoms. *Reports on Progress in Physics*, 54(10):1333–1372, oct 1991.
- [29] MARGARET M. MURNANE, HENRY C. KAPTEYN, MORDECAI D. ROSEN, and ROGER W. FALCONE. Ultrafast x-ray pulses from laser-produced plasmas. *Science*, 251(4993):531–536, 1991.
- [30] P Gibbon and E Förster. Short-pulse laser - plasma interactions. *Plasma Physics and Controlled Fusion*, 38(6):769–793, jun 1996.
- [31] W. L. Kruer. *The Physics of Laser Plasma Interactions*. Addison Wesley, New-York, 1988.
- [32] J. D. Kmetec, C. L. Gordon, J. J. Macklin, B. E. Lemoff, G. S. Brown, and S. E. Harris. Mev x-ray generation with a femtosecond laser. *Phys. Rev. Lett.*, 68:1527–1530, Mar 1992.
- [33] A. W. CASTLEMAN and R. G. KEESEE. Gas-phase clusters: Spanning the states of matter. *Science*, 241(4861):36–42, 1988.
- [34] T. Ditmire. Atomic clusters in ultrahigh intensity light fields. *Contemporary Physics*, 38(5):315–328, 1997.

- [35] V.P. Krainov and M.B. Smirnov. Cluster beams in the super-intense femtosecond laser pulse. *Physics Reports*, 370(3):237 – 331, 2002.
- [36] U Saalmann, Ch Siedschlag, and J M Rost. Mechanisms of cluster ionization in strong laser pulses. *Journal of Physics B: Atomic, Molecular and Optical Physics*, 39(4):R39, 2006.
- [37] Th. Fennel, K.-H. Meiwes-Broer, J. Tiggesbäumker, P.-G. Reinhard, P. M. Dinh, and E. Suraud. Laser-driven nonlinear cluster dynamics. *Rev. Mod. Phys.*, 82:1793–1842, Jun 2010.
- [38] O. F. Hagen and W. Obert. Cluster formation in expanding supersonic jets: Effect of pressure, temperature, nozzle size, and test gas. *The Journal of Chemical Physics*, 56(5):1793–1802, 1972.
- [39] T. D. Donnelly, T. Ditmire, K. Neuman, M. D. Perry, and R. W. Falcone. High-order harmonic generation in atom clusters. *Phys. Rev. Lett.*, 76:2472–2475, Apr 1996.
- [40] J W G Tisch, T Ditmire, D J Fraser, N Hay, M B Mason, E Springate, J P Marangos, and M H R Hutchinson. Investigation of high-harmonic generation from xenon atom clusters. *Journal of Physics B: Atomic, Molecular and Optical Physics*, 30(20):L709, 1997.
- [41] B. Shim, G. Hays, R. Zgadzaj, T. Ditmire, and M. C. Downer. Enhanced harmonic generation from expanding clusters. *Phys. Rev. Lett.*, 98:123902, Mar 2007.
- [42] T. Ditmire, J. Zweiback, V. P. Yanovsky, T. E. Cowan, G. Hays, and K. B. Wharton. Nuclear fusion from explosions of femtosecond laser-heated deuterium clusters. *Nature (London)*, 398:489–492, 1999.

Bibliography

- [43] J. Zweiback, R. A. Smith, T. E. Cowan, G. Hays, K. B. Wharton, V. P. Yanovsky, and T. Ditmire. Nuclear fusion driven by coulomb explosions of large deuterium clusters. *Phys. Rev. Lett.*, 84:2634–2637, Mar 2000.
- [44] Kirk W. Madison, Pravesh K. Patel, Matt Allen, Dwight Price, and Todd Ditmire. Investigation of fusion yield from exploding deuterium-cluster plasmas produced by 100-tw laser pulses. *J. Opt. Soc. Am. B*, 20(1):113–117, Jan 2003.
- [45] L. V. Keldysh. Ionization in the field of a strong electromagnetic wave. *Sov. Phys. JETP*, 20:1307, 1965.
- [46] H. Barry Bebb and Albert Gold. Multiphoton ionization of hydrogen and rare-gas atoms. *Phys. Rev.*, 143:1–24, Mar 1966.
- [47] V M Morton. Multi-photon absorption in monatomic gases. *Proceedings of the Physical Society*, 92(2):301–310, oct 1967.
- [48] P. Agostini, G. Barjot, J. Bonnal, G. Mainfray, C. Manus, and J. Morellec. Multiphoton ionization of hydrogen and rare gases. *IEEE Journal of Quantum Electronics*, 4(10):667–669, October 1968.
- [49] Farhad H.M. Faisal. *Theory of Multiphoton Processes*. Springer, US, 1987.
- [50] M. D. Perry, O. L. Landen, A. Szöke, and E. M. Campbell. Multiphoton ionization of the noble gases by an intense 10^{14} -w/cm² dye laser. *Phys. Rev. A*, 37:747–760, Feb 1988.
- [51] Eric Mevel, Pierre Breger, Rusty Trainham, Guillaume Petite, Pierre Agostini, Arnold Migus, Jean-Paul Chambaret, and Andre Antonetti. Atoms in strong optical fields: Evolution from multiphoton to tunnel ionization. *Phys. Rev. Lett.*, 70:406–409, Jan 1993.

- [52] M. Protopapas, C. H. Keitel, and P. L. Knight. Atomic physics with super-high intensity lasers. *Reports on Progress in Physics*, 60:389–486, April 1997.
- [53] V S Popov. Tunnel and multiphoton ionization of atoms and ions in a strong laser field (keldysh theory. *PHYS-USP*, 47(9):855–885, 2004.
- [54] L.D. Landau and E.M. Lifshitz. *Quantum Mechanics Non-Relativistic Theory*. Pergamon Press, Oxford, third edition, 1977.
- [55] M.V. Ammosov, N.B. Delone, and V.P. Krainov. Tunnel ionization of complex atoms and of atomic ions in an alternating electromagnetic field. *Sov. Phys. JETP*, 64:1191, 1986.
- [56] Dimitri Batani, Charles J. Joachain, S. Martellucci, and Arthur N. Chester. *Atoms, Solids, and Plasmas in Super-Intense Laser Fields*. Springer, US, 2012.
- [57] P. Agostini, F. Fabre, G. Mainfray, G. Petite, and N. K. Rahman. Free-free transitions following six-photon ionization of xenon atoms. *Phys. Rev. Lett.*, 42:1127–1130, Apr 1979.
- [58] Y Gontier and M Trahin. Energetic electron generation by multiphoton absorption. *Journal of Physics B: Atomic and Molecular Physics*, 13(22):4383–4390, nov 1980.
- [59] F Fabre, G Petite, P Agostini, and M Clement. Multiphoton above-threshold ionisation of xenon at 0.53 and 1.06 m. *Journal of Physics B: Atomic and Molecular Physics*, 15(9):1353–1369, may 1982.
- [60] G Petite, P Agostini, and H G Muller. Intensity dependence of non-perturbative above-threshold ionisation spectra: experimental study. *Journal of Physics B: Atomic, Molecular and Optical Physics*, 21(24):4097–4105, dec 1988.

Bibliography

- [61] J H Eberly and J Javanainen. Above-threshold ionisation. *European Journal of Physics*, 9(4):265–275, oct 1988.
- [62] W. Becker, F. Grasbon, R. Kopold, D. B. Milosevic, G. G. Paulus, and H. Walther. Above-threshold ionization: From classical features to quantum effects. *volume 48 of Advances In Atomic, Molecular, and Optical Physics*, pages 35-98. Academic Press, 2002.
- [63] Yousef I. Salamin, S.X. Hu, Karen Z. Hatsagortsyan, and Christoph H. Keitel. Relativistic high-power laser-matter interactions. *Physics Reports*, 427(2):41 – 155, 2006.
- [64] H.A. Bethe and E.E. Salpeter. *Quantum Mechanics of One and Two Electron Atoms*. Springer, Berlin, 1957.
- [65] D. BAUER. Plasma formation through field ionization in intense laser-matter interaction. *Laser and Particle Beams*, 21(4):489–495, 2003.
- [66] E. M. Snyder, S. A. Buzza, and A. W. Castleman, Jr. Intense field-matter interactions: Multiple ionization of clusters. *Phys. Rev. Lett.*, 77:3347–3350, Oct 1996.
- [67] D. Bauer and A. Macchi. Dynamical ionization ignition of clusters in intense short laser pulses. *Phys. Rev. A*, 68:033201, Sep 2003.
- [68] Christian Siedschlag and Jan M. Rost. Enhanced ionization in small rare-gas clusters. *Phys. Rev. A*, 67:013404, Jan 2003.
- [69] D Bauer. Small rare gas clusters in laser fields: ionization and absorption at long and short laser wavelengths. *Journal of Physics B: Atomic, Molecular and Optical Physics*, 37(15):3085, 2004.

- [70] Isidore Last and Joshua Jortner. Electron and nuclear dynamics of molecular clusters in ultraintense laser fields. i. extreme multielectron ionization. *The Journal of Chemical Physics*, 120(3):1336–1347, 2004.
- [71] M. Kundu, P. K. Kaw, and D. Bauer. Laser-cluster interaction with subcycle pulses. *Phys. Rev. A*, 85:023202, Feb 2012.
- [72] Cornelia Deiss, Nina Rohringer, Joachim Burgdörfer, Emily Lamour, Christophe Prigent, Jean-Pierre Rozet, and Dominique Vernhet. Laser-cluster interaction: X-ray production by short laser pulses. *Phys. Rev. Lett.*, 96:013203, Jan 2006.
- [73] Andreas Heidenreich, Isidore Last, and Joshua Jortner. Extreme ionization of xe clusters driven by ultraintense laser fields. *The Journal of Chemical Physics*, 127(074305), 2007.
- [74] Wolfgang Lotz. An empirical formula for the electron-impact ionization cross-section. *Zeitschrift für Physik*, 206(2):205–211, Apr 1967.
- [75] Wolfgang Lotz. Electron-impact ionization cross-sections and ionization rate coefficients for atoms and ions from hydrogen to calcium. *Zeitschrift für Physik*, 216(3):241–247, Jun 1968.
- [76] J. S. Zweiback. *Resonance effects in laser cluster interactions*. PhD thesis, LAWRENCE LIVERMORE NATIONAL LABORATORY, University of California, Livermore, California, 1999.
- [77] S. Rand. Inverse bremsstrahlung with high-intensity radiation fields. *Phys. Rev.*, 136:B231–B237, Oct 1964.
- [78] M V Fedorov and R V Karapetyan. Stimulated bremsstrahlung in the presence

Bibliography

- of an intense electromagnetic wave. *Journal of Physics A: Mathematical and General*, 9(8):L103–L106, aug 1976.
- [79] L. Schlessinger and J. Wright. Inverse-bremsstrahlung absorption rate in an intense laser field. *Phys. Rev. A*, 20:1934–1945, Nov 1979.
- [80] I. Yu. Kostyukov. Inverse-bremsstrahlung absorption of an intense laser field in cluster plasma. *Journal of Experimental and Theoretical Physics Letters*, 73(8):393–397, Apr 2001.
- [81] M. Moll, Th. Bornath, M. Schlages, and V. P. Krainov. Inverse bremsstrahlung heating rate in atomic clusters irradiated by femtosecond laser pulses. *Physics of Plasmas*, 19(3):033303, 2012.
- [82] Zachary B. Walters, Robin Santra, and Chris H. Greene. Interaction of intense vuv radiation with large xenon clusters. *Phys. Rev. A*, 74:043204, Oct 2006.
- [83] O. F. Kostenko and N. E. Andreev. Heating and ionization of metal clusters in the field of an intense femtosecond laser pulse. *Plasma Physics Reports*, 33(6):503–509, Jun 2007.
- [84] L. Spitzer. *Physics of Fully Ionized Gases*. Interscience Publishers, Inc., New York, 1956.
- [85] F. F. Chen. *Introduction to Plasma Physics and Controlled Fusion*, volume 1. Plenum Press, New York, 1984.
- [86] V.P. Silin. Nonlinear high-frequency plasma conductivity. *Sov. Phys. JETP*, 20(6):1510, 1965.

- [87] P. Mulser and M. Kanopathipillai. Collisionless absorption in clusters out of linear resonance. *Phys. Rev. A*, 71:063201, Jun 2005.
- [88] T. Liseykina, P. Mulser, and M. Murakami. Collisionless absorption, hot electron generation, and energy scaling in intense laser-target interaction. *Physics of Plasmas*, 22(3), 2015.
- [89] F. Brunel. Not-so-resonant, resonant absorption. *Phys. Rev. Lett.*, 59:52–55, Jul 1987.
- [90] S. C. Wilks and W. L. Kruer. Absorption of ultrashort, ultra-intense laser light by solids and overdense plasmas. *IEEE Journal of Quantum Electronics*, 33(11):1954–1968, Nov 1997.
- [91] Paul Gibbon and A. R. Bell. Collisionless absorption in sharp-edged plasmas. *Phys. Rev. Lett.*, 68:1535–1538, Mar 1992.
- [92] L. M. Chen, J. Zhang, Q. L. Dong, H. Teng, T. J. Liang, L. Z. Zhao, and Z. Y. Wei. Hot electron generation via vacuum heating process in femtosecond laser-solid interactions. *Physics of Plasmas*, 8(2925), 2001.
- [93] Thomas M. Antonsen, Toshihiro Taguchi, Ayush Gupta, John Palastro, and Howard M. Milchberg. Resonant heating of a cluster plasma by intense laser light. *Physics of Plasmas*, 12(5), 2005.
- [94] A. V. Getz and V. P. Krainov. Vacuum heating of large atomic clusters by a superintense femtosecond laser pulse. *JETP*, 101(80), 2005.
- [95] Boris N. Breizmanc, Alexey V. Arefiev, and Mykhailo V. Fomyts“kyi”. Nonlinear physics of laser-irradiated microclusters. *Physics of Plasmas*, 12(056706), 2005.

Bibliography

- [96] D. R. Symes, M. Hohenberger, A. Henig, and T. Ditmire. Anisotropic explosions of hydrogen clusters under intense femtosecond laser irradiation. *Phys. Rev. Lett.*, 98:123401, Mar 2007.
- [97] W. L. Kruer and Kent Estabrook. J \times b heating by very intense laser light. *Physics of Fluids*, 28(1):430–432, 1985.
- [98] E. Springate, N. Hay, J. W. G. Tisch, M. B. Mason, T. Ditmire, J. P. Marangos, and M. H. R. Hutchinson. Enhanced explosion of atomic clusters irradiated by a sequence of two high-intensity laser pulses. *Phys. Rev. A*, 61:044101, Mar 2000.
- [99] M. Kundu and D. Bauer. Collisionless energy absorption in the short-pulse intense laser-cluster interaction. *Phys. Rev. A*, 74:063202, Dec 2006.
- [100] I. Kostyukov and J.-M. Rax. Collisional versus collisionless resonant and autoresonant heating in laser-cluster interaction. *Phys. Rev. E*, 67:066405, Jun 2003.
- [101] Malay Dalui, M. Kundu, T. Madhu Trivikram, Krishanu Ray, and M. Krishnamurthy. Manifestation of anharmonic resonance in the interaction of intense ultrashort laser pulses with microstructured targets. *Physics of Plasmas*, 23(10):103101, 2016.
- [102] M. Krishnamurthy, M. Kundu, Kartik Bane, Amit D. Lad, Prashant Kumar Singh, Gourab Chatterjee, G. Ravindra Kumar, and Krishanu Ray. Enhanced x-ray emission from nano-particle doped bacteria. *Opt. Express*, 23(14):17909–17922, Jul 2015.
- [103] H. M. Milchberg, S. J. McNaught, and E. Parra. Plasma hydrodynamics of the intense laser-cluster interaction. *Phys. Rev. E*, 64:056402, Oct 2001.

- [104] Isidore Last, Israel Schek, and Joshua Jortner. Energetics and dynamics of coulomb explosion of highly charged clusters. *The Journal of Chemical Physics*, 107(17):6685–6692, 1997.
- [105] Isidore Last and Joshua Jortner. Dynamics of the coulomb explosion of large clusters in a strong laser field. *Phys. Rev. A*, 62:013201, Jun 2000.
- [106] Isidore Last and Joshua Jortner. Electron and nuclear dynamics of molecular clusters in ultraintense laser fields. iii. coulomb explosion of deuterium clusters. *The Journal of Chemical Physics*, 121(7):3030–3043, 2004.
- [107] Enrique Parra, Ilya Alexeev, Jingyun Fan, Kiong Y. Kim, Stuart J. McNaught, and Howard M. Milchberg. Hydrodynamic time scales for intense laser-heated clusters. *J. Opt. Soc. Am. B*, 20(1):118–124, Jan 2003.
- [108] Yuji Fukuda, Koichi Yamakawa, Yutaka Akahane, Makoto Aoyama, Norihiro Inoue, Hideki Ueda, and Yasuaki Kishimoto. Optimized energetic particle emissions from xe clusters in intense laser fields. *Phys. Rev. A*, 67:061201, Jun 2003.
- [109] Christian Jungreuthmayer, Lora Ramunno, Jurgen Zanghellini, and Thomas Brabec. Intense VUV laser cluster interaction in the strong coupling regime. *IOP Publishing*, 38(16):3029–3036, aug 2005.
- [110] Michael P. Allen and Dominic J. Tildesley. *Computer simulations of liquids*. Oxford Science Publications. Oxford Science Publications, Oxford, UK, 1988.
- [111] Daan Frenkel and Berend Smit. *Understanding Molecular Simulation*. Academic Press, San Diego, second edition, 2002.
- [112] D. C. Rapaport. *The Art of Molecular Dynamics Simulation*. Cambridge University Press, Cambridge, UK, second edition, 2004.

Bibliography

- [113] C.K. Birdsall and A.B. Langdon. *Plasma Physics via Computer Simulation*. McGraw-Hill, New York, 1985.
- [114] R. W. Hockney and J. W. Eastwood. *Computer simulation using particles*. IOP Publishing, Bristol, 1988.
- [115] G. E. P. Box and Mervin E. Muller. A note on the generation of random normal deviates. *Ann. Math. Statist.*, 29(2):610–611, 06 1958.
- [116] S. V. Fomichev, D. F. Zaretsky, D. Bauer, and W. Becker. Classical molecular-dynamics simulations of laser-irradiated clusters: Nonlinear electron dynamics and resonance-enhanced low-order harmonic generation. *Phys. Rev. A*, 71:013201, Jan 2005.
- [117] G. M. Petrov, J. Davis, A. L. Velikovich, P. Kepple, A. Dasgupta, and R. W. Clark. Dynamics of a xe cluster plasma produced by an intense ultrashort pulse krf laser. *Physics of Plasmas*, 12(6), 2005.
- [118] Gaurav Mishra, Amol R. Holkundkar, and N.K. Gupta. Effect of laser pulse time profile on its absorption by argon clusters. *Laser and Particle Beams*, 29:305–313, 9 2011.
- [119] Gaurav Mishra and N. K. Gupta. Molecular dynamic studies on anisotropic explosion of laser irradiated xe cluster. *Physics of Plasmas*, 19(9), 2012.
- [120] Rong Cheng, Chunyan Zhang, Li-Bin Fu, and Jie Liu. Molecular dynamics simulations of anisotropic explosions of small hydrogen clusters in intense laser pulses. *Journal of Physics B: Atomic, Molecular and Optical Physics*, 48(3):035601, 2015.

- [121] Amol R. Holkundkar, Gaurav Mishra, and N. K. Gupta. Molecular dynamic simulation for laser–cluster interaction. *Physics of Plasmas*, 18(5), 2011.
- [122] F. Greschik, L. Arndt, and H.-J. Kull. Absorption of few-cycle laser pulses by outer ionization of atomic clusters. *EPL (Europhysics Letters)*, 72(3):376, 2005.
- [123] W.C. Swope, C. Hans, H.C. Andersen, P.H. Berens, and K.R. Wilson. A computer simulation method for the calculation of equilibrium constants for the formation of physical clusters of molecules: Application to small water clusters. *The Journal of Chemical Physics*, 76:637–649, 1982.
- [124] Loup Verlet. Computer "experiments" on classical fluids. i. thermodynamical properties of lennard-jones molecules. *Phys. Rev.*, 159:98–103, Jul 1967.
- [125] John C. Butcher. *Numerical Analysis of Ordinary Differential Equations*. Wiley, Chichester, UK, 1987.
- [126] O.V. Batishchev, A.A. Batishcheva, V.Yu. Bychenkov, C.M. Albukrek, A.V. Brantov, and W. Rozmus. Molecular dynamics model for heating of coulomb clusters by laser field. *Computer Physics Communications*, 164(1–3):53 – 59, 2004.
- [127] Roman G Bystryi and Igor V Morozov. Electronic oscillations in ionized sodium nanoclusters. *Journal of Physics B: Atomic, Molecular and Optical Physics*, 48(1):015401, 2015.
- [128] T. Döppner, Th. Fennel, Th. Diederich, J. Tiggesbäumker, and K. H. Meiwes-Broer. Controlling the coulomb explosion of silver clusters by femtosecond dual-pulse laser excitation. *Phys. Rev. Lett.*, 94:013401, Jan 2005.

Bibliography

- [129] S. Zamith, T. Martchenko, Y. Ni, S. A. Aseyev, H. G. Muller, and M. J. J. Vrakking. Control of the production of highly charged ions in femtosecond-laser cluster fragmentation. *Phys. Rev. A*, 70:011201, Jul 2004.
- [130] M. Kundu, S. V. Popruzhenko, and D. Bauer. Harmonic generation from laser-irradiated clusters. *Phys. Rev. A*, 76:033201, Sep 2007.
- [131] Thomas Fennel, Lora Ramunno, and Thomas Brabec. Highly charged ions from laser-cluster interactions: Local-field-enhanced impact ionization and frustrated electron-ion recombination. *Phys. Rev. Lett.*, 99:233401, Dec 2007.
- [132] T. Ditmire, J. W. G. Tisch, E. Springate, M. B. Mason, N. Hay, J. P. Marangos, and M. H. R. Hutchinson. High energy ion explosion of atomic clusters: Transition from molecular to plasma behavior. *Phys. Rev. Lett.*, 78:2732–2735, Apr 1997.
- [133] V. Kumarappan, M. Krishnamurthy, and D. Mathur. Asymmetric high-energy ion emission from argon clusters in intense laser fields. *Phys. Rev. Lett.*, 87:085005, Aug 2001.
- [134] V. Kumarappan, M. Krishnamurthy, D. Mathur, and L. C. Tribedi. Effect of laser polarization on x-ray emission from Ar_n ($n = 200 \sim 10^4$) clusters in intense laser fields. *Phys. Rev. A*, 63:023203, Jan 2001.
- [135] M. Krishnamurthy, D. Mathur, and V. Kumarappan. Anisotropic “charge-flipping” acceleration of highly charged ions from clusters in strong optical fields. *Phys. Rev. A*, 69:033202, Mar 2004.
- [136] V. Kumarappan, M. Krishnamurthy, and D. Mathur. Two-dimensional effects in the hydrodynamic expansion of xenon clusters under intense laser irradiation. *Phys. Rev. A*, 66:033203, Sep 2002.

- [137] E. Springate, N. Hay, J. W. G. Tisch, M. B. Mason, T. Ditmire, M. H. R. Hutchinson, and J. P. Marangos. Explosion of atomic clusters irradiated by high-intensity laser pulses: Scaling of ion energies with cluster and laser parameters. *Phys. Rev. A*, 61:063201, May 2000.
- [138] E. Springate, S. A. Aseyev, S. Zamith, and M. J. J. Vrakking. Electron kinetic energy measurements from laser irradiation of clusters. *Phys. Rev. A*, 68:053201, Nov 2003.
- [139] V. Kumarappan, M. Krishnamurthy, and D. Mathur. Asymmetric emission of high-energy electrons in the two-dimensional hydrodynamic expansion of large xenon clusters irradiated by intense laser fields. *Phys. Rev. A*, 67:043204, Apr 2003.
- [140] J Jha, D Mathur, and M Krishnamurthy. Enhancement of x-ray yields from heteronuclear cluster plasmas irradiated by intense laser light. *Journal of Physics B: Atomic, Molecular and Optical Physics*, 38(18):L291, 2005.
- [141] J. Jha, D. Mathur, and M. Krishnamurthy. Engineering clusters for table-top acceleration of ions. *Applied Physics Letters*, 88(4), 2006.
- [142] L. M. Chen, F. Liu, W. M. Wang, M. Kando, J. Y. Mao, L. Zhang, J. L. Ma, Y. T. Li, S. V. Bulanov, T. Tajima, Y. Kato, Z. M. Sheng, Z. Y. Wei, and J. Zhang. Intense high-contrast femtosecond k -shell x-ray source from laser-driven ar clusters. *Phys. Rev. Lett.*, 104:215004, May 2010.
- [143] P. Mulser, S. M. Weng, and Tatyana Liseykina. Analysis of the brunel model and resulting hot electron spectra. *Physics of Plasmas*, 19(4), 2012.

Bibliography

- [144] F Megi, M Belkacem, M A Bouchene, E Suraud, and G Zwicknagel. On the importance of damping phenomena in clusters irradiated by intense laser fields. *Journal of Physics B: Atomic, Molecular and Optical Physics*, 36(2):273, 2003.
- [145] J. P. Geindre, R. S. Marjoribanks, and P. Audebert. Electron vacuum acceleration in a regime beyond brunel absorption. *Phys. Rev. Lett.*, 104:135001, Mar 2010.
- [146] S. V. Popruzhenko, M. Kundu, D. F. Zaretsky, and D. Bauer. Harmonic emission from cluster nanoplasmas subject to intense short laser pulses. *Phys. Rev. A*, 77:063201, Jun 2008.
- [147] M. Kundu and D. Bauer. Optimizing the ionization and energy absorption of laser-irradiated clusters. *Physics of Plasmas*, 15(3), 2008.
- [148] J. Posthumus. *Molecules and Clusters in Intense Laser Fields*. Cambridge University Press, Cambridge, UK, September 2009.